MODELING, ANALYSIS AND CONTROL OF PRINT REGISTRATION

IN ROLL-TO-ROLL PRINTING PRESSES

By

ARAVIND SESHADRI

Bachelor of Engineering
Mechanical Engineering
University of Madras
Tamil Nadu, India
2003

Master of Science
Mechanical Engineering
Oklahoma State University
Stillwater, Oklahoma
2007

Submitted to the Faculty of the
Graduate College of the
Oklahoma State University
in partial fulfillment of
the requirements for
the Degree of
Doctor of Philosophy
May 2013

MODELING, ANALYSIS AND CONTROL OF PRINT REGISTRATION

IN ROLL-TO-ROLL PRINTING PRESSES

Dissertation Approved:

Dr. Prabhakar R. Pagilla
Dissertation Advisor and Committee Chair

Dr. Lawrence L. Hoberock
Committee Member

Dr. Karl N. Reid
Committee Member

Dr. Martin Hagan
Committee Member

Acknowledgments

To my parents.

I am fortunate to be around wonderful people who have directly and indirectly contributed to this dissertation. I thank everyone with whom I have interacted with during my stay at OSU, for providing me a warm and welcoming place and for motivating me to succeed in my endeavors. Without their support I would have not had the chance to complete this work.

I have no words to express my gratitude to my advisor Dr. Prabhakar Pagilla. He recognized the potential in me to pursue a doctoral degree, which I definitely did not see in myself. He has always provided tremendous support, both monetarily and morally. There was never a time during my degree I had to worry about funding for my graduate school. Whenever possible he had found monies from other sources to supplement my assistantship without me ever taking the initiative. He went above and beyond when he took the initiative to send me to France to conduct research as part of the National Science Foundation, International Research and Education in Engineering program. I am really grateful for all his support.

Dr. Pagilla kept me motivated and pushed me to publish frequently. Even though I have several publications, I am sure he would have liked me to have even more. And I could have if I didn't get involved with all the extra-curricular activities at OSU. He has been very patient and supportive of my activities with the student organizations on-campus, even though my involvement significantly affected my research productivity for a period of three years. My on-campus involvement has been a great learning experience, and I thank him for providing me an opportunity to pursue them.

I thank him for his patience in reading all my writings and for making my writings read well. I am sure he would have spent a significant amount of time

to correct all my documents. I am really amazed how meticulous he is to every minute detail while reading manuscripts.

Finally, I thank him for convincing me to stay at OSU after my Masters degree. My life has changed significantly since that decision and I am really glad I made that decision.

I would also like to thank my committee members, Dr. Karl Reid, Dr. Larry Hoberock, Dr. Martin Hagan and also Dr. John Shelton, for their valuable suggestions and guidance during the course of my Ph.D. studies.

Armstrong World Industries, particularly Jamie Lynch and Tim Gottlob, allowed me to conduct research at their Stillwater facility by providing me access to their machines. Jamie, thank you so much for spending a lot of time with me to explain how things work, and for giving me all the freedom to work with the machinery even during production runs. Your insights and guidance have definitely helped me understand, and successfully solve the problems in my dissertation. Tim, I am really thankful for your willingness to help and spend time with me even when you had to manage two positions in the plant. Thank you!

I would also like to thank National Science Foundation and Oklahoma Center for Advancement of Science and Technology for sponsoring the research I was involved in, ConocoPhillips for the graduate fellowship, and the graduate college for the supplementary fellowship, the tuition waivers and health insurances.

Carlo Branca and Mauro Cimino, you both have taught me so much about control theory, and I couldn't have finished my dissertation without you guys. Our discussions in the graduate office, both academic and non-academic, have definitely enriched my experience at OSU and I thank you both for that. Both of you have motivated and supported me and I am grateful for having you both as

my friends. I would like to thank Pramod Raul, Diao Yu, Ramamurthy Dwivedula and Yunfei Zou for their time and enjoyable conversations that we shared, and all my other fellow graduate students advised by Dr. Pagilla.

I have make great friends at OSU and everyone has directly or indirectly supported me during my stay at OSU. I would especially like to thank Brenda Morales (my fiancé), Pedro Velasco, Paolo Sanza and Awilda Rodriguez for their friendship, motivation and support. Brenda, you have kept me motivated and have provided me a lot of moral and emotional support, and love. You definitely destressed me when the days were tough. Pedro, thank you for putting up with me and being my golf partner; golf definitely helped me de-stress, reflect on my thoughts and think about fresh ideas for my research and other things that were on my mind. Paolo and Awilda, you both are like a big brother and big sister to me. I always enjoyed your company and conversations, the conversations definitely helped me have a perspective about life.

I would also like to thank all the colleagues that I worked with during my days as the President and Vice President of the Graduate and Professional Student Government Association and as the Creativity Innovation Entrepreneurship scholar. You guys definitely helped me balance both my research and campus involvement.

I would also like to thank staff members from the School of Mechanical and Aerospace Engineering, Daleene Caldwell, Sharon Green and Dianne Compton, for helping me navigate the administrative, research and teaching activities while being a graduate assistant at OSU. Thanks to staff member at the OSU International Students and Scholar office, Regina Henry, Linda Dunbar and Tim Huff, for taking care of my legal status in the US and helping me navigate the immigration

and tax requirements during my stay at OSU.

Last by not least I thank my family; they have provided significant moral, emotional, and of course monetary support during my entire student tenure at OSU. Mom and Dad, you both have made a lot of sacrifices so that I can lead a better life. Even though I have disappointed you in many occasions, you both believed in me, trusted me, and supported me during this very long journey. I Thank you both for your motivation, support, understanding and faith in me. I wouldn't be in the US, nor in this position without the unconditional support from my brother, Sriram Seshadri (Anna). Anna, I thank you for supporting me in all my decisions and sticking with me during my high and low times. You have always been a motivation to me, and I am who I am because of you. Thank you!

Acknowledgements reflect the views of the author and are not endorsed by committee members or Oklahoma State University.

Name: Aravind Seshadri

Date of Degree: May 2013

Title of Study: MODELING, ANALYSIS AND CONTROL OF PRINT REGISTRATION IN ROLL-TO-ROLL PRINTING PRESSES

Major Field: Mechanical and Aerospace Engineering

ABSTRACT

Print registration in roll-to-roll (R2R) printing process is investigated in this dissertation. Print registration is the process of aligning multiple images that are printed in consecutive print units. The quality of the print output depends on the proper alignment of these images. A new mathematical model for print registration is developed by considering the effect of key process variables, such as web tension and transport velocity, print cylinder angular position and velocity, and the compensator roller position. Sources of machine induced disturbances and their effect on print registration are also investigated and machine design recommendations to mitigate these disturbances are given. Propagation of disturbances between print units due to web transport is investigated. The interaction, or the disturbance propagation behavior, between print units is studied by developing a new interaction metric called the Perron Root based Interaction Metric (PRIM). The new interaction metric, for large-scale interconnected systems employing decentralized controllers, is developed using tools from the Perron-Frobenius theory. A systematic procedure to minimize interaction is given by designing pre-filters for decentralized control systems. The disturbance propagation behavior with two registration control strategies is compared using the PRIM and it is found that a compensator based registration control (CRC) has smaller magnitude of disturbance propagation when compared to a print cylinder angular position based registration control (PARC). It is also found that a simple, decentralized, memoryless, state feedback controllers stabilizes print units with CRC. Results from a number of model simulations and experiments are provided to support the recommendations and conclusions.

Contents

Contents ix

List of Tables xi

List of Figures xii

1 Introduction 1

1.1 Web Handling 2

1.2 Roll-to-Roll Printing 3

1.3 Focus Application 7

1.4 Problems and Opportunities in Roll-to-roll Printing 8

1.5 Contributions 11

2 Modeling Print Registration and Print Section Dynamics 14

2.1 Governing Equation for Print Registration Error 15

2.2 Print Registration Experiments and Model Simulations 20

2.3 Governing Equation for Web Strain 31

2.4 Print Section Velocity Dynamics 34

2.5 Print Cylinder Velocity Dynamics due to Web Wrapped Impression Roller 47

2.6 Design Recommendations to Minimize Strain Variations within Print Units 50
2.7 Remarks 55

3 Interaction Analysis in Decentralized Control Systems 56
3.1 Introduction 56
3.2 Perron-Frobenius Theory 59
3.3 Perron-Root Based Interaction Measure 61
3.4 Interaction Analysis and Minimization in Roll-to Roll Systems 70
3.5 Discussion of PRIM and Other Interaction Metrics 83

4 Analysis and Control of Print Registration 89
4.1 Analysis of Interaction in R2R Printing 91
4.2 Comparison of Registration Control Strategies 98
4.3 Remarks 115

5 Summary and Conclusions 130
5.1 Summary 130
5.2 Conclusions 134
5.3 Future Work 135

Bibliography 136

List of Tables

2.1 Doctor blade stroke length and crank arm position during out-of-phase run for various print units. The stroke length is given in centimeters and relative crank arm angular position is represented in terms of the needle of the clock. 52

3.1 Parameter of the Euclid line and web transport conditions used in the linearized model. 75

4.1 Web transport parameters used in interaction analysis. 96

List of Figures

1.1 Schematic of an example roll-to-roll processing machinery. 2

1.2 Schematic of a rotogravure print unit. 4

1.3 An illustrative example showing a properly registered print pattern (left) and an improperly registered print pattern (right). Both machine direction and cross machine direction registration issues are shown in the illustration. 5

1.4 Patterns are printed successively to form a multicolor image. Registration flags are printed along with the pattern on the web; the registration error sensor measures the distance (or time) between registration flags which can be used to determine the registration error. . . . 6

1.5 Schematic of the Armstrong print line. 7

2.1 A schematic showing the web between two successive print cylinders; some of the idle rollers are ignored. 16

2.2 Measured web tension and registration error in print cylinder 7 from a production run. 22

2.3 FFT of the relative tension and registration error data in print cylinder 7 from a production run. 22

2.4 Comparison of model output data and actual data (Run 1) 23

2.5 Comparison of model output data and actual data (Run 2) 24
2.6 Web strain from prints units 5 – 7 during a production run (Run 1). Web strain is determined from web tension measurements based on the assumption that the web material is elastic. 26
2.7 Web strain from prints units 5 – 7 during a production run (Run 2). . . . 26
2.8 Comparison of input to the registration error integrator in the three models; data corresponds to production Run 1. 27
2.9 Comparison of input to the registration error integrator in the three models; data corresponds to production Run 2. 27
2.10 Web strain from prints units 5 – 7 during a production run (Run 3). A slow drift in the web strain can be observed in print unit 5 during this run. 28
2.11 Web strain from prints units 5 – 7 during a production run. A sudden shift in the web strain can be observed in print unit 5 during this run. . 29
2.12 Comparison of input to the registration error integrator in the three models; data corresponds to production Run 3. 29
2.13 Comparison of input to the registration error integrator in the three models; data corresponds to production run with sudden shift in web strain. 30
2.14 Comparison of model output data and actual data (Run 3) 30
2.15 Comparison of model output data and actual data (Run 2) 30

2.16 A schematic showing the print section mechanical transmission with angles used in this work. The print section motor drives the common shaft which in turn transmits power to print unit gear boxes. The print cylinder and doctor blade assembly in each print unit is driven by the torque transmitted through the gear box. 35
2.17 Doctor Blade Assembly 36
2.18 A side view of the doctor blade assembly and the print cylinder. 36
2.19 Effect of change in r/l ratio on the normalized f_i as a function of crank arm position 41
2.20 Effect of change in r/l ratio on the normalized $\frac{\partial f_i}{\partial \theta_m}$ as a function of crank arm position 42
2.21 A sketch showing the frictional forces on the print cylinder and the web. 47
2.22 Measured web tension in print unit 5 and print unit 6. 51
2.23 FFT of differential tension and registration error at various print units when doctor blade oscillations are out-of-phase with each other. 53
2.24 FFT of differential tension and registration error at various print units when doctor blade oscillations are in with each other. 54

3.1 Picture of the experimental web platform; a line schematic is shown in Figure 3.2. 70
3.2 Schematic of the experimental web platform 70
3.3 Decentralized tension control structure for roll-to-roll systems with an inner velocity loop and an outer tension loop 71
3.4 Perron root interaction metric for the linearized model of the roll-to-roll system 74

3.5 Tension measurement at the unwind, pull roll and rewind section with sinusoidal velocity disturbances at the S-wrap section; web transport in the forward direction. The alternate shaded and light regions show the sinusoidal velocity disturbances with six distinct frequencies with a 5 ft/min magnitude; the annotation in the top plot indicates the frequencies. 76
3.6 Tension measurement at the unwind, pull roll and rewind section with sinusoidal velocity disturbances at the S-wrap section; web transport in the reverse direction. The alternate shaded and light regions show the sinusoidal velocity disturbances with six distinct frequencies with a 5 ft/min magnitude. 77
3.7 Comparison of PRIM for two different web materials. Tyvek web: EA=2200 lbf; Polyethylene web: EA=7000 lbf. 77
3.8 Tension measurement at the unwind, pull roll and rewind section with sinusoidal velocity disturbances at the S-wrap section; web transport in the forward direction. 78
3.9 Tension measurement at the unwind, pull roll and rewind section with sinusoidal velocity disturbances at the S-wrap section; web transport in the reverse direction. 78
3.10 FFT of tension measurement in the three tension zones with Tyvek and polyethylene webs; web is transported in the forward direction. . . 79
3.11 FFT of tension measurement in the three tension zones with Tyvek and polyethylene webs; web is transported in the reverse direction. . . . 79
3.12 Perron vector elements in the frequency range of interest 80

3.13 Pre-filters for the three tension loops designed by fitting stable, minimum phase ration transfers for the elements of the Perron right eigenvector 81

3.14 Interaction in the experimental platform with pre-filter; tension measurement at the unwind, pull roll and rewind section with sinusoidal velocity disturbances at the S-wrap section; web transport in the forward direction. 82

3.15 Interaction in the experimental platform with pre-filter; tension measurement at the unwind, pull roll and rewind section with sinusoidal velocity disturbances at the S-wrap section; web transport in the reverse direction. 82

3.16 FFT of tension measurement in the three tension zones with and without pre-filter; web is transported in the forward direction. 83

3.17 FFT of tension measurement in the three tension zones with and without pre-filter; web is transported in the reverse direction. 84

3.18 Top and bottom plots show the closed-loop magnitude response ($|\overline{h}_i(s)|$) for the three tension loops (dashed and dotted lines) without and with pre-filter for the diagonal system $\overline{G(s)}$. The solid line is the stability constraint ($\frac{1}{p_{L_H}}$) for the overall system G. 84

3.19 PRIM and SSVIM for the linearized R2R platform model with Tyvek and Polyethylene webs. 88

4.1 A schematic showing the web between two successive print cylinders; some of the idle rollers are ignored. 92

4.2 Schematic of a print section with seven print units and eight print cylinders. 94

4.3 Perron root interaction metric for print units with CRC and PARC. 96

4.4 $M-\Delta$ loop representation of the system in (4.8) 100

4.5 Stability constraints for print units with compensator based control for print registration. For the stability condition dependent on delay the maximum delay for τ_1 was chosen as $r_1 = 19$ seconds and $r_2 = 7$ seconds for τ_2. 109

4.6 Delay-dependent stability condition as a function of magnitude of span length correction. The plots show 10 to 100 % of the registration error correction per second. 110

4.7 Stability condition dependent on delay for the print section with the dynamics in Equation 4.7 controlled using a electronic line shaft based registration control with gain $k_0 = 1000$ and $k_{ii} = [0 \quad -275 \quad 1000]$ for a maximum delay value for τ_1 to be $\overline{r}_1 = 0.27$ seconds. 114

4.8 Interaction in CRC with a pulse width of 14 seconds and magnitude of 0.0401 in/sec. 117

4.9 Interaction in PARC with a pulse width of 14 seconds and input torque magnitude of 0.5643 lb-in. 118

4.10 Interaction in CRC with a pulse width of 1.5 seconds and magnitude of 0.0401 in/sec. 118

4.11 Interaction in PARC with a pulse width of 1.5 seconds and input torque magnitude of 0.5643 lb-in. 119

4.12 Interaction in CRC with a sinusoidal input magnitude of 0.0401 in/sec and frequency of 0.05 Hz. 119

4.13 Interaction in PARC with a sinusoidal torque input magnitude of 0.5643 lb-in and frequency of 0.05 Hz. 120

4.14 Interaction in CRC with a sinusoidal input magnitude of 0.0401 in/sec and frequency of 0.1 Hz. 120
4.15 Interaction in PARC with a sinusoidal torque input magnitude of 0.5643 lb-in and frequency of 0.1 Hz. 121
4.16 Interaction in CRC with a sinusoidal input magnitude of 0.0401 in/sec and frequency of 0.5 Hz. 121
4.17 Interaction in PARC with a sinusoidal torque input magnitude of 0.5643 lb-in and frequency of 0.5 Hz. 122
4.18 Interaction in CRC with a sinusoidal input magnitude of 0.0401 in/sec and frequency of 1 Hz. 122
4.19 Interaction in PARC with a sinusoidal torque input magnitude of 0.5643 lb-in and frequency of 1 Hz. 123
4.20 Interaction in CRC with a sinusoidal input magnitude of 0.0401 in/sec and frequency of 1.5 Hz. 123
4.21 Interaction in PARC with a sinusoidal torque input magnitude of 0.5643 lb-in and frequency of 1.5 Hz. 124
4.22 Initial condition response of the print section dynamics without compensator correction. The initial conditions for the variational web strain in the seven print units were taken as $[-1.5, -1, -0.5, 0, 0.5, 1, 1.5]\times 10^{-5}$. 124
4.23 Initial condition response of the print section dynamics without compensator correction. The initial conditions for registration error in print unit 4 was taken as 0.01 mils. 125

4.24 Initial condition response of the print section dynamics without compensator correction. The initial conditions for variational web velocity in print cylinder 4 was taken as 10^{-4} rad/sec or 8.5944×10^{-4} in/sec. 125

4.25 Initial condition response of the print section dynamics with state feedback CRC. The initial conditions for the variational web strain in the seven print units were taken as $[-1.5, -1, -0.5, 0, 0.5, 1, 1.5] \times 10^{-5}$.126

4.26 Initial condition response of the print section dynamics with state feedback CRC. The initial conditions for registration error in print unit 4 was taken as 0.01 mils. 126

4.27 Initial condition response of the print section dynamics with state feedback CRC. The initial conditions for variational web velocity in print cylinder 4 was taken as 10^{-4} rad/sec or 8.5944×10^{-4} in/sec. 127

4.28 Propagation of disturbance in the print section without compensator correction. A pulse disturbance magnitude of 1×10^{-6} in variational web strain was introduced in the span upstream of the print section. . . 127

4.29 Propagation of disturbance in the print section without compensator correction. A sinusoidal disturbance with magnitude of 1×10^{-6} and frequency of $(1/300)$ Hz in variational web strain was introduced in the span upstream of the print section. 128

4.30 Propagation of disturbance in the print section with CRC. A pulse disturbance magnitude of 1×10^{-6} in variational web strain was introduced in the span upstream of the print section. 128

4.31 Propagation of disturbance in the print section with CRC. A sinusoidal disturbance with magnitude of 1×10^{-6} and frequency of (1/300) Hz in variational web strain was introduced in the span upstream of the print section. 129

Abbreviations

CRC : Compensator based Registration Control
DSP : Digital Signal Processor
ELS : Electronic Line Shaft
FFT : Fast Fourier Transform
IMC : Internal Model Control
LTI : Linear Time Invariant
MLS : Mechanical Line Shaft
MSV : Maximum Singular Value
NP-hard : Non-deterministic Polynomial-time hard
PARC : Print cylinder Angular position based Registration Control
PLC : Programmable Logic Controller
PRIM : Perron Root based Interaction Metric
R2R : Roll-to-Roll
RFID : Radio-Frequency IDentification
SISO : Single-Input Single-Output
SSV : Structured Singular Value
SSVIM : Structured Singular Value Interaction Metric

Notations

$\mathscr{R}$: Set of real numbers

$\mathscr{C}$: Set of complex numbers

$\mathscr{C}^+$: Set of complex numbers in open right half plane

$\mathscr{R}^n$: Set of real vectors of length n

$\mathscr{C}^n$: Set of complex vectors of length n

$\mathscr{R}^{n\times m}$: Set of real $n \times m$ matrices

$\mathscr{C}^{n\times m}$: Set of complex $n \times m$ matrices

$|(.)|$: Absolute value of elements in $\mathscr{R}$ or $\mathscr{C}$

$||(.)||_1$: One norm of elements in $\mathscr{R}^n$ or $\mathscr{C}^n$

$||(.)||$: Induced matrix norm of elements in $\mathscr{R}^{n\times m}$ or $\mathscr{C}^{n\times m}$

I : Identity matrix of appropriate dimension

$\mathbf{0}$: Matrix will all zeros of appropriate dimension

For $n \times n$ square matrix, $A_{n\times n}$:

$\lambda_i(A)$: Eigenvalue of A

$\rho(A)$: Spectral radius of A, maximum absolute value of

$\sigma(A)$: Spectrum of A, the set of all eigenvalues of A

$\det(A)$: Determinant of the matrix A

$A \geq 0$: All the elements of the matrix A are nonnegative

$\mathscr{P}(A)$: Perron root of irreducible nonnegative matrix A

For $n \times m$ matrix, $M_{n\times m}$:

$\overline{\sigma}(M)$: Maximum singular value of M

$\mu_\Delta(M)$: Structured singular value of M with respect to the structure Δ

CHAPTER 1

Introduction

Roll-to-roll (R2R) manufacturing is a continuous process in which a continuous, flexible material is passed through processing machinery to create a finished product; the continuous, thin, flexible material is often termed as a web. A variety of common consumer products are manufactured in rolled form, materials such as paper, plastic, metals, textiles, etc., since roll-to-roll manufacturing is efficient with high yields due to high speed automation. A typical web processing machine (see Figure 1.1) consists of an unwind section which consists of a material roll and other dynamic elements, such as accumulators and web guides, process sections where the required processing operations are carried out, and a rewind section where the finished material is wound back into rolls or cut into sheets; operations such as printing, coating, lamination, etc., are carried out on the continuously moving web material to create a finished product. The transport of webs through processing machinery is facilitated by a number of driven rollers and idle rollers throughout the machine.

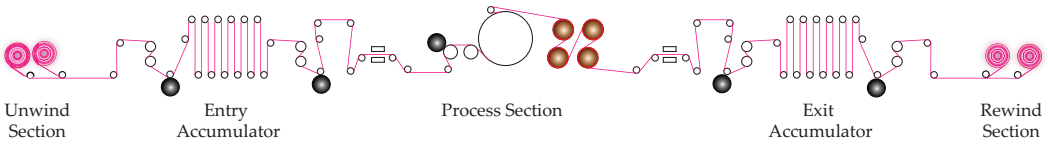

Figure 1.1: *Schematic of an example roll-to-roll processing machinery.*

1.1 Web Handling

As the web is transported over rollers, the moving web experiences fluctuations in all three directions; these fluctuations have to be controlled in order to obtain a quality finished product. The machine direction or the transport direction behavior of the moving web is termed as longitudinal dynamics; the cross-machine direction behavior is often termed as lateral dynamics and the transverse fluctuations are often referred to as web flutter. The study of web behavior as it is transported over rollers is called web handling. The key variable that describes the longitudinal behavior of the web as it is transported over the rollers is the tension in the web between two adjacent rollers. The transport of web, assuming that sufficient friction is available to prevent web slippage over rollers, also results in transport of strain which may cause propagation of strain variations (tension variations) from upstream spans to downstream spans. The propagation of tension variations will cause variations in roller velocities as the two variables, web tension and roller velocities, are inherently coupled through their governing equations and affect each other. The web behavior during transport on rollers depends on the transport conditions such as web transport velocity, web tension, etc., web material properties such as Young's modulus of the material, cross-sectional dimensions of the web, etc., and machine installation properties such as roller size and span length between rollers, etc. To efficiently transport webs

on rollers without defects, most web handling processes require regulation of web tension and web transport velocity. The transport velocity is controlled using driven rollers and web tension is controlled by using either (1) driven rollers under speed or torque control [1] or (2) an active or a passive dancer [2].

Control of lateral motion (called web guiding) is critical for operation of all R2R process lines since uncontrolled lateral movement of the web may cause wrinkles or slackness in the web which may damage or break the material. A mechanism called the web guide is used for controlling the lateral motion. Depending on the location of use within the web machine, web guides are categorized as (a) terminal guides, used on the unwind and rewind rolls and (b) intermediate guides, used in the intermediate sections of the processing machinery. Electro-mechanical or electro-hydraulic actuators are used to control web guides and sensors that detect the position of the web are used as feedback devices for the controllers. Additional details about lateral dynamics and control can be found in [3, 4, 5, 6, 7] and references therein.

This work is focused on controlling the longitudinal behavior of the web such as control of web velocity and web tension or web strain which are critical for roll-to-roll printing applications.

1.2 Roll-to-Roll Printing

R2R printing involves transport of web through print units where the required pattern is printed on the material. Several types of R2R printing technologies, such as offset-printing, flexo-printing and rotogravure printing, are available. This work is concerned with studying the fundamental web behavior in printing presses irrespective of the technologies used for printing. The main objective in

a printing process is to ensure a quality print output by transporting the material through print units by appropriately controlling various web handling process variables, such as web transport velocity, web tension or web strain, etc.

In R2R printing, the web is transported through one or more printing rollers (also called as print cylinder) where the image/pattern on the print cylinder(s) is transferred onto the web material. Figure 1.2 shows a schematic of a rotogravure printing unit. The gravure print cylinder is engraved to form wells to create print patterns on the cylinder surface. As the print cylinder rotates within the ink bath, ink is collected onto the wells or cells in the surface of the gravure print cylinder. The excess ink from the surface of the print cylinder is scraped by a device called doctor blade so that only the region of the gravure cylinder with the pattern contains the ink and the rest of the region is devoid of ink. As the web passes between the nipped impression roller and the print cylinder, ink is transferred from the print cylinder to the web. The printed web with wet ink is transported over idle rollers in the drying section and cooled using a downstream cooling roller.

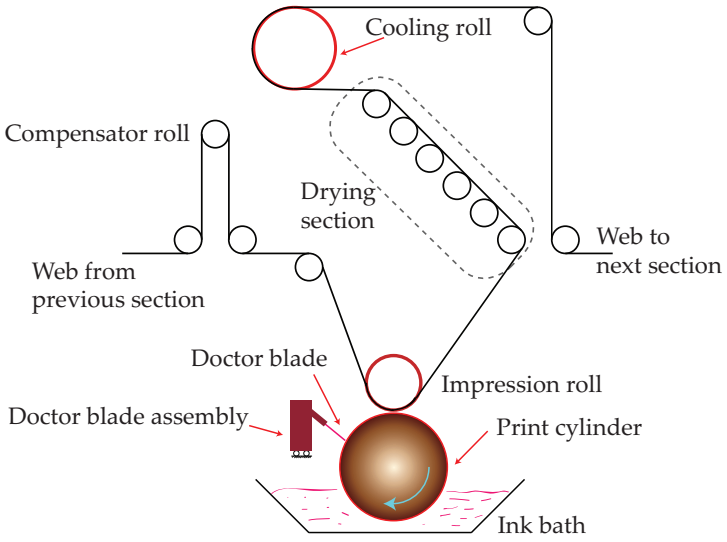

Figure 1.2: *Schematic of a rotogravure print unit.*

The quality of the print output depends on maintaining appropriate web transport conditions, such as regulation of web tension and web transport velocity [8]. Apart from maintaining web tension and web transport velocity – to minimized transport related web defects such as wrinkling, creasing, or even web breakage – printing requires spatial positioning of the web. When multiple print cylinders are used to print a complex multicolor pattern, it is critical to have successively printed patterns to align appropriately on top of each other; this in addition to maintaining web tension at desired value presents additional challenges in R2R printing.

The process of aligning successive print patterns on the web material to form a multicolor pattern is called registration or print registration. The position misalignment in the successive patterns may occur in either the machine direction (transport direction) or the cross machine direction (perpendicular to the transport direction and in the plane of the web) or both. Figure 1.3 shows an illustrative example of an improperly registered and a properly registered print image. The defect in print registration is quantified by a metric often termed as registration error; the focus of this work is primarily on studying the causes of machine direction registration error and its mitigation.

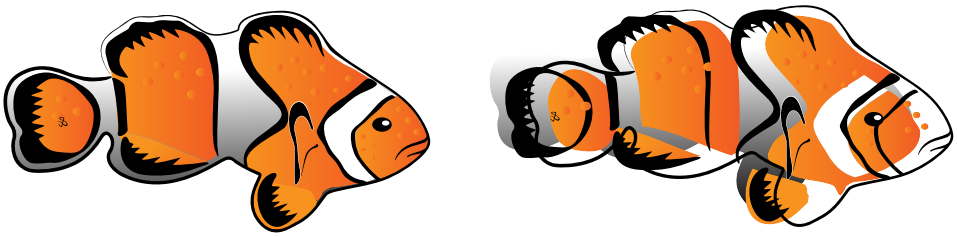

Figure 1.3: *An illustrative example showing a properly registered print pattern (left) and an improperly registered print pattern (right). Both machine direction and cross machine direction registration issues are shown in the illustration.*

The process of print registration can be explained using the illustrations in

Figure 1.4. Whenever a pattern is printed onto the web, along with the pattern a registration flag is also printed on the web near its edge. The next pattern, along with the registration flag, is printed at the subsequent print unit. If the successive prints are aligned, then the distance between the two registration flags is equal to a predetermined fixed distance. The registration error is the difference between the predetermined fixed distance and the actual distance measured between the two registration flags; an optical sensor is used to measure the distance between the registration flags.

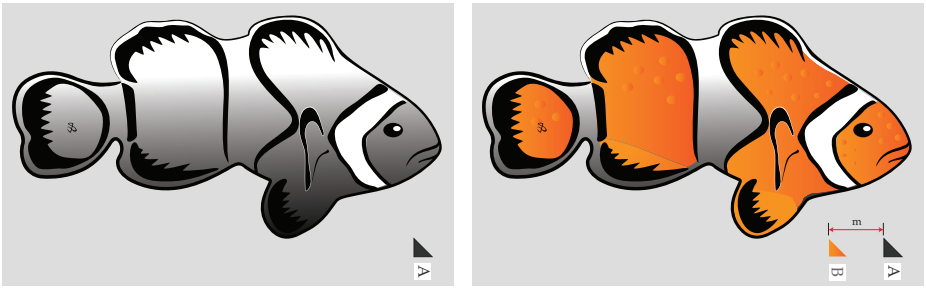

Figure 1.4: *Patterns are printed successively to form a multicolor image. Registration flags are printed along with the pattern on the web; the registration error sensor measures the distance (or time) between registration flags which can be used to determine the registration error.*

In order to maintain print quality, registration error is actively controlled within print units. Depending on the type of the printing press either the linear position of a compensator roller or the angular position of a print cylinder is controlled to minimize the registration error. Modeling, analysis and control of registration error in R2R printing presses are studied in this work.

The optical sensor does not directly measure the distance between the registration flags; rather the time passage between the occurrence of the registration flags is measured, and based on the web transport velocity the registration error is inferred.

1.3 Focus Application

A real-world example of a roll-to-roll printing application is considered in this work. Armstrong World Industries manufacture flooring materials in their Stillwater, Oklahoma plant which require printing of the flooring patterns on composite web materials. A large mechanically coupled rotogravure printing press is used by Armstrong to print on composite flooring materials. Figure 1.5 shows a schematic of the print line at Armstrong World Industries. The print line is one of the three web processing lines in Armstrong. The plant manufactures different types of flooring material from a base felt material; layers of composite materials are calendared, coated and deposited to form a composite web material in the base line; different types of flooring patterns are printed in the print line (or the press); further barrier coating and chemical curing is carried out to form the finished flooring product in the coating and fusion (C & F) line .

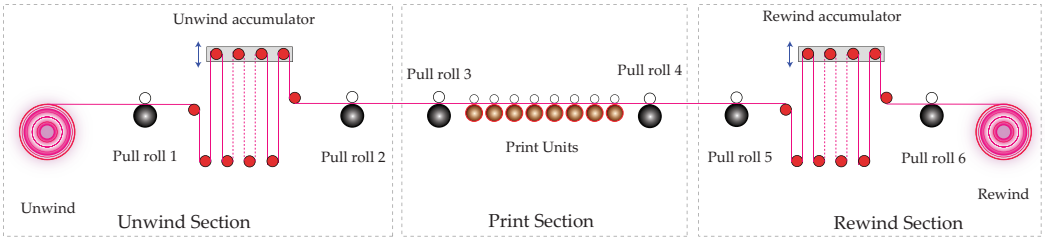

Figure 1.5: *Schematic of the Armstrong print line.*

The print line consists of a print section with eight rotogravure print units, an unwind section with an unwind accumulator and a rewind section with a rewind accumulator. Each print unit consists of a gravure print cylinder, an impression roller, a back-up roller, a cooling roller, a registration error compen-

The width of the web that is typically transported in the printing press is about 10 to 14 feet and the print section can thread at least 300 feet of web material.

sator roller, and many idle rollers that support the web during transport (see Figure 1.2). All eight print units in the print section are driven by a single print section drive motor. The print section motor shaft is connected to various print units through a mechanical transmission system. Accumulators in the printing line facilitate continuous and uninterrupted transport of the web through the print units during unwind and rewind material roll changes [9]. The transport velocity and web tension within various sections of the printing line are controlled using driven rollers called pull rolls. For example, as shown in Figure 1.5, pull roll 3 regulates web tension and web transport velocity of the material entering the print section, and pull roll 4 regulates the transport variables at the exit side of the print section.

Actual measurements from Armstrong print line, such as registration error, web tension and other web transport conditions, collected during production runs are used to corroborate the models developed in this work. In certain situations targeted experiments were conducted during production runs with slightly changed operating conditions to collect the required key process variable data, which was used to aid in the validation of the models developed and to test the various hypotheses presented in this dissertation.

1.4 Problems and Opportunities in Roll-to-roll Printing

With the demand to increase productivity and to minimize waste and costs, different materials with different mechanical and physical properties are transported within the same printing presses with higher speeds. For example, in the Armstrong plant different composite flooring materials with different thickness and mechanical properties are transported within the same printing press. But in

order to efficiently transport them with minimum material wastage it is necessary to clearly understand the behavior of the web within the printing press. Therefore, it is critical to develop good mathematical models which accurately describe and predict the process behavior and which can be used to design efficient model based control algorithms that provide higher print quality.

Often web machine manufacturers do not consider the effect of the web dynamics during the machine design process. Because of this, unwanted machine dynamics can significantly affect the web dynamics and may result in transport related defects. There is a need to understand how the machine dynamics influence the print registration process and how improvements can be made to minimize machine induced disturbances.

When multiple print cylinders are employed to print a complex pattern, control of the registration error in one print unit will affect the registration error in subsequent units because of strain transport, interaction between printing units is unavoidable; this is often not addressed in the literature. There is a need to understand how the interaction can be minimized and how different control mechanisms cause or minimize the interaction. There is also a need to evaluate whether a centralized control strategy or a decentralized control strategy would be efficient in minimizing print registration error.

Registration error in R2R printing can be controlled by employing different control mechanisms. One of the control mechanisms that dates back to the origins of R2R printing, which is also in substantial use in current machines, utilized a compensator roller that changes the span length between successive print units to control registration. With the advent of electronic line shafting technologies, the current trend is to control print registration by directly controlling the

angular position of the print cylinders. There are advantages and disadvantages with both methods; but a clear understanding of the effect of these control strategies on web transport through print units is currently lacking; this understanding will assist in the selection of a method as well as development of strategies to improve the method. A comparison of the effectiveness of these control mechanisms would greatly benefit the roll-to-roll manufacturing community.

1.4.1 Flexible Printed Electronics

Flexible printed electronics is touted to be a significant part of future of roll-to-roll printing industry. Several electronic devices, such as RFID tags (Radio Frequency IDentification), low-cost displays and lighting devices, polymer solar cells, sensors, etc., are already being manufactured commercially on a flexible substrate using roll-to-roll machines.

In recent years there has been a significant focus towards printing electronics on a flexible substrate using R2R printing methods since printing of functional materials on a substrate is cost effective compared to conventional photolithography techniques [10, 11, 12, 13, 14, 15, 16]. These studies have primarily dealt with the feasibility of printing electronic components such as thin metal lines, electrodes, capacitors, thin film transistors, etc., on a flexible substrate. The web handling aspects related to roll-to-roll printing of flexible electronics have not been adequately addressed; challenges related to design of web handling machines for roll-to-roll manufacture of flexible printed electronics are discussed in [17, 18]. The registration requirements for printing electronics on a flexible substrate are much higher, in the order of tens of microns, than conventional printing requirements, which is in the order of a few millimeters. Better understanding of the registration process and the substrate behavior as it is

transported in a printing press is necessary to realize roll-to-roll printing of electronics. It is envisioned that further understanding of the web handling and machine design aspects related to print registration would be of substantial benefit towards the development of R2R manufacturing technologies for flexible printed electronic devices.

1.5 Contributions

The contributions of this dissertation are focused towards better registration control in roll-to-roll printing presses. In order to achieve improved registration performance it is important to understand the print registration process. A new mathematical model for print registration is developed in this work. It is also important to study and understand the possible sources of disturbances within print units. A systematic study of machine induced disturbances that affect print registration and machine design recommendations that can minimize these disturbances are presented. Understanding and minimization of the propagation of disturbances within roll-to-roll processing machines will also enable improved registration performance. The interaction, or the disturbance propagation behavior, between tension zones is studied using a new interaction metric based on the Perron-Frobenius theory and a systematic pre-filter design procedure to minimize interaction is also presented in this work. The proposed new interaction metric is also used to analyze the interaction in printing presses with a compensator based registration control (CRC) strategy and a print cylinder angular position based registration control (PARC) strategy. Stability characteristics and registration performance of CRC and PARC are compare. The outline of each chapter and contributions are provided in the following:

Chapter 2: A new mathematical model for print registration is developed by considering the effect of web strain adjacent to the print cylinders, dynamics of the print section machine including the print cylinder, doctor-blade assembly and impression roller, and span length changes due to the motion of the compensator roller. The model includes governing equations for registration error and web strain in a print unit, print cylinder velocities, doctor blade position, and impression roller velocities. Interaction between machine and web dynamics is studied and its effect on registration error is included in the model. The developed model can be utilized for designing algorithms for control of print registration by using either CRC strategy or a PARC strategy. Based on the analysis of the model, mechanical design recommendations to minimize interaction between machine and web dynamics, in order to minimize registration error, are also discussed. Measured data from production runs on an industrial printing press are used to corroborate the model and compare it with the models available in the literature.

Chapter 3: Interaction in roll-to-roll systems is quantified by considering a new interaction metric which is based on the Perron-root of a nonnegative matrix. The Perron-root based interaction metric (PRIM) can be used to analyze any decentralized large-scale interconnected system, such as a roll-to-roll processing system. A systematic design procedure to minimize interaction is also presented based on the Perron-Frobenius theory. The PRIM also provides constraints on stability of decentralized large-scale interconnected systems. To demonstrate the usability of the theory to a practical application, a large R2R system is considered and a number of experiments

are conducted to evaluate the PRIM and the effectiveness of the dynamic pre-filters designed to minimize interaction.

Chapter 4: The compensator based registration control strategy and print cylinder angular position based registration control strategies are compared using PRIM to evaluate the disturbance propagation behavior within print units. Results and discussions are provided to compare the PRIM analysis and the time domain model simulations with CRC and PARC. The control of registration error with either strategy is complicated because of the presence of internal state delays in the print registration model. Frequency domain based stability analysis for delayed differential equations is employed to analyze the stability of the decentralized, memoryless, state feedback control algorithm developed for CRC. The control law for existing PARC algorithms in the literature require communication of state measurements between adjacent print units and knowledge of past state measurements to stabilize the system. The uniqueness of the developed CRC algorithm is its simple decentralized control structure with a memoryless state feedback control law. Model simulations are conducted to evaluate the performance of the CRC algorithm in terms of its disturbance attenuation performance.

Chapter 5: In this chapter concluding remarks and directions for future research are presented.

CHAPTER 2

Modeling Print Registration and Print Section Dynamics

In this chapter a first principles based approach is followed to model the print registration process. The model developed is corroborated based on actual measurements collected from production runs from Armstrong print line. Existing models in the literature are also compared with the developed model based on the actual production run data. The interaction between machine and web dynamics, specifically sources of machine induced disturbances are identified based on print section machine dynamics. The print section machine dynamics for the Armstrong print press with eight print units driven by a single mechanical line shaft are derived based on Euler-Lagrange equations. The effect of compliance in torque transmission in mechanical line shafts and the effect of doctor blade oscillations on print cylinder velocities and eventually on print registration are studied. Recommendations to minimize machine induced disturbances are also discussed in this chapter.

2.1 Governing Equation for Print Registration Error

There has not been much fundamental work reported in the literature on modeling of print registration other than the models given in [19] and [20]; further, there has been no experimental corrobration of the proposed models. In [21, 22] the modeling approach given in [19] and [20] is used for designing controllers to minimize registration error. A mathematical model for the print registration process in an offset printing press was developed in [19]. A governing equation for the registration error is obtained by taking into account the elongation (or strain) experienced by the web as it passes through two successive print units and the difference of the actual web strain and its nominal value for each print unit span is used in the governing equation. A similar model, but considering the actual strain in each print unit span, was developed in [20]. In these existing models it is assumed that the print cylinder angular positions are synchronized and that the print cylinders rotate at a constant velocity.

Consider the print unit shown in Figure 2.1 which consists of two successive print cylinders and the web between them; a print unit span is the web between two adjacent print cylinders. The web strains in the span upstream of print cylinder 1, in the print unit span and downstream of print cylinder 2 are denoted by ϵ_1, ϵ_2, and ϵ_3, respectively. The angular velocity of the print cylinders are ω_1 and ω_2 at the respective print cylinder. The control volume containing the web between the two print cylinders is shown in Figure 2.1. The web velocity entering the control volume is denoted by V_1 and the web velocity at the exit by V_2. Each printed pattern travels the web path length L within the control volume; the path length L is a function of the linear position x of the compensator roller. The path length L is equal to $l = 2\pi n r_1$ when the compensator roller is at its nominal po-

sition which is set as $x = 0$, where n is an integer and r_1 is the radius of print cylinder 1. The change in span length when $x \neq 0$ is represented by the quantity $\tilde{l} = L - l$.

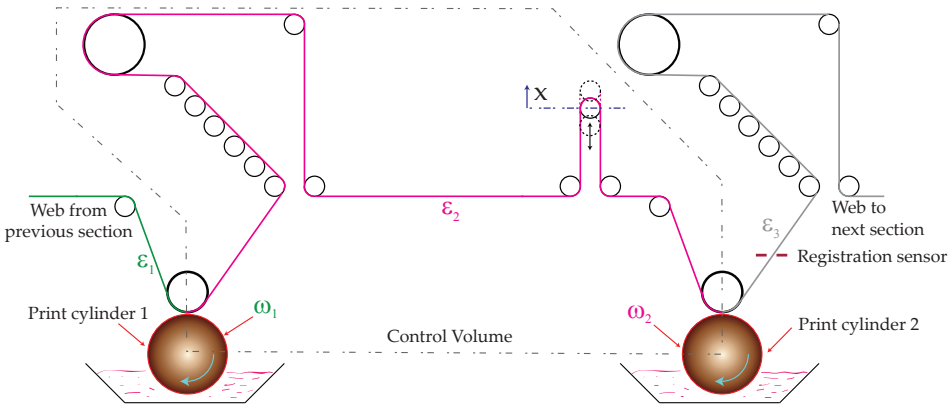

Figure 2.1: *A schematic showing the web between two successive print cylinders; some of the idle rollers are ignored.*

Consider an ideal state where the angular positions of the two print cylinders are the same at any instant and web strain in all spans to be the same. If the distance traveled by the pattern is an integer multiple of print cylinder 1 circumference, i.e., $L = l$, then the patterns will register correctly. But in practice there are no ideal machine components and it is seldom possible to maintain ideal operating conditions. The occurrence of the registration error is mainly due to three process conditions: strain variations, compensator roller linear velocity, and print cylinder velocity variations. It is assumed that each of these effects are independent and may be combined to obtain the governing equation for the registration error by considering that there is no slip between the web and the roller surface and web strain is uniform along the length of the print unit span.

2.1.1 Effect of Web Strain

As the web is transported through the print unit, web elongation due to strain changes results in the improper registration since the distance the printed image needs to travel within the control volume changes; with a positive strain the net distance a portion of print image needs to travel decreases whereas with a negative strain the distance increases. In order to clearly understand the effect consider the following assumptions:

- There is no slip between the web and the print cylinder, and the web and the impression roller.
- The angular positions of consecutive print cylinders are the same and the cylinders have the same radius, i.e., $\theta_1(t) = \theta_2(t)\ \forall t,\ r_1 = r_2$.
- The compensator roller is fixed at $x = 0$ so that $L = l$.
- The print cylinder velocity variations and strain variations are small and do not cause a change in time τ_1, where τ_1 is the time delay for a point on the web to travel from the upstream print cylinder to the downstream print cylinder.

Note that when the image is printed on the web at the upstream print cylinder, the web is in a stretched state with strain ϵ_1. Now as the printed image travels in the control volume additional elongation may be experienced and this elongation per unit length is given by $\overline{\epsilon}_{21} \triangleq \epsilon_2 - \epsilon_1$. Note that if both the upstream strain and the downstream strain are the same, then the same length of unstretched web passes both the print cylinders which results in no registration error; the registration error is a function of the relative stretched length or relative strain

$\overline{\epsilon}_{21}$. The registration error is neither a function of the absolute strain ϵ_2 as discussed in [20] nor it is a function of the difference between the absolute strain ϵ_2 and its nominal value as discussed in [19, 23].

Because of the relative elongation the net distance traveled by the web from the upstream to the downstream print cylinder in time τ_1 would increase or decrease based on the additional elongation; this length change affects registration and the registration error due to web strain is

$$e_r(t) = l - \int_{t-\tau_1}^{t} \frac{r_1 \omega_1(\tau)}{1+\overline{\epsilon}_{21}(\tau)} d\tau. \tag{2.1}$$

2.1.2 Effect of Compensator Roller Motion

The direct effect of the compensator roller motion on registration error is due change in web path length because of its linear motion. Indirectly, its motion may also cause strain variations which is implicitly accounted for in equation (2.1). As the compensator moves, the span length that the web needs to travel before reaching the next print cylinder increases or decreases. The additional distance traveled by the printed portion of web due to the motion of the compensator can be obtained from the net span length change during that period when the printed web travels from the upstream print cylinder to the downstream print cylinder. Note that the distance traveled by the web once it is past the compensator will always be the same. Hence when a printed portion of the web moves past the compensator roller, the compensator motion from that point forward in time would not change the web span length for that portion of the web. Let τ_2 be the time taken by a point on the web from the upstream print cylinder to reach the span downstream of the compensator roller; $\tau_1 > \tau_2$. And if it is assumed that the compensator motion does not cause a change in time delays τ_1 and τ_2, the

governing equation for the registration error due to web strain and compensator motion is

$$e_r(t) = l + \int_{t-\tau_1}^{t-\tau_2} \dot{\bar{l}}(\tau) d\tau - \int_{t-\tau_1}^{t} \frac{r_1 \omega_1(\tau)}{1+\bar{\epsilon}_{21}(\tau)} d\tau. \tag{2.2}$$

2.1.3 Effect of Print Cylinder Angular Position

Velocity variations between the print cylinders will result in the angular position misalignment between the two print cylinders which will result in the registration error. It is imperative that the angular position of the print cylinders are aligned at the start of the printing process and with mechanical line shafts they are aligned using a key mechanism. Under ideal conditions, if the angular position and angular velocity of the two print cylinders are the same, then a registration mark on the web from the upstream print cylinder at time $t-\tau_1$ will overlap exactly with a registration mark on the downstream print cylinder at time t provided that the effect of strain variations and span length variations are neglected, that is, when $\theta_1(t-\tau_1) = \theta_2(t)$. But if the print cylinder velocities are not the same, then the registration error would be a function of the angular position difference between the two print cylinders and can be given by

$$e_{r2}(t) = r_1\theta_1(t-\tau_1) - r_2\theta_2(t) \tag{2.3}$$

Note that, when the effect of strain is considered then the position error due to velocity variations of upstream print cylinder has to be compensated for the strain changes since that patch of the web would be elongated as it reaches the downstream print cylinder.

Hence a overall registration error equation that includes the effect of print cylinder velocity variations, strain variations and compensator roller motion is

$$e_r(t) = l - \int_{t-\tau_1}^{t} \frac{r_1 \omega_1(\tau)}{1+\bar{\epsilon}_{21}(\tau)} d\tau - \left[r_2\theta_2(t) - \frac{r_1\theta_1(t-\tau_1)}{1+\bar{\epsilon}_{21}(t)} \right] + \int_{t-\tau_1}^{t-\tau_2} \dot{\bar{l}}(\tau) d\tau. \tag{2.4}$$

The governing equation for the registration error can be obtained from equation (2.4) by taking the time derivative:

$$\dot{e}_r(t) = r_1\left[\frac{1}{1+\overline{\epsilon}_{21}(t)}\left[\omega_1(t-\tau_1)-\omega_1(t)\right]+\frac{\omega_1(t-\tau_1)}{1+\overline{\epsilon}_{21}(t-\tau_1)}\right]-r_2\omega_2(t) \\ -\frac{r_1\theta_1(t-\tau_1)\dot{\overline{\epsilon}}_{21}(t)}{\left[1+\overline{\epsilon}_{21}(t)\right]^2}+\left(\dot{\overline{l}}(t-\tau_2)-\dot{\overline{l}}(t-\tau_1)\right). \tag{2.5}$$

This equation (2.5) is applicable to any type of rotary printing presses. Note that in presses with mechanical line shafts, independent control of print cylinder velocities is not possible and hence the compensator roller is used as the active control device to minimize the registration error. But in the case of printing presses with electronic line shafts, independent control of print cylinder velocities facilitate direct control of the registration error without the need for the compensator roller. Hence in printing presses with electronic line shafts the registration error governing equation can be obtained from equation (2.5) by neglecting the span length variation terms $\dot{\overline{l}}(t-\tau_2)$ and $\dot{\overline{l}}(t-\tau_1)$.

2.2 Print Registration Experiments and Model Simulations

The actual production run measurements from Armstrong printing press is used to corroborate the developed model. Each print unit contains a roller mounted on load cells to measure web tension. Registration error data is also measured immediately downstream of each print cylinder by a registration sensor. Measurement of web tension in each print unit is used to compute web strain in each print unit by using a constitutive relation between web strain and tension under the assumption that the material is elastic; this assumption is reasonable as the composite webs are transported with reference strain corresponding to the low strain region of the stress-strain curve of the material. Different types of materials and operating conditions were used during many production runs: webs

that are 12 – 14 feet wide, modulus of elasticity ranging from 50,000 – 75,000 psi, transport speed in the range of 150 – 180 feet per minute, and web tension in the range of 200 – 500 pounds.

Figure 2.2 shows a representative sample of tension and registration error data collected during a production run. The top plot shows the relative tension at print cylinder 7 which is the difference between web tension in the spans upstream and downstream of print cylinder 6. The bottom plot shows the registration error measured immediately downstream of print cylinder 7. From the figure it is observed that the relative tension and registration error are correlated. To clearly see the correlation between relative tension and registration error the Fast Fourier Transform (FFT) of the time domain data is shown in Figure 2.3. Several distinct peaks in the tension and registration error data are observed; the first peak is observed at 0.0315 Hz and the remaining peaks are higher-order harmonics. Data from a number of production runs support the fact that relative strain between two adjacent print unit spans has a significant effect on registration error in each print unit.

Simulations are conducted using the registration error equation (2.5) with the measured tension data as input, that is, strain is computed using measured tension data and used as input in equation (2.5). The registration error data from these simulations are compared with the actual registration error data. A constant web velocity is assumed at all the print cylinders and the effect of compensator motion and the effect of print cylinder velocity variations are neglected in the model simulations; the web is assumed to be elastic and web strain based on measured web tension, with one second sampling time, is used in the model to obtain registration error. Figures 2.4 – 2.5 show a representative sample of the

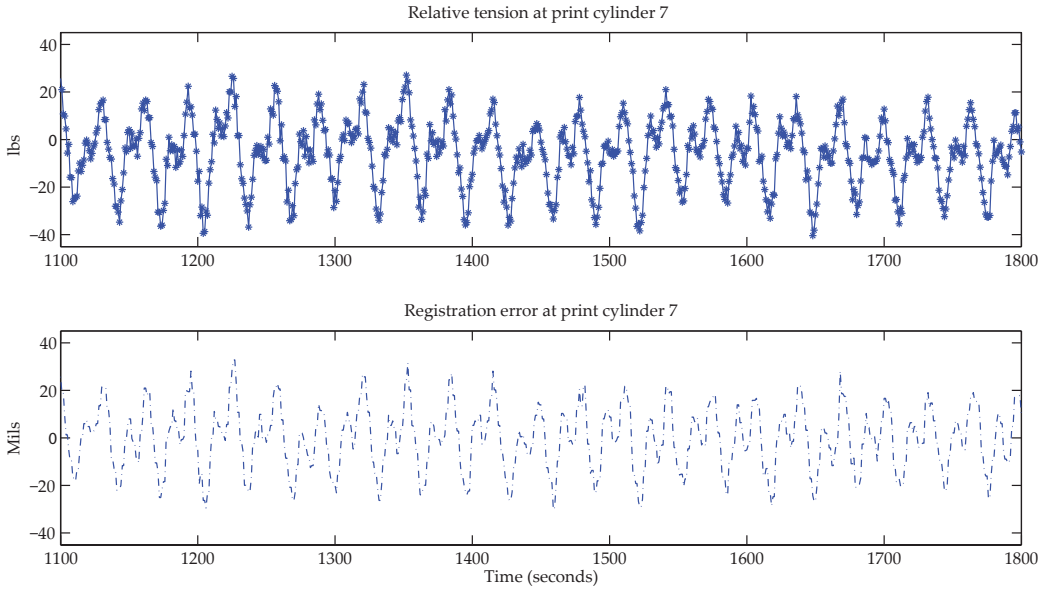

Figure 2.2: *Measured web tension and registration error in print cylinder 7 from a production run.*

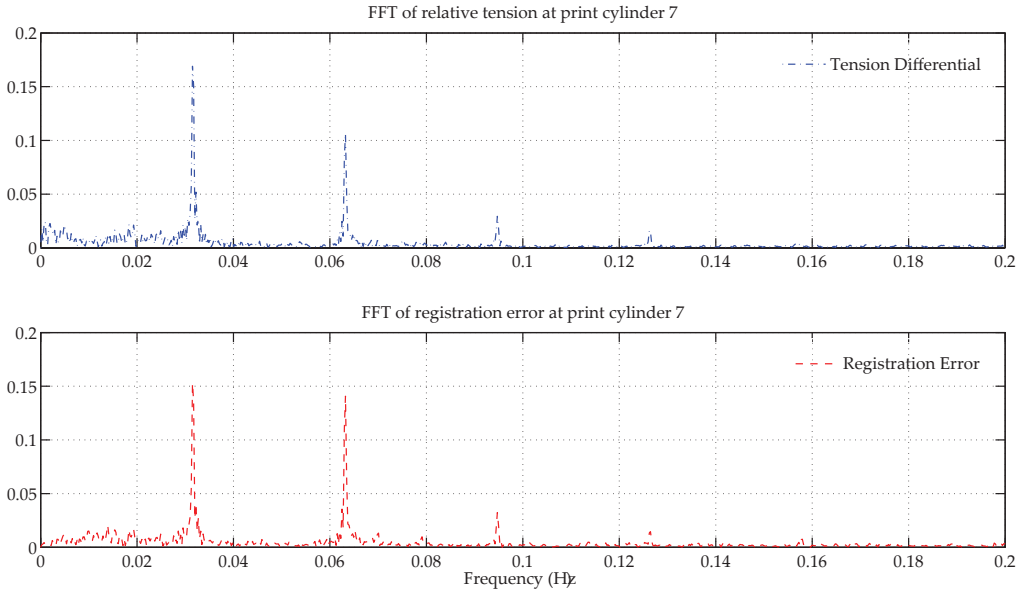

Figure 2.3: *FFT of the relative tension and registration error data in print cylinder 7 from a production run.*

data comparing the model output and the actual registration error data collected at print units 7 and 8. From these plots it is evident that without considering the effect of print cylinder velocity variations and span length changes due to compensator motion, the proposed model output data correlates well with the actual registration error data. It is expected that with additional measurements, such as the print cylinder velocities, compensator rate, one may obtain better correlation between the output of the full model and the measured registration error from experiments. In this industrial printing press, print cylinder velocity measurements are not available because of the inability to instrument in the explosion proof environment around the print cylinders and the compensator roller position measurements are also not available from the original equipment manufacturer.

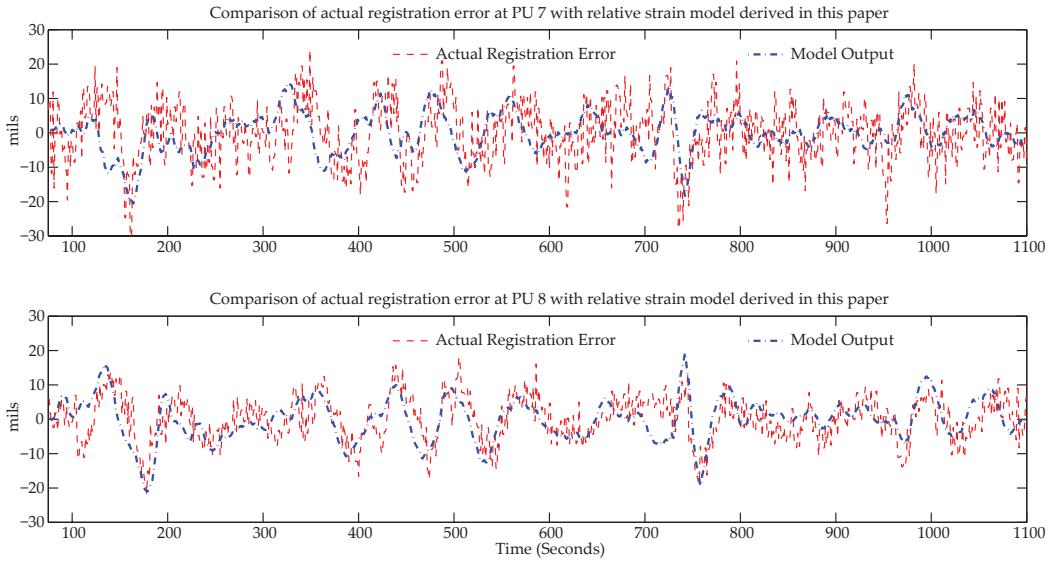

Figure 2.4: *Comparison of model output data and actual data (Run 1)*

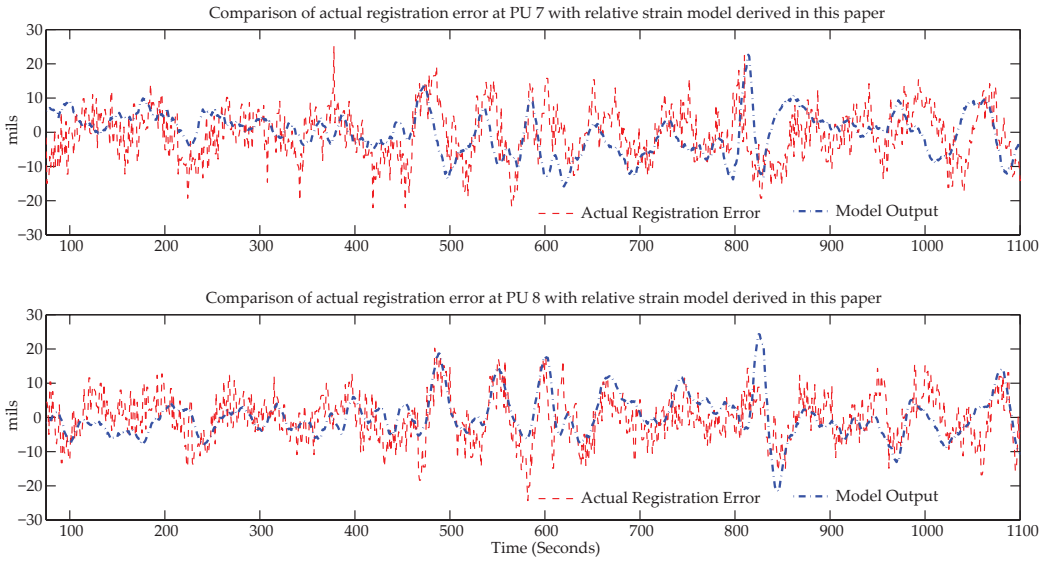

Figure 2.5: *Comparison of model output data and actual data (Run 2)*

2.2.1 Comparison with Other Models in the Literature

To further illustrate the accuracy of the developed model, it is compared with available models in the literature. By considering a constant web speed at print cylinders and neglecting compensator motion, the registration error governing equation (2.5) reduces to

$$-\dot{e}_r(t) = \frac{v_s^*}{1+\overline{\epsilon}_{21}(t)} - \frac{v_s^*}{1+\overline{\epsilon}_{21}(t-\tau_1)} \tag{2.6}$$

where v_s^* is the steady-state web velocity at the print cylinders. The following equation for the registration error is presented in [19, 23]

$$\dot{e}_r(t) = \frac{v_s^*}{1+\tilde{\epsilon}_2(t)} - \frac{v_s^*}{1+\tilde{\epsilon}_1(t-\tau_1)} \tag{2.7}$$

where $\tilde{\epsilon}_i$ is the strain variation above the nominal value. And the following registration error equation is presented in [20]:

$$\dot{e}_r(t) = \frac{v_s^*}{1+\epsilon_2(t)} - \frac{v_s^*}{1+\epsilon_1(t-\tau_1)}. \tag{2.8}$$

The model proposed in this paper uses relative strain, whereas absolute strain is used in [20] and strain over nominal value is used in [19, 23]. Data from production runs are used to compare these three models. Tension measurements are used to obtain the registration error based on the models in equations (2.6) – (2.8). Figures 2.6–2.10 show web strain in the three print units during production runs. From the data it is evident that the web strains between print units are not the same. In practice a draw is deliberately introduced between successive print units and hence the mean web strain in each span will increase progressively. Therefore, any model based on absolute strain is not accurate because the right-hand-side in the registration error equation (input to the registration error integrator), (2.8), will have a non-zero mean value which will result in the unboundedness of the registration error. Figures 2.8–2.12 show the inputs to the registration error integrator for the three models in print units 7 and 8 during a particular production run, Run 2. The top and bottom plots show the integrator input data corresponding to registration error in print unit 6 and print unit 7, respectively. From these plot it is evident that the absolute strain model presented in [20] does not provide a good representation of the actual system.

In order to compare the proposed model with the one presented in [23], it is assumed that the mean strain in print unit is the nominal web strain within the print unit. It is noted that since web tension is seldom maintained within print units, it is unlikely that the mean web strain in a print unit will be same as the nominal web strain in many practical situations. From Figures 2.9 and 2.8 it may appear as if the input to the integrator signal for the model in [23] to have zero-mean but that is not the case. In many industrial situations there may be a drift in tension value within a span due to strain transport especially when tension

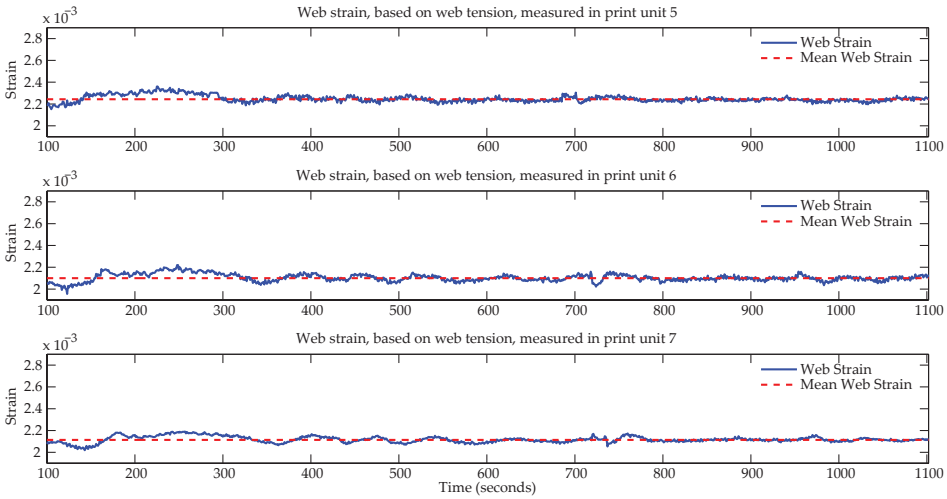

Figure 2.6: *Web strain from prints units 5 – 7 during a production run (Run 1). Web strain is determined from web tension measurements based on the assumption that the web material is elastic.*

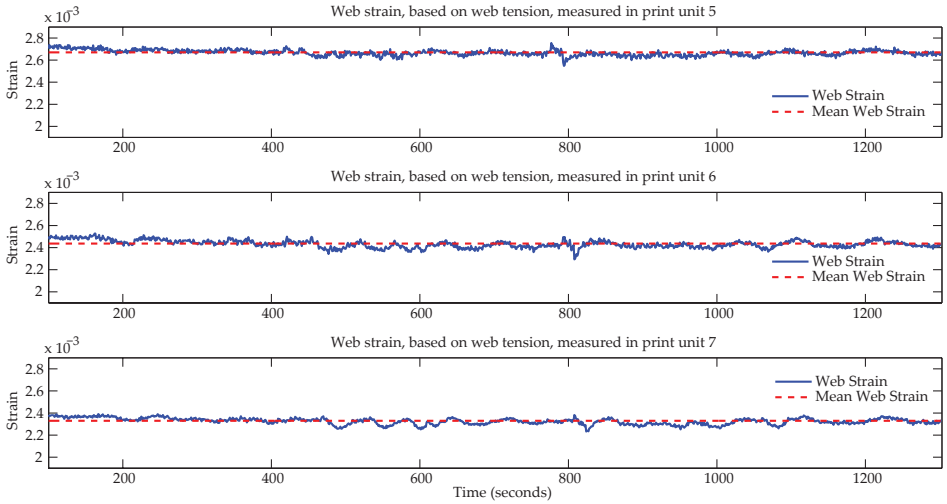

Figure 2.7: *Web strain from prints units 5 – 7 during a production run (Run 2).*

is not actively controlled. Hence, introduction of the difference between actual strain and its nominal value into the governing equation for registration error is not appropriate as the nominal value of the strain is not well defined. To highlight this observation a representative sample of production runs during which the mean strain within a print unit span changed during the runs is shown in

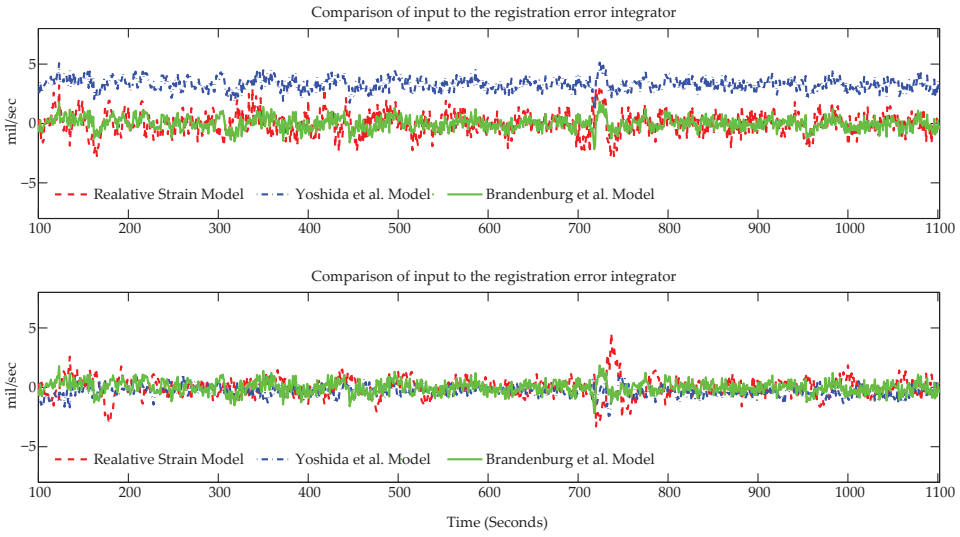

Figure 2.8: *Comparison of input to the registration error integrator in the three models; data corresponds to production Run 1.*

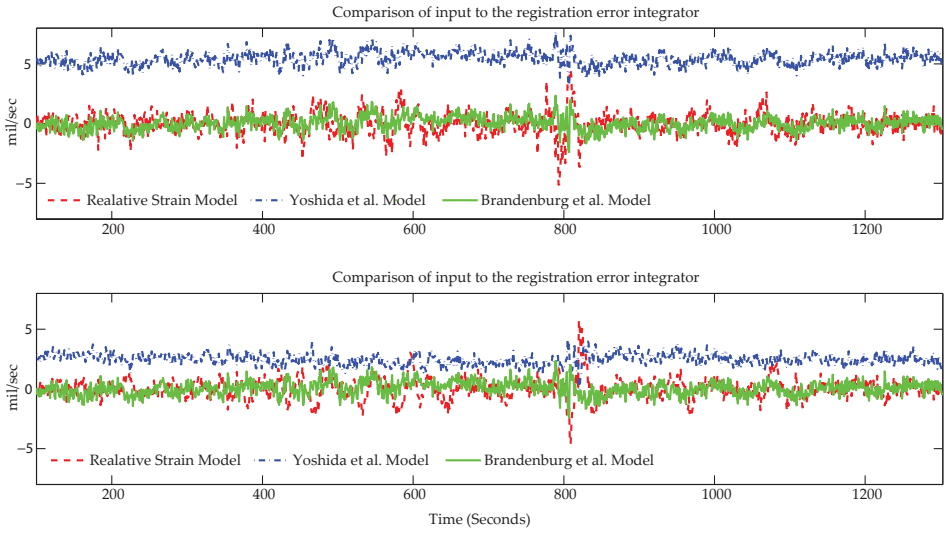

Figure 2.9: *Comparison of input to the registration error integrator in the three models; data corresponds to production Run 2.*

Figures. 2.10 and 2.11; the corresponding inputs to the registration error integrator is shown in Figures 2.12 and 2.13. From these figures it is evident that the models presented in [23, 20] do not sufficiently capture the web transport behavior when web strains within the print units are not the same and when a drift

in web strain is observed. The relative strain model presented in this paper captures the dynamic behavior of the print registration process better than the two models compared here. The relative strain registration model output for the two production runs with strain drift is shown in Figures 2.14 and 2.15. From these figures it is evident that the proposed model captures the overall print registration dynamic behavior although a constant bias in the model output is observed in the data. The span length change due to compensator motion that is neglected in the registration error governing equation (2.6) may be the cause for this bias.

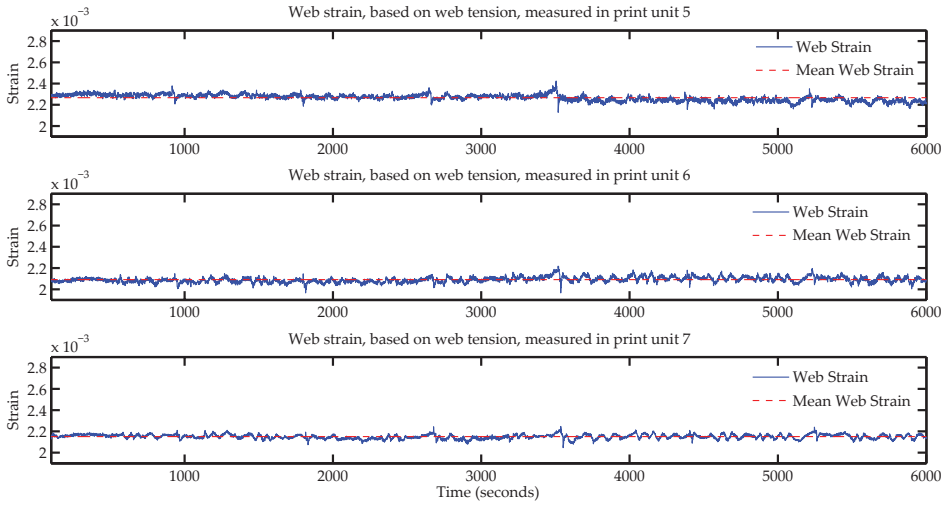

Figure 2.10: *Web strain from prints units 5 – 7 during a production run (Run 3). A slow drift in the web strain can be observed in print unit 5 during this run.*

Analysis of the print registration model and data obtained from actual production runs clearly show the influence of relative strain on the registration error. In practice, strain is seldom actively controlled within the print units. In printing presses with mechanical line shafts, independent control of print cylinder velocities is not possible; hence compensator rollers are used to compensate for registration error. But the motion of the compensator roller causes strain vari-

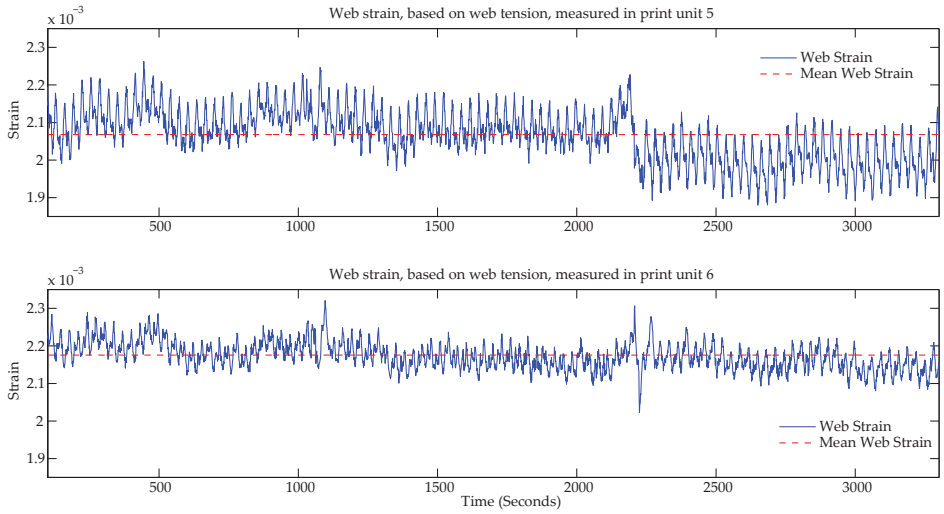

Figure 2.11: *Web strain from prints units 5 – 7 during a production run. A sudden shift in the web strain can be observed in print unit 5 during this run.*

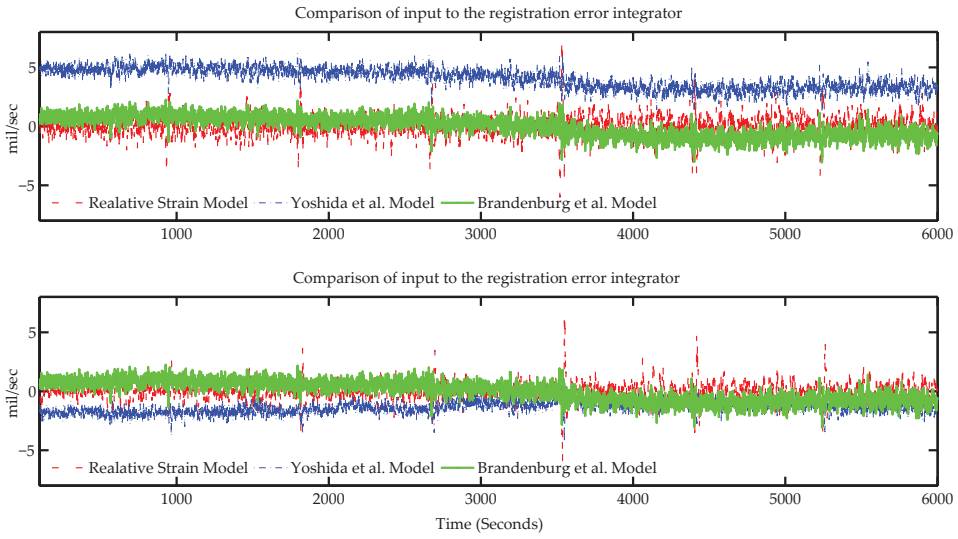

Figure 2.12: *Comparison of input to the registration error integrator in the three models; data corresponds to production Run 3.*

ations in the print unit. Similarly, direct control of each print cylinder angular position also results in strain variations within the print unit. With strain transport the tension disturbances occurring in spans preceding the print units are likely to cause strain variations in succeeding print units. Machine induced dis-

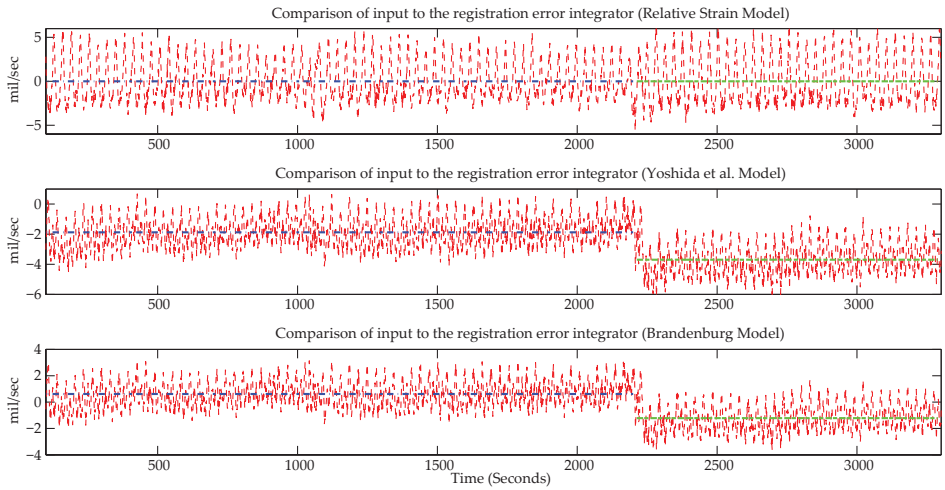

Figure 2.13: *Comparison of input to the registration error integrator in the three models; data corresponds to production run with sudden shift in web strain.*

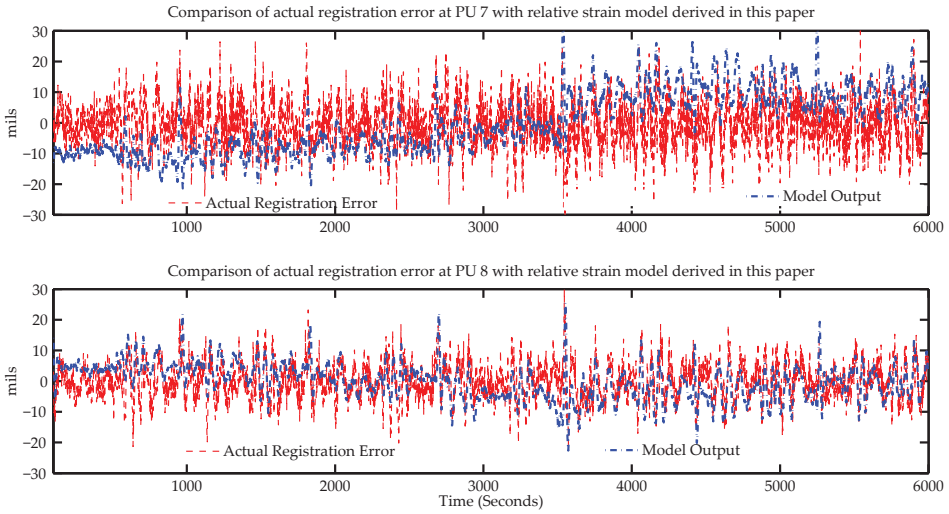

Figure 2.14: *Comparison of model output data and actual data (Run 3)*

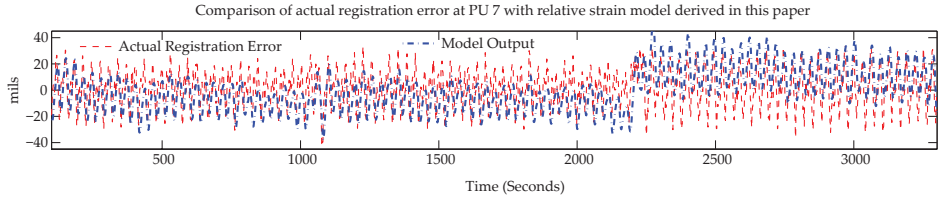

Figure 2.15: *Comparison of model output data and actual data (Run 2)*

turbances in the print units, such as eccentric or out-of-round rollers, may also cause strain variations that can affect registration error. Hence, control strategies have be designed such that both strain variations and registration error are minimized simultaneously. In the following section, a governing equation for web strain in a print unit with a compensator roller is presented to understand how the web strain dynamics is affected by compensator motion and print cylinder velocity variations.

2.3 Governing Equation for Web Strain

The compensator roller is a control device used in mechanical line shafted print units to control registration error, see Figure 2.1. The compensator roller is positioned linearly, using parallel ball screw mechanisms, to adjust the length of the span between the two print cylinders. The motion of the compensator roller not only results in a span length change between the two print cylinders but also affects web strain within the span.

Following the assumptions and the procedure outlined in [24] and without the small strain assumption, the governing equation for strain due to compensator motion and print cylinder velocities can derived as follows. From the law of conservation of mass, the rate of change of mass in the control volume encompassing the span is equal to the difference in mass flow rate entering the control volume and mass flow rate exiting the volume; it can be written as

$$\frac{dm}{dt} = \frac{d}{dt}\left[\int_{y_1}^{y_2} \rho(y,t)A(y,t)dy\right] = \rho(y_1,t)A(y_1,t)V_1(t) - \rho(y_2,t)A(y_2,t)V_2(t) \tag{2.9}$$

where dm/dt is the rate of change of mass in the control volume, $\rho(y,t)$ is the density of the web in the control volume, $A(y,t)$ is the cross sectional area of the

web, $\rho(y_1,t),\rho(y_2,t)$ are the density of the web at the entry and exit of the control volume, $A(y_1,t),A(y_2,t)$ are the cross sectional area of the web at the entry and exit of the control volume, $V_1(t),V_2(t)$ are the web velocities at the entry and exit of the control volume and y_1,y_2 are the entry and exit position of the web in machine direction along the span.

To further simplify the derivation of the governing equation for tension, it is assumed that the density and modulus of elasticity of the unstretched web are constant over the cross sectional area and the unstretched web cross sectional area is assumed constant along its length (machine direction). Consider an unstretched web of infinitesimal length dy_u with cross sectional area A_u and density ρ_u. As this web is stretched the density changes to ρ, the cross sectional area changes to A and the length to dy. Since the mass of the web is constant we have

$$m=\rho_u A_u dy_u=\rho A dy=\rho A(1+\epsilon_y)dy_u \tag{2.10}$$

where ϵ_y is the strain in machine direction. From the above equation we get

$$\rho A=\frac{\rho_u A_u}{1+\epsilon_y}. \tag{2.11}$$

Substituting the above relationship in equation (2.9) we get

$$\frac{d}{dt}\left[\int_{y_1}^{y_2}\frac{\rho_u(y,t)A_u(y,t)}{1+\epsilon_y(y,t)}dy\right]=\frac{\rho_u(y_1,t)A_u(y_1,t)}{1+\epsilon_y(y_1,t)}V_1(t)-\frac{\rho_u(y_2,t)A_u(y_2,t)}{1+\epsilon_y(y_2,t)}V_2(t). \tag{2.12}$$

From the assumption that the web density, modulus and cross sectional area are constant in the unstretched state, and that the strain is uniform along the length, we get

$$\frac{d}{dt}\left[\int_{y_1}^{y_2}\frac{1}{1+\epsilon_2(t)}dy\right]=\frac{V_1(t)}{1+\epsilon_1(t)}-\frac{V_2(t)}{1+\epsilon_2(t)}. \tag{2.13}$$

Note that if the compensator is fixed at a position such that $\tilde{l}=0$ then the limits of integration are constant. But since the compensator is free to move up and

down, one of the limits of the integration would be a function of time. With this we get

$$\frac{d}{dt}\left[\int_{y_1}^{y_2(t)} \frac{1}{1+\epsilon_2(t)} dy\right] = \frac{V_1(t)}{1+\epsilon_1(t)} - \frac{V_2(t)}{1+\epsilon_2(t)}. \tag{2.14}$$

In order to differentiate an integral of a function with variable limits the following Liebniz integral rule is used.

$$\frac{d}{dt}\int_{y_1(t)}^{y_2(t)} f(x,t)dx = \frac{d}{dt}y_2(t)f(y_2(t),x) - \frac{d}{dt}y_1(t)f(y_1(t),x) + \int_{y_1(t)}^{y_2(t)} \frac{\partial}{\partial t}f(x,t)dx \tag{2.15}$$

Note that the $y_2(t)$ can be written as $y_2(t) = \overline{y}_2 + \tilde{l}(t)$ where $\overline{y}_2$ is a constant and hence $\dot{y}_2(t) = \dot{\tilde{l}}(t)$. Application of Liebniz integral rule to equation (2.14) gives

$$\frac{\dot{\tilde{l}}(t)}{1+\epsilon_2(t)} - \frac{\dot{\epsilon}_2(t)(l+\tilde{l}(t))}{(1+\epsilon_2(t))^2} = \frac{V_1(t)}{1+\epsilon_1(t)} - \frac{V_2(t)}{1+\epsilon_2(t)} \tag{2.16}$$

which can be simplified to

$$\dot{\epsilon}_2(t) = \frac{1+\epsilon_2(t)}{l+\tilde{l}(t)}\left[V_2(t) + \dot{\tilde{l}}(t) - V_1(t)\frac{1+\epsilon_2(t)}{1+\epsilon_1(t)}\right]. \tag{2.17}$$

For print units with electronic line shafts, $\dot{\tilde{l}}(t)$ and $\tilde{l}(t)$ in Equation (2.17) will be zero, and therefore, web strain will be influenced only by the two print cylinder velocities.

Since strain is not a measurable quantity, the longitudinal web dynamics is represented in terms of measurable tensile force. To obtain the governing equation for web tension using the equation for strain, one must choose a constitutive material relation that relates web strain and web tension. Assuming the web material to be elastic, the following constitutive relation cab be used.

$$T(t) = EA\epsilon(t) \tag{2.18}$$

where E is the modulus of elasticity of the web and $T(t)$ is the tension in the web span. Hence, the governing equation for tension in the print unit span is given

by

$$\dot{T}_2(t) = \frac{EA + T_2(t)}{l + \tilde{l}(t)} \left[\left(V_2(t) + \dot{\tilde{l}}(t) \right) - V_1(t) \frac{EA + T_2(t)}{EA + T_1(t)} \right]. \tag{2.19}$$

It is evident that the compensator roller linear velocity and position affect web strain in the print unit span. In order to regulate web strain within a print unit, independent control of web velocity at the upstream and downstream print cylinders is necessary; and since the print cylinders are not controlled independently, movement of the compensator roller to minimize registration error would result in web strain variations in the span. For the rotogravure printing press considered in this work, neither the print cylinder velocities nor the strain is actively controlled. It is well known that, even with active draw control, strain within spans can be seldom maintained at its nominal value. The use of a single print section motor to drive all the print units, as is done in mechanical line shafting, worsens the problem even further. Small variations in print cylinder velocities can significantly affect strain, and in turn the registration error. The compliance in the mechanical line shafts and other transmission dynamics can cause print cylinder velocity variations. In the following section a dynamic model for the print section mechanical transmission and print cylinders is developed. The interaction between machine and web dynamics is also considered. Based on the developed model, design recommendations are provided to minimize print cylinder velocity variations and strain variations within the print units.

2.4 Print Section Velocity Dynamics

The print section in the Armstrong printing press contains eight identical print units. For simplicity, the speed and angular synchronization of all the print cylinders are maintained by using a mechanical line shaft that connects all the print

cylinders to a single print section motor; each print unit is equipped with a gear box that transmits power from the line shaft to the print cylinder. To better understand the configuration and the dynamical behavior, the print section can be represented as an equivalent system having eight inertial disks connected to a single shaft as shown in Figure 2.16. The print cylinders are driven rollers that facilitate web transport within the print section but the speed of each print cylinder cannot be controlled independently because of the mechanical coupling to a single motor.

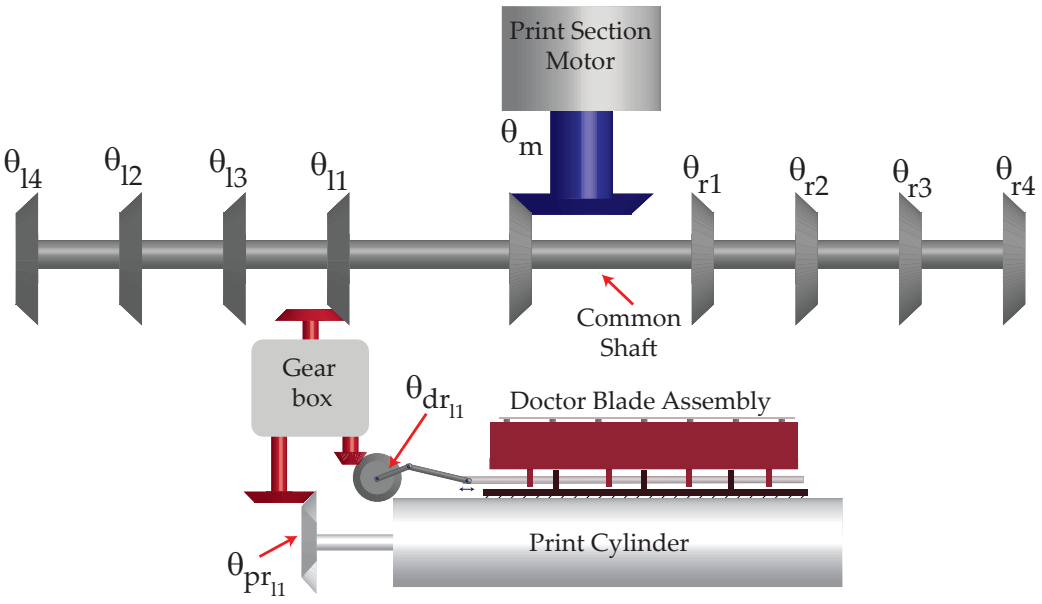

Figure 2.16: *A schematic showing the print section mechanical transmission with angles used in this work. The print section motor drives the common shaft which in turn transmits power to print unit gear boxes. The print cylinder and doctor blade assembly in each print unit is driven by the torque transmitted through the gear box.*

Apart from driving the print cylinder, the power transmitted through the

The print cylinder can be engaged and disengaged as per the printing requirements by using a clutch mechanism.

gear box also drives a device called the doctor blade which is used to wipe excess ink off the print cylinder. The doctor blade is mounted on a blade holder which pivots on an assembly frame. Figures 2.17 and 2.18 show a schematic of the doctor blade assembly. Pneumatic cylinders, housed on the doctor blade assembly frame, are used to apply pressure on the doctor blade holder such that adequate pressure is applied at the contact between the doctor blade and the print cylinder surface to wipe off excess ink.

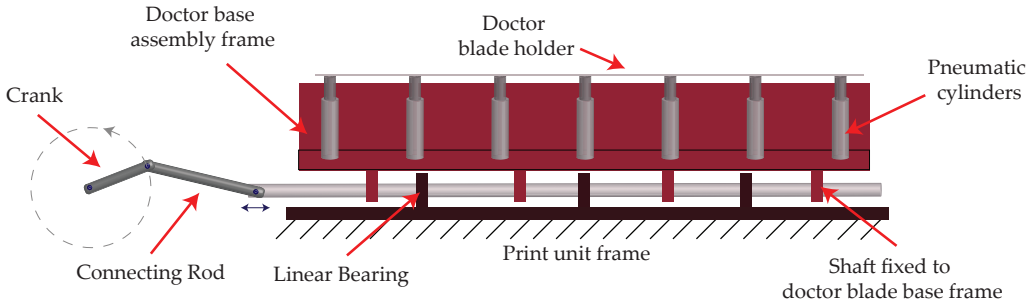

Figure 2.17: *Doctor Blade Assembly*

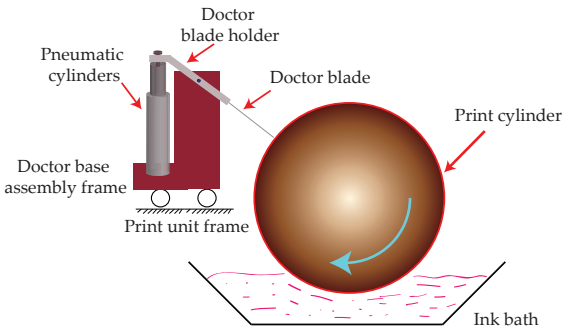

Figure 2.18: *A side view of the doctor blade assembly and the print cylinder.*

In order to produce even wear on the doctor blade, the doctor blade is made to slide back and forth on the print cylinder as it wipes the ink off. To facilitate the rocking motion the entire doctor blade assembly is moved back and

forth. A linear bearing facilitates the sliding motion of the doctor blade assembly and a crank mechanism as shown in Figure 2.17 provides the power for the motion. Whenever the print cylinder is engaged by the clutch mechanism, the doctor blade assembly oscillates; but the doctor blade makes contact with the print cylinder only when the pneumatic cylinders are engaged. The frequency of oscillation of the doctor blade assembly is based on the gearing ratio and is usually fixed; the stroke length may be varied based on the crank radius. Since the same gear box drives the print cylinder and the doctor blade assembly, the motion of the doctor blade assembly will affect the print cylinder velocity dynamics due to mechanical compliance.

Since all the print units are mechanically coupled, loading in one print unit will be reflected back to the print motor and will eventually affect all the print units. Note that the print cylinder velocity dynamics is affected by the compliance in the transmission, the doctor blade assembly dynamics, and web tension in adjacent spans. Even if all the print cylinders rotate with a constant surface velocity, strain transport and compensator roller motion would result in web tension variations in the print units. Moreover, uncontrolled tension variations within the print units may result in web slippage over the print cylinder which may further degrade the print quality.

2.4.1 Model with Rigid Transmission Elements

A model assuming rigid transmission elements is considered in order to see the effect of print unit loading on the print section motor. Let θ_m and ω_m be the angular position and angular velocity of the print section motor. Let θ_{pr_i} and ω_{pr_i} be the angular position and angular velocity of the i^{th} print cylinder. Let the transmission ratio (through the drive shaft and gear box) between print sec-

tion motor and the i^{th} print cylinder be n_{pr_i} so that $\theta_{pr_i} = \theta_m/n_{pr_i}$ and $\omega_{pr_i} = \omega_m/n_{pr_i}$. Let the transmission ratio between the crank, that drives the doctor blade of the i^{th} print cylinder, and the print section motor be n_{dr_i}; then the angular position of the crank with respect to the print section motor can be given by $\theta_{dr_i} = (\theta_m/n_{dr_i}) + \phi_{dr_i}$ where, θ_{dr_i} is the angular position of the crank and ϕ_{dr_i} the phase difference. Let r_i be the radius of the i^{th} print cylinder crank and l_i be the length of the connecting rod.

Let x_{dr_i} denote the position of the i^{th} doctor blade assembly position from the center of the doctor blade crank. The position of the doctor blade assembly as a function of the doctor blade crank angle can be obtained as

$$x_{dr_i} = r_i \cos\theta_{dr_i} + \sqrt{l_i^2 - r_i^2 \sin^2\theta_{dr_i}} \tag{2.20}$$

Since the doctor blade assembly is powered by the motion of the rotary crank, the equation for the linear oscillatory velocity of the doctor blade assembly can be derived as

$$\dot{x}_{dr_i} = \frac{dx_{dr_i}}{dt} = \frac{dx_{dr_i}}{d\theta_{dr_i}}\frac{d\theta_{dr_i}}{dt} = -\left[r_i \sin\theta_{dr_i} + \frac{r_i^2 \sin\theta_{dr_i}\cos\theta_{dr_i}}{\sqrt{l_i^2 - r_i^2\sin^2\theta_{dr_i}}}\right]\omega_{dr_i}$$

The linear velocity of doctor blade assembly in terms of print motor coordinates can be represented as

$$\frac{dx_{dr_i}}{dt} = -\frac{\omega_m}{n_{dr_i}}\left[r_i \sin\left(\frac{\theta_m}{n_{dr_i}} + \phi_{dr_i}\right) + \frac{r_i^2 \sin\left(\frac{\theta_m}{n_{dr_i}} + \phi_{dr_i}\right)\cos\left(\frac{\theta_m}{n_{dr_i}} + \phi_{dr_i}\right)}{\sqrt{l_i^2 - r_i^2\sin^2\left(\frac{\theta_m}{n_{dr_i}} + \phi_{dr_i}\right)}}\right] \tag{2.21}$$

To determine the dynamics using Euler-Lagrange equation of motion we need to determine the kinetic and potential energy of the system in terms of a set of suitable coordinates; in this case print section motor angular velocity ω_m and angular position θ_m are used. Assuming all the transmission elements are rigid

and gravity does not contribute to the dynamics, we can neglect any potential energy in the system. The total kinetic energy is the sum of kinetic energies of different rotating and translating masses and is given by

$$T = T_m + \sum_{i=1}^{8} T_{pr_i} + \sum_{i=1}^{8} T_{dr_i} \tag{2.22}$$

where T_m is the kinetic energy due to the print section motor, T_{pr_i} kinetic energy due to print cylinders and T_{dr_i} is the kinetic energy due to doctor blade assembly motion. Expressions for these kinetic energies are given by

$$T_m = \frac{1}{2} J_m \omega_m^2, \quad T_{pr_i} = \frac{1}{2} J_{pr_i} \omega_{pr_i}^2, \quad T_{dr_i} = \frac{1}{2} M_{dr_i} \dot{x}_{dr_i}^2 \tag{2.23}$$

Hence the Lagrangian L is given by

$$\begin{aligned} L &= T - V \\ &= T_m + \sum_{i=1}^{8} T_{pr_i} + \sum_{i=1}^{8} T_{dr_i} = \frac{\omega_m^2}{2} \left(J_m + \sum_{i=1}^{8} J_{pr_i} \frac{1}{n_{pr_i}^2} + \sum_{i=1}^{8} M_{dr_i} \frac{1}{n_{dr_i}^2} f_i(\theta_m, \phi_i) \right) \end{aligned} \tag{2.24}$$

where

$$f_i(\theta_m, \phi_i) = g_i(\theta_m, \phi_i)^2 \text{ and} \tag{2.25a}$$

$$g_i(\theta_m, \phi_i) = \left[r_i \sin\left(\frac{\theta_m}{n_{dr_i}} + \phi_{dr_i} \right) + \frac{r_i^2 \sin\left(\frac{\theta_m}{n_{dr_i}} + \phi_{dr_i} \right) \cos\left(\frac{\theta_m}{n_{dr_i}} + \phi_{dr_i} \right)}{\sqrt{l_i^2 - r_i^2 \sin^2\left(\frac{\theta_m}{n_{dr_i}} + \phi_{dr_i} \right)}} \right] \tag{2.25b}$$

Therefore, using Euler-Lagrange equation, the governing equations for the print motor angular position is given by

$$\begin{aligned} \frac{d}{dt}\left(\frac{\partial L}{\partial \dot{\theta}_m} \right) - \frac{\partial L}{\partial \theta_m} = \tau_m - b_m \dot{\theta}_m - \sum_{i=1}^{8} b_{pr_i} \frac{\omega_m}{n_{pr_i}} - \sum_{i=1}^{8} r_{pr_i} F_{pr_i} \\ - \sum_{i=1}^{8} F_{dr_i} g_i(\theta_m, \phi_i) + \sum_{i=1}^{8} b_{dr_i} \frac{\omega_m}{n_{dr_i}} g_i(\theta_m, \phi_i) \end{aligned} \tag{2.26}$$

where τ_m is the print motor torque and b_m is the print motor viscous friction coefficient. For the i^{th} print cylinder: b_{pr_i} is the viscous friction coefficient of the

print cylinder bearing, b_{dr_i} is the viscous friction coefficient in the linear bearing of the doctor blade assembly, F_{pr_i} is the friction force opposing the print cylinder rotary motion due to doctor blade contact, F_{dr_i} is the friction force opposing the doctor blade linear motion due to doctor blade contact. The left hand side of Equation (2.26) can be obtained as

$$\frac{d}{dt}\left(\frac{\partial L}{\partial \dot{\theta}_m}\right) = \underbrace{\left[J_m + \sum_{i=1}^{8} J_{pr_i}\left(\frac{1}{n_{pr_i}^2}\right) + \sum_{i=1}^{8} M_{dr_i}\left(\frac{1}{n_{dr_i}^2}\right) f_i(\theta_m,\phi_i)\right]}_{J_{eq}(\theta_m,\phi_i)} \ddot{\theta}_m \tag{2.27a}$$

$$+ \sum_{i=1}^{8} M_{dr_i}\left(\frac{1}{n_{dr_i}^2}\right) \frac{\partial f_i(\theta_m,\phi_i)}{\partial \theta_m} \dot{\theta}_m^2 \tag{2.27b}$$

$$\frac{\partial L}{\partial \theta_m} = \frac{1}{2} \sum_{i=1}^{8} M_{dr_i}\left(\frac{1}{n_{dr_i}^2}\right) \frac{\partial f_i(\theta_m,\phi_i)}{\partial \theta_m} \dot{\theta}_m^2 \tag{2.27c}$$

where

$$\frac{\partial f_i(\theta_m,\phi_i)}{\partial \theta_m} = 2r_i \frac{g_i(\theta_i,\phi_i)}{n_{dr_i}} \left[\frac{r_i\left(\cos^2\beta - \sin^2\beta\right)}{q} + \frac{r_i^3 \cos^2\beta \sin^2\beta}{q^3} + \cos\beta\right], \tag{2.28}$$

$\beta = \frac{\theta_m}{n d r_i} + \phi_i$ and $q = \sqrt{l_i^2 - r_i^2 \sin^2\beta}$. Hence, the equation of motion is given by

$$\begin{aligned} J_{eq}(\theta_m,\phi_i)\ddot{\theta}_m + b_m\dot{\theta}_m = \tau_m &- \sum_{i=1}^{8} b_{pr_i}\frac{\omega_m}{n_{pr_i}} - \frac{1}{2}\sum_{i=1}^{8} M_{dr_i}\left(\frac{1}{n_{dr_i}^2}\right)\dot{\theta}_m^2 \frac{\partial f_i(\theta_m,\phi_i)}{\partial \theta_m} \\ &- \sum_{i=1}^{8} r_{pr_i} F_{pr_i} - \sum_{i=1}^{8} F_{dr_i} g_i(\theta_m,\phi_i) \\ &+ \sum_{i=1}^{8} b_{dr_i}\frac{\omega_m}{n_{dr_i}} g_i(\theta_m,\phi_i). \end{aligned} \tag{2.29}$$

Note that the equivalent inertia J_{eq} is not a constant but it is a function of the linear position (or the crank angle) of the doctor blade assembly of each print unit. The equivalent inertia changes due to the doctor blade assembly motion since $f_i(\theta_m,\phi_i)$ is a function of the print motor angular position; note that J_m, J_{pr_i}, M_{dr_i}, n_{pr_i}, n_{dr_i} are all constant. Figure 2.19 shows the normalized $f_i(\theta_m,\phi_i)/l^2$ as a function of the print section motor angular position for several r/l ratios. From

the plot it is evident that the r/l ratio must be small to ensure small variations in J_{eq}. The same conclusion can be reached by using the following logic. When the crank arm rotates at a constant velocity the period of oscillation of the doctor blade assembly is fixed. By increasing the crank arm radius the stroke length is increased and hence the doctor blade assembly would have to reach higher velocities to travel a longer distance within the same period of time. Hence, more kinetic energy is required to accelerate the doctor blade assembly; this results in large variations in equivalent inertia as the mass accelerates. In order to avoid large variations in the equivalent inertia J_{eq} the stroke length of the doctor blade assembly has to be small.

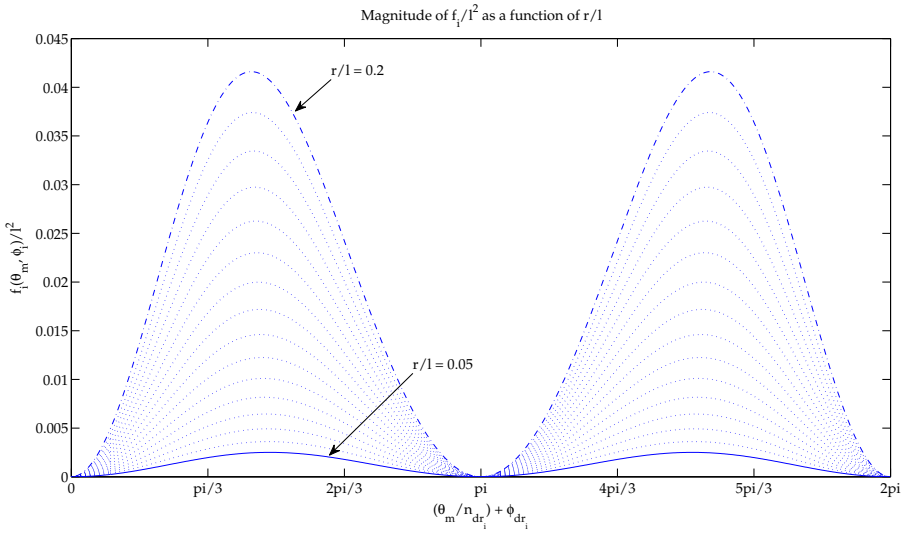

Figure 2.19: *Effect of change in r/l ratio on the normalized f_i as a function of crank arm position*

Similar to the equivalent inertia the input load disturbance due to doctor blade assembly also varies as a function of the print section motor angular position; normalized input load disturbance as a function of angular position is shown in Figure 2.20. From the plot it is evident that r/l has to be maintained

small to reduce the magnitude of input disturbances. Unlike equivalent inertia, load disturbances have sign changes. In order to avoid large input disturbances the stroke length of the doctor blade assembly has to be small.

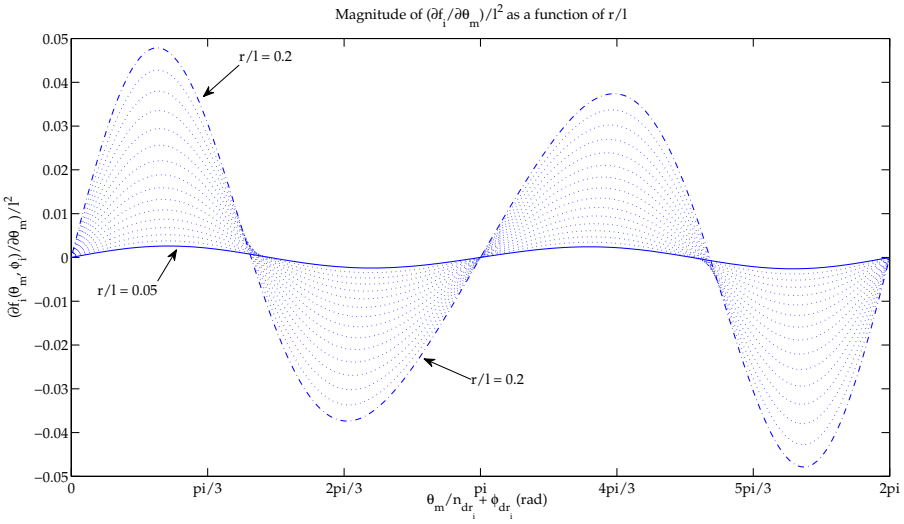

Figure 2.20: *Effect of change in r/l ratio on the normalized $\frac{\partial f_i}{\partial \theta_m}$ as a function of crank arm position*

Note that the print section motor dynamics is affected by the equivalent inertia and input load disturbances from all the print units; the overall disturbance seen at the print section motor is a cumulative effect. Hence it is important to observe the effect of phase difference between doctor blade oscillations on the print section motor dynamics. Irrespective of the value of the r/l ratio, oscillations in doctor blade assemblies in all print units need to be out of phase with each other to reduce dynamic variations in equivalent inertia and input load disturbances. To reduce dynamic input load and equivalent inertia variations, no two crank arms should be in phase and the phase of all crank arms should be equally spaced around a circle.

The model developed in this section provides an understanding of how print

unit loading due to doctor blade oscillations can affect the print section motor; but the assumption that the transmission elements are rigid in the dynamic model development may not provide an accurate representation of the real system. A model considering compliance in the common shaft is developed and analyzed in the following section.

2.4.2 Model Assuming Print Unit Compliance

A dynamic model of the print section can be obtained by appropriately combining the rotary motion of the print cylinders and the linear motion of the doctor blade assemblies in terms of the rotary motion of the print section motor. The common shaft and the print unit gear box transmission elements are considered to be compliant but the crank and the connecting rod of the doctor blade assembly are assumed to be rigid. The equations of motion are obtained using Euler-Lagrange equations by considering the total potential and kinetic energy in the print section. The total kinetic energy is given by

$$\begin{aligned} T =& \frac{1}{2}J_m\dot{\theta}_m^2 + \sum_{i=1}^{4}\frac{1}{2}J_{li}\dot{\theta}_{li}^2 + \sum_{i=1}^{4}\frac{1}{2}J_{ri}\dot{\theta}_{ri}^2 + \sum_{i=1}^{4}\frac{1}{2}J_{pr_{li}}\dot{\theta}_{pr_{li}}^2 + \sum_{i=1}^{4}\frac{1}{2}J_{pr_{ri}}\dot{\theta}_{pr_{ri}}^2 \\ &+ \sum_{i=1}^{4}\frac{1}{2}M_{dr_{li}}\dot{x}_{dr_{li}}^2 + \sum_{i=1}^{4}\frac{1}{2}M_{dr_{r_i}}\dot{x}_{dr_{r_i}}^2 + \sum_{i=1}^{4}\frac{1}{2}J_{dr_{li}}\dot{\theta}_{dr_{li}}^2 + \sum_{i=1}^{4}\frac{1}{2}J_{dr_{r_i}}\dot{\theta}_{dr_{r_i}}^2. \end{aligned} \tag{2.30}$$

The total potential energy is given by

$$\begin{aligned} V =& \frac{1}{2}K(\theta_m - \theta_{l1})^2 + \frac{1}{2}K(\theta_m - \theta_{r1})^2 + \frac{1}{2}K\sum_{i=1}^{3}(\theta_{li} - \theta_{li+1})^2 + \frac{1}{2}K\sum_{i=1}^{3}(\theta_{ri} - \theta_{ri+1})^2 \\ &+ \frac{1}{2}K_{gr}\sum_{i=1}^{4}\left(\frac{\theta_{li}}{n_{pr_{li}}} - \theta_{pr_{li}}\right)^2 + \frac{1}{2}K_{gr}\sum_{i=1}^{4}\left(\frac{\theta_{ri}}{n_{pr_{ri}}} - \theta_{pr_{ri}}\right)^2 \\ &+ \frac{1}{2}K_{gr}\sum_{i=1}^{4}\left(\frac{\theta_{li}}{n_{dr_{li}}} - \theta_{dr_{li}}\right)^2 + \frac{1}{2}K_{gr}\sum_{i=1}^{4}\left(\frac{\theta_{ri}}{n_{dr_{ri}}} - \theta_{dr_{ri}}\right)^2 \end{aligned} \tag{2.31}$$

where θ_m is the print section motor angular position, θ_q is the angular position of the common shaft at the qth position, θ_{pr_q} is the angular position of the print cylinder at the qth print unit, θ_{dr_q} is the angular position of the doctor blade crank at the qth print unit, J_q is the inertia of the common shaft at the qth position, M_{dr_q} is the mass of the doctor blade assembly at the qth print unit, K is the stiffness of the common shaft and K_{gr} is the gear box stiffness, and $q = li, ri, i = 1,\ldots,4$.

The equation of motion for the print section motor can be obtained as

$$J_m\ddot{\theta}_m + K(\theta_m - \theta_{r1}) + K(\theta_m - \theta_{l1}) = \tau_m - b_m\dot{\theta}_m \tag{2.32}$$

where τ_m is the torque supplied to the print section motor and b_m is the print section motor viscous friction coefficient. Equations for other inertias on the common shaft (J_{li}, J_{ri}) may be obtained in a similar fashion. Torque from the common shaft is transmitted to the gear boxes in a series on either side of the common shaft (see Figure 2.16). To derive the equations of motion for print cylinders, viscous bearing friction (b_{pr_q}) as well as the frictional effect (F_{pr_q}) of the doctor blade contact with the print cylinder surface are taken into consideration. In order to simplify the model, it is assumed that the friction force due to the axial motion of doctor blade does not affect the dynamics of the print cylinder; friction force that is tangential to the surface of the print cylinder due to contact with the doctor blade is considered. Therefore, the dynamics for the print cylinders can be obtained as

$$J_{pr_q}\ddot{\theta}_{pr_q} + b_{pr_q}\dot{\theta}_{pr_q} = K_{gr}\left(\frac{\theta_q}{n_{pr_q}} - \theta_{pr_q}\right) - r_{pr_q}F_{pr_q} \tag{2.33}$$

where r_{pr_q} is the radius of the print cylinder at the qth print unit.

Note that the velocity of the doctor blade assembly may be obtained from the doctor blade crank angular velocity by the following transformation (assum-

ing the crank and the connecting rod to be rigid):

$$\dot{x}_q = -\left[r_q \sin\theta_q + \frac{r_q^2 \sin\theta_q \cos\theta_q}{\sqrt{l_q^2 - r_q^2 \sin^2\theta_q}} \right] \dot{\theta}_q, \quad q = dr_{li}, dr_{ri}, \quad i = 1,\ldots,4 \tag{2.34}$$

where $\dot{x}_q$ is the linear velocity of the doctor blade assembly at the qth print unit, r_q is the radius of crank and l_q is the length of the connecting rod at the qth print unit.

Then the dynamics of the q^{th} doctor blade assembly is given by

$$\begin{aligned} \underbrace{\left(M_{dr_q} f_q(\theta_{dr_q}) + J_{dr_q}\right)}_{J_{eq_{dr_q}}} \ddot{\theta}_{dr_q} = & K_{gr}\left(\frac{\theta_q}{n_{dr_q}} - \theta_{dr_q}\right) - \underbrace{\frac{1}{2} M_{dr_q} \frac{\partial f_q(\theta_{dr_q})}{\partial \theta_{dr_q}} \dot{\theta}_{dr_q}^2}_{W_{dr_q}} \\ & - F_{dr_q} g_q(\theta_{dr_q}) + b_{dr_q} \underbrace{g_q(\theta_{dr_q}) \dot{\theta}_{dr_q}}_{-\dot{x}_{dr_q}} \end{aligned} \tag{2.35}$$

where

$$g_q(\theta_{dr_q}) = \left[r_{dr_q} \sin\theta_{dr_q} + \frac{r_{dr_q}^2 \sin\theta_{dr_q} \cos\theta_{dr_q}}{\sqrt{l_{dr_q}^2 - r_{dr_q}^2 \sin^2\theta_{dr_q}}} \right], \; f_q(\theta_{dr_q}) = g_q(\theta_{dr_q})^2. \tag{2.36}$$

Note that the equivalent inertia $J_{eq_{dr_q}}$ and the input disturbance W_{dr_q} are functions of the crank angle. Since rigid elements are assumed to transmit power to the doctor blade assembly, the equivalent inertia and input disturbances are functions of the linear position of the doctor blade. From the dynamics it is evident that the doctor blade motion causes velocity variations at the print cylinder due to variations in equivalent inertia and load disturbance. The variations in both the equivalent inertia $J_{eq_{dr_q}}$ and the input disturbance W_{dr_q} may be reduced by reducing the stroke length of the doctor blade assembly.

A friction model that includes the viscous and Coulomb effects is considered, accounting for lubricating effect of the ink contributing to the viscous friction and the doctor blade loading contributing to the Coulomb friction. The net

friction force is therefore given by

$$F = F_{c_q}\,\mathrm{sgn}(v_{r_q}) + F_{v_q}\,v_{r_q}, \quad v_{r_q} = \sqrt{v_{s_q}^2 + \dot{x}_{dr_q}^2} \tag{2.37a}$$

$$v_{s_q} = r_{pr_q}\dot{\theta}_{pr_q}, \quad \dot{x}_{dr_q} = -g_q(\theta_{dr_q})\dot{\theta}_{dr_q} \tag{2.37b}$$

where F_{c_q} and F_{v_q} are Coulomb and viscous friction coefficients, respectively, at print cylinder q, v_{r_q} is the relative velocity between the print cylinder and doctor blade in print unit q, v_{s_q} is the surface velocity of print cylinder q, and r_{pr_q} is the radius of the print cylinder q. Hence, the friction forces on the print cylinder and doctor blade assembly are given by

$$F_{pr_q} = F\frac{v_{s_q}}{v_{r_q}}, \qquad F_{dr_q} = F\frac{\dot{x}_{dr_q}}{v_{r_q}} \tag{2.38}$$

The model is a function of the relative velocity between the doctor blade linear velocity and the print cylinder surface velocity. Note that the surface velocity of the print cylinder is much larger in magnitude than the doctor blade velocity.

If the doctor blade is actuated by an independent motor, then the print cylinder velocity will be influenced by doctor blade oscillations only through the frictional contact and not through mechanical coupling. In the case of print units with electronic line shafting, the torque transmitted through the mechanical coupling in Equation (2.33) should be replaced by the torque generated by the independent motor of the print cylinder. Even in this case the doctor blade frictional contact will influence print cylinder velocity. But with electronic line shafting the angular misalignment between print cylinders due to shaft compliance is eliminated which enables increase in line speed and machine size due to reduced mechanical vibrations [25].

2.5 Print Cylinder Velocity Dynamics due to Web Wrapped Impression Roller

An impression roller, with a backup roller, is used to nip the web with the print cylinder for efficient transfer of ink from the print cylinder to the web; see Figures 2.1 and 2.21. The nipping action also increases traction between the web and the roller. The print cylinder velocity model presented in the previous section did not include the loading due to the impression roller and the web. Without engaging the print units the web transport is facilitated by the two pull rolls on either side of the print section. When the web wrapped impression rollers are nipped to the print cylinders additional energy is imparted to the web to further facilitate transport. In this section a model that includes this loading on the print cylinder will be presented.

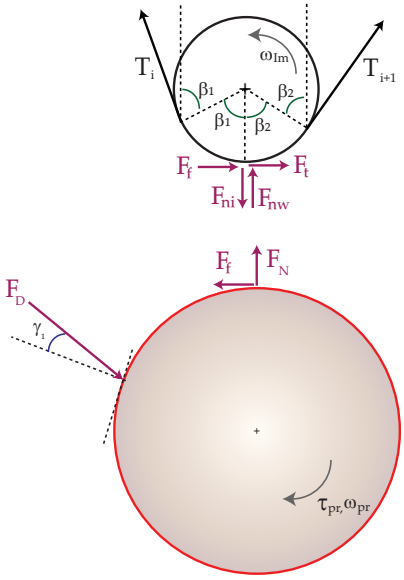

Figure 2.21: *A sketch showing the frictional forces on the print cylinder and the web.*

Figure 2.21 shows the forces involved at the contact of the print cylinder and

the impression roll; let the web wrap angle be $\beta_1 + \beta_2$ as shown in the figure. Denote the tension upstream and downstream of the q^{th} print cylinder to be T_{i_q} and T_{i+1_q} (note that the subscript q is omitted from the variables in the figure). Let F_{D_q} be the force applied on the doctor blade and let γ_{1_q} be the doctor blade contact angle as shown in Fig. 2.21. When the web does not make contact with the print cylinder, the impression roller acts as an idle roller and is driven by the relative tension in the spans upstream and downstream of the roller. When the impression roller is nipped onto the print cylinder, frictional forces between the web and the print cylinder affect the rotational dynamics of the impression roller. In Fig. 2.21, F_t is the force due to the tension differential and F_f is the force due to friction. Based on the wrap angle and the tension upstream and downstream of the impression roll, a normal force $\mathrm{F_{nw}}$ acting upwards opposes the nip force $\mathrm{F_{ni}}$ and the net normal force is $\mathrm{F_N} = \mathrm{F_{ni}}$ - $\mathrm{F_{nw}}$.

A friction model that includes stiction, Coulomb and viscous effects is considered to describe the friction force between the web and the print cylinder. Since ink fills the grooves in the gravure print cylinder, viscous effect is added to a basic model of friction with stiction and Coulomb friction effects. Define the relative velocity between the web and the print cylinder surface to be $\delta_{v_q} = r_{pr_q}\omega_{pr_q} - r_{I_q}\omega_{I_q}$. Let μ_{sw_q} denote the static friction coefficient, μ_{dw_q} denote the dynamic friction coefficient, and F_{vw_q} denote the viscous friction coefficient. The friction force between the web and the print cylinder is given by

$$\mathrm{F}_{f_q} = \begin{cases} \underbrace{\mu_{sw_q}\mathrm{F_{N_q}}}_{F_{swq}}, & \text{if } \delta_{v_q} = 0 \\ \underbrace{\mu_{dw_q}\mathrm{F_{N_q}}}_{F_{cwq}}\,\mathrm{sgn}(\delta_{v_q}) + F_{vw_q}\delta_{v_q}, & \text{otherwise} \end{cases}$$

The following assumptions are considered to obtain the model:

1. The coefficient of friction between the web and the impression roller is greater than the coefficient of friction between the web and the print cylinder; the surface of the impression roller is usually covered with rubber elastomers to increase traction.

2. There is no slip between the surface of the impression roller and the web; this is typically achieved by employing an adequate wrap angle and an appropriate nipping force.

3. The thickness of the web is negligible compared to the radius of the impression roller; this allows for the assumption that the surface velocity of the web is same as the peripheral velocity of the impression roll.

The dynamics of the q^{th} impression roll is given by

$$J_{I_q}\dot{\omega}_{I_q} + b_{Im_q}\omega_{I_q} = r_{I_q}\left(\mathrm{F}_{t_q} + \mathrm{F}_{f_q}\right) \tag{2.39a}$$

$$\mathrm{F}_{t_q} = T_{i+1_q} - T_{i_q}, \quad \mathrm{F}_{f_q} = f(\mathrm{F}_{\mathrm{N}_q}, \delta_{v_q}) \tag{2.39b}$$

$$\mathrm{F}_{\mathrm{N}_q} = \mathrm{F}_{\mathrm{ni}_q} - \left[T_{i_q}\sin(\beta_1) + T_{i+1_q}\sin(\beta_2)\right], \tag{2.39c}$$

where web tension can be obtained from the strain equation (2.17) by assuming the web to be perfectly elastic, i.e., $T_{i_q} = EA\epsilon_{i_q}$.

The print cylinder dynamics when nipped by the web wrapped impression roller is given by

$$J_{pr_q}\ddot{\theta}_{pr_q} + b_{pr_q}\dot{\theta}_{pr_q} = K_{gr}\left(\frac{\theta_q}{n_{pr_q}} - \theta_{pr_q}\right) - r_{pr_q}\left(F_{pr_q} + F_{fq}\right) \tag{2.40}$$

where F_{pr_q} is given by equation (2.38) with $F_{cq} = \mu_{pr_q}\cos(\gamma_{1q})F_{D_q}$; μ_{pr_q} is the friction coefficient between the print cylinder and the doctor blade, γ_{1q} is the doctor blade contact angle, and F_{D_q} is the load force on the doctor blade.

The model for registration error given previously did not consider the effect of web slip on the print cylinder; the model can be modified to the following to include slip:

$$e_r(t) = l - \int_{t-\tau_1}^{t} \frac{r_{I_q}\omega_{I_q}(\tau)}{1+\overline{\epsilon}_{21}(\tau)} d\tau - \left[r_2\theta_2(t) - \frac{r_1\theta_1(t-\tau_1)}{1+\overline{\epsilon}_{21}(t)} \right] + \int_{t-\tau_1}^{t-\tau_2} \dot{\overline{l}}(\tau) d\tau. \quad (2.41)$$

Note that when web slips on the print cylinder the web velocity $r_{I_q}\omega_{I_q}$ will be either greater than or less than the print cylinder surface velocity.

2.6 Design Recommendations to Minimize Strain Variations within Print Units

The model for the print cylinder velocity dynamics provides insights into how various mechanical elements can be designed to minimize web strain variations within the print unit. First, the doctor blade oscillation may cause print cylinder velocity variations which in turn may cause strain variations. As shown earlier, the stroke length of the doctor blade oscillation affects the equivalent inertia $J_{eq_{dr_q}}$ and the input disturbance W_{dr_q}. As the stroke length increases more kinetic energy is required to accelerate the doctor assembly since the period of oscillation of the doctor blade assembly is fixed by the gear ratio; hence this affects the print cylinder velocity due to gear box compliance. Additionally, since all the print units are connected to the common shaft, the doctor blade oscillations at different print units have a cumulative effect on the print section motor due to compliance; the load disturbance on the print section motor due to doctor blade motions can be minimized if the oscillations of the doctor blades in the print section are out-of-phase with each other. Independent motors to drive the doctor blade assemblies can significantly reduce print cylinder velocity variations due

to doctor blade oscillations.

Recall the plots shown in Figure 2.3. The first peak observed at 0.0315 Hz coincides with the fundamental frequency of oscillation of the doctor blade assembly. Therefore, it appears that the motion of the doctor blade affects both web tension and registration error. Observation of the tension signals upstream and downstream of print cylinder 6 (see Figure 2.22) indicate that oscillations in web tension are not due to transport of strain from upstream spans but are created in the print unit span itself.

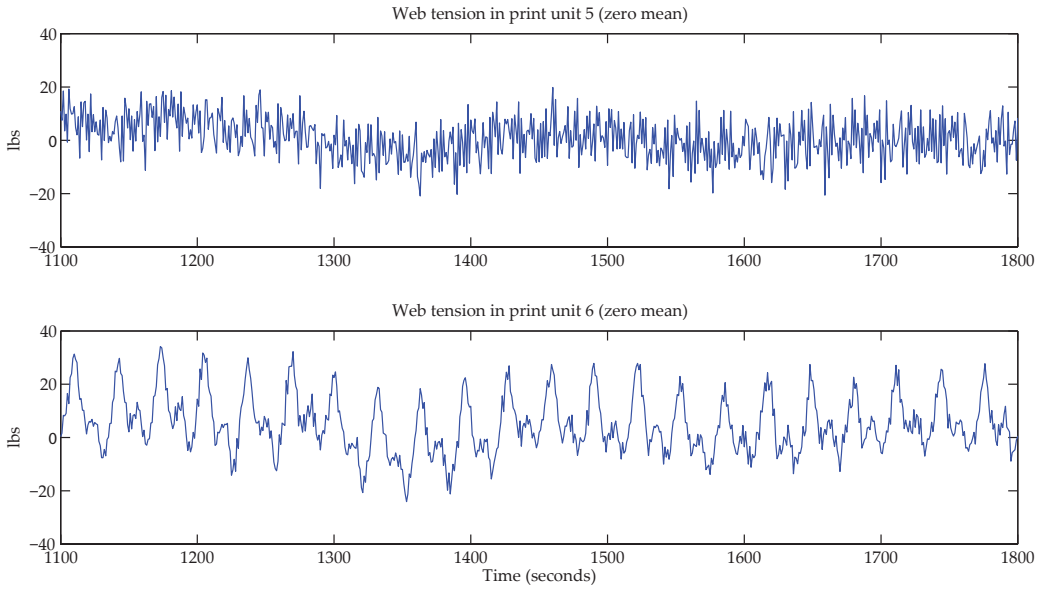

Figure 2.22: *Measured web tension in print unit 5 and print unit 6.*

Observations based on the data collected during various production runs revealed that the distinct peak observed at 0.0315 Hz in Figure 2.3 does not appear in all production runs. To ascertain the exact cause for the occurrence of the peak at 0.0315 Hz, modifications to doctor blade oscillations were made. It was

It is noted that the modifications were made during production runs, hence only small incremental modifications were possible.

Print Unit #	Stroke Length	Crank position
4	2.1 cm	7 o'clock
5	1.9 cm	10 o'clock
6	4.5 cm	8 o'clock
7	1.1 cm	1 o'clock
8	1.9 cm	6 o'clock

Table 2.1: *Doctor blade stroke length and crank arm position during out-of-phase run for various print units. The stroke length is given in centimeters and relative crank arm angular position is represented in terms of the needle of the clock.*

hypothesized that the possible cause for the occurrence of the peak is due to the phase difference between different doctor blade oscillations. The phase of the oscillation of a doctor blade can be characterized based on the crank angular position. Two sets of data were collected by either synchronizing the doctor blade crank position or by ensuring that the crank positions at various print units are out-of-phase; no changes to the stroke lengths were made. The crank positions for the out-of-phase runs and the stoke length for various print units are shown in Table 2.1. Since all the doctor blades oscillate with the same frequency, the angular orientation of each crank with respect to every other crank will remain the same at any instant. When the doctor blades are made to oscillate in-phase, each crank will have the same angular position at any instant of time.

The FFT of relative tension and registration error data for the two scenarios are shown in Figures 2.23 and 2.24. It is evident that the peak at 0.0315 Hz is visible when the doctor blades oscillates in phase with each other while the peak is nonexistent when the doctor blade oscillations are out-of-phase. Additionally, comparing the amplitudes of the peaks with the stoke lengths at each print unit, a positive correlation between the stoke length and the peak amplitude is also evident. The data corroborates the hypothesis that doctor blade oscillations need to be out-of-phase and the stoke lengths need to be small.

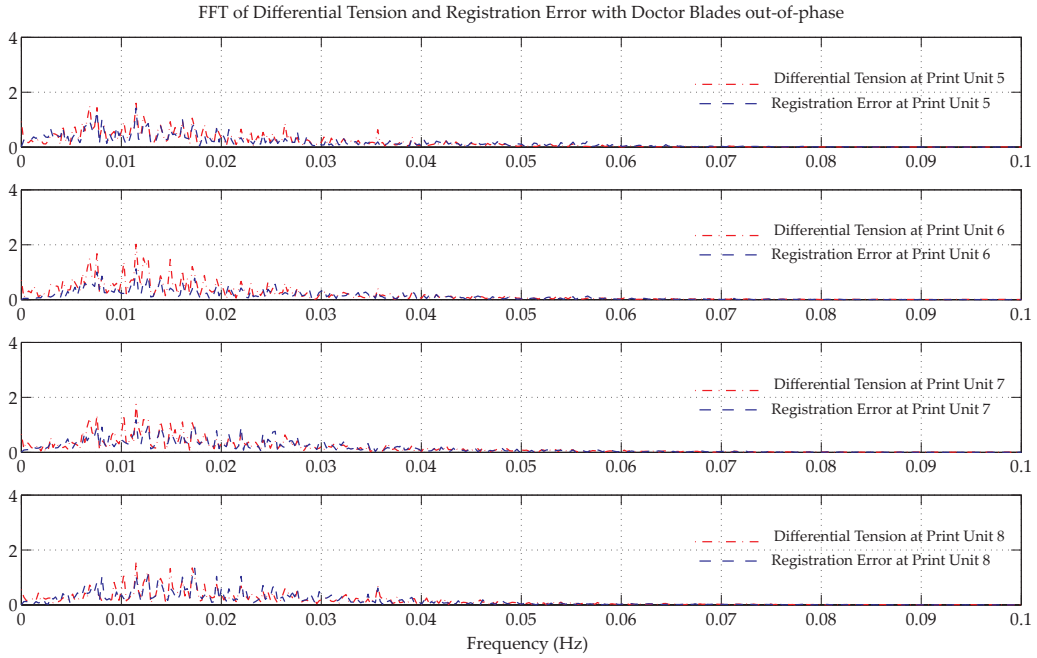

Figure 2.23: *FFT of differential tension and registration error at various print units when doctor blade oscillations are out-of-phase with each other.*

Even when the doctor blade assemblies are driven by independent motors, print cylinder velocities are affected by the frictional contact of the doctor blades. Note that the relative velocity between doctor blade oscillation and print cylinder surface velocity has less variations if the linear velocity of the doctor blade is much smaller in magnitude when compared to the surface velocity of the print cylinder; this implies that the friction force opposing the print cylinder velocity will have less variations. Therefore, even when an independent motor is used for the doctor blade, the stroke length and velocity of oscillation need to be small.

Excessive contact force between the doctor blade and print cylinder may result in print cylinder velocity variations due to frictional contact and hence a suitable doctor blade loading force needs to be maintained. Depending on the

The ideal situation is to have no doctor blade oscillation, and since that is not possible, the stroke length of oscillation and linear velocity of doctor blade need to be small.

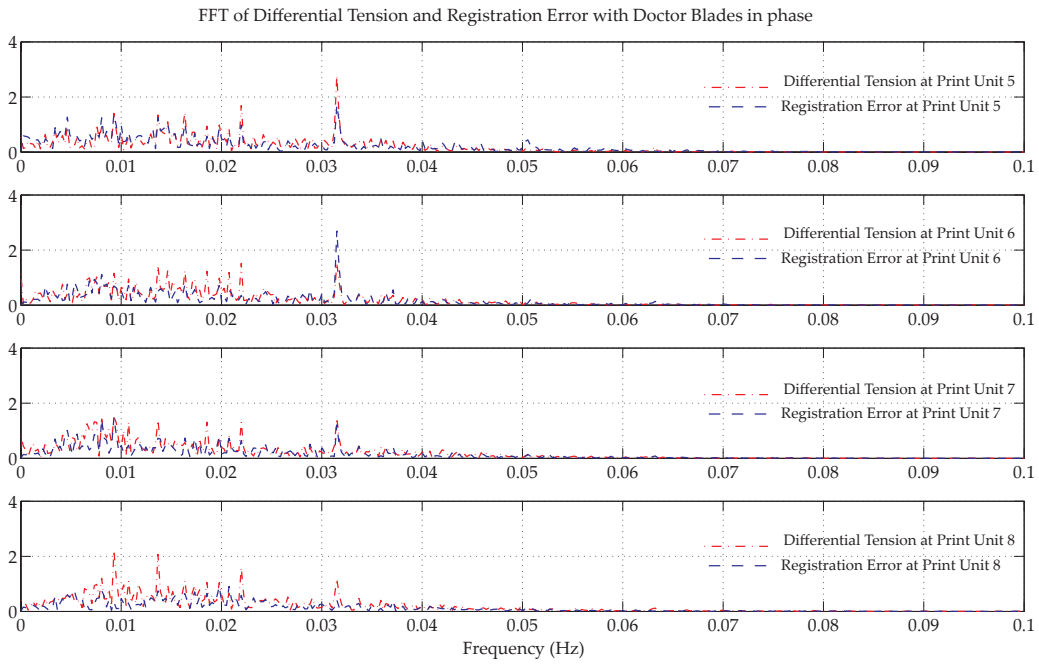

Figure 2.24: *FFT of differential tension and registration error at various print units when doctor blade oscillations are in with each other.*

choice of the material for the doctor blade it may be possible to reduce doctor blade loading force.

Another cause for strain variations within the print unit is the motion of the compensator roller, which is evident from equation (2.17). The rate at which the compensator is linearly positioned, at the required location to compensate for the registration error, has a significant effect on web strain in the print unit. Additionally, without rate constraints, large strain variations due to compensator motion may result in web slippage on the print cylinder if adequate nipping force is not maintained, which is evident from equation (2.39).

2.7 REMARKS

Based on the analysis of the model and from experimental data it is evident that a primary cause for misregistration is variations in web strain from one print unit to the other. Therefore, to minimize registration error, tension variations must be minimized. In practice, it appears that web tension is not regulated within the print units, rather registration error is directly controlled using a compensator roller or by controlling the print cylinder velocities.

Although expensive to install and maintain, the current trend in printing presses is to use electronic line shafts (ELS) to synchronize the motion of the print cylinders [25]. By using ELS, fine control over print cylinder velocities is achieved and it is generally argued in the literature that there is no longer a need for a compensator to correct registration error. But from the print registration model developed in this dissertation it is evident that the strain variations need to be minimized to reduce the registration error. It is hypothesized that a compensator in addition to ELS will provide better registration control compared to the use of just electronic line shafts. This will be investigated further in Chapter 4.

It is evident from the dynamic models and experimental data that the registration error in one print unit can influence registration in subsequent print units. Therefore, it is important to analyze the effect of interaction between different print units. Development of a suitable control strategy to minimize propagation of registration error throughout the print section is also a topic for interest which will be investigated in the following chapter.

CHAPTER 3

Interaction Analysis in Decentralized Control Systems

3.1 Introduction

In many large-scale interconnected system applications decentralized controllers are often employed due to the ease of their implementation and simplicity. Typically these decentralized controllers are designed based on the dynamics of each subsystem without considering the interconnection between subsystems; interconnections are sometimes treated as unknown disturbances but seldom the decentralized controllers are designed to specifically minimize the effect of the interconnections or the interaction. There may be a desire to minimize interaction between subsystems for many reasons, and one of these reasons may be to minimize propagation of disturbances from one subsystem to another. This chapter focuses on quantifying interaction by introducing a Perron-root based interaction metric (PRIM), design of decentralized filters to minimize interaction, and applying this to roll-to-roll (R2R) manufacturing systems through a comprehen-

sive experimental study on a large R2R experimental platform.

A R2R system is a large-scale system with several subsystems interconnected by the web transport. Decentralized control strategies are typically used in R2R machines because of their simplicity and ease of implementation [26, 27, 28], where each driven roller is controlled based on measurements, such as web speed and web span tension, from that section (subsystem).

Interaction between the machine dynamics and web dynamics is inevitable as the web is transported on rollers through processing machinery, and it has been an active topic of interest in web handling. Extensive work has been done to investigate web behavior as it is transported on rollers through processing machinery and its interaction with machine dynamics (see [1, 29, 27, 30] and references therein). In addition to interaction between the web and machine dynamics, interaction between adjacent web tension zones (adjacent subsystems) exists in roll-to-roll processing machines; a tension zone is typically defined as the web between two driven rollers. As the web is transported, web tension disturbances are propagated both upstream and downstream of each tension zone due to strain transport [1, 29]. A systematic analysis of the overall interaction in roll-to-roll systems employing decentralized controllers is not currently available in the literature, which is the focus of this chapter.

In a roll-to-roll printing process with multiple print units, the registration error in each print unit is minimized either by using a compensator roller or by directly controlling the angular position of the print cylinder in that print unit. Because of strain transport, the compensation of registration error in one print unit will affect the error in subsequent print units. This interaction has not been studied in the literature. Currently, with no coordinated control between print

units, the problem is basically treated in a decentralized manner without any analysis. A new interaction metric for decentralized control developed in this chapter will be used in the following chapter to analyze interaction in roll-to-roll printing.

In general interaction in multivariable systems may be described as the influence of each input (output) on all the outputs (inputs). The level of interaction may be investigated by representing the input-output relationship of the multivariable system as a transfer function matrix; for example, if all the off-diagonal entries of the transfer function matrix are zero, then there is no interaction. Prior work related to interaction analysis in multivariable systems (multivaribale process control applications) dealt with the determination of ideal loop-paring between the input and output variables [31, 32, 33, 34] because of the destabilizing effect of various input–output combinations. Interaction measures that quantify constraints on stability with decentralized controllers due to the effect of interaction have been studied in [35, 36]. Whereas, a R2R system is a large-scale interconnected system with clearly defined subsystems which interact with each other and hence the need for analysis of interaction to determine the ideal looping paring is irrelevant. Moreover, the existing interaction measures that provide constraints on stability does not provide a systematic procedure to design controllers and filters in order to minimize interaction in the system. The main contribution of this chapter is an interaction metric that provides information about the level of interaction in the system and that provides a systematic procedure to minimize interaction in decentralized large-scale interconnected systems.

3.2 Perron-Frobenius Theory

The Perron-Frobenius theory provides tools to study spectral properties of square, real, nonnegative matrices; and specifically to a special family of nonnegative matrices. In this section the preliminaries needed to understand the development of the new interaction metric would are presented and discussed.

A matrix is said to be positive if all the elements of the matrix are positive. Square, real, positive matrices exhibit some unique spectral properties and these were first studied by Perron in detail. Substantial extensions to the positive matrix theory to include nonnegative matrices were developed by Frobenius [37]. A matrix is nonnegative if all the elements of the matrix are real and nonnegative. Mathematically, $A \in \mathscr{R}^{m\times n}$ is a nonnegative matrix if its elements a_{ij} satisfy $a_{ij} \geq 0, \forall i, j$; $A \geq 0$ is the notation used to represent the nonnegative matrix A. But nonnegative matrices with special structure have spectral properties similar to those of positive matrices as shown by Frobenius. These special matrices are called irreducible matrices.

Irreducible Matrix

$A_{n\times n}$ is said to be an reducible matrix [37] when there exist a permutation matrix P such that

$$P^{\top}AP = \begin{pmatrix} X & Y \\ 0 & Z \end{pmatrix}, \quad \text{where } X \text{ and } Y \text{ are both square.}$$

Otherwise A is said to be an irreducible matrix.

Irreducibility in graph theory means that any node can be reached from any other node in the graph, i.e., the graph is strongly connected.

PRIMITIVE MATRIX

A nonnegative irreducible matrix $A_{n\times n}$ having only one eigenvalue, $r=\rho(A)$, on its spectral circle is said to be a primitive matrix [37].

The Perron-Frobenius theorem is stated in the following [37].

PERRON-FROBENIUS THEOREM

If $A_{n\times n}\geq 0$ is irreducible, then the following statements are true.

- $r=\rho(A)\in\sigma(A)$ and $r>0$ (r is the Perron root)
- r is a simple eigenvalue
- There exists a vector $x>0$ such that $Ax=rx$
- The Perron vector is the unique vector defined by

$$Ap=rp,\quad p>0,\quad \text{and}\quad \|p\|_1=1,$$

  and, except for positive multiples of p, there are no other nonnegative eigenvector for A, regardless of the eigenvalue.

- The Collatz-Wielandt formula holds – i.e., $r=\max_{x\in\mathcal{N}} f(x)$, where

$$f(x)=\min_{1\leq i\leq n,\ x_i\neq 0}=\frac{[Ax]_i}{x_i}\ \text{and}\ \mathcal{N}=\{x|x\geq 0\ \text{with}\ x\neq 0\}.$$

where $\rho(A)$ is the spectral radius of A, $\sigma(A)$ is the set containing the eigenvalues of A, $x>0$ implies that all elements of x are greater than zero or x is a positive vector and $\|(.)\|_1$ is the one-norm or the sum of the elements in the vector (.). The Perron-Frobenius theorem is powerful and elegant. First, the largest eigenvalue of the matrix A is real, simple and it lies on the spectral radius of A. There is always a positive eigenvector for the matrix A and it can only be a positive

multiple of the unique eigenvector p corresponding to the eigenvalue r. Finally, the Collatz-Wielandt formula is valid for all nonnegative matrices including reducible matrices.

3.3 Perron-Root Based Interaction Measure

The Perron-root based interaction metric developed in this chapter is applicable to a class of large-scale interconnected systems where each subsystem can be reduced to a single-input single-output subsystem. In general the metric can be applied to any multivariable system with equal number of inputs and outputs not necessarily large-scale interconnected systems. In a general framework consider a multivariable system with the following input-output relationship: $y = G(s)u$, where $u \in \mathscr{R}^n$ is the input vector, $y \in \mathscr{R}^n$ is the output vector and $G(s)$ is the $n \times n$ rational, plant transfer function matrix. The interaction in the system is due to the off-diagonal elements in the transfer function matrix; and by quantifying the relative effect of off-diagonal elements on a particular input-output relationship one can see the effect of interaction on a particular subsystem. Let G be separated as $G = \overline{G} + \widetilde{G}$ where $\overline{G}$ has diagonal elements of G and $\widetilde{G}$ has off-diagonal elements of G; interaction may be quantified by the size of $\widetilde{G}$. The relative effect of the off-diagonal elements on a particular output can be understood by observing the size of the relative error matrix $L_H \triangleq \widetilde{G}\overline{G}^{-1}$.

3.3.1 Quantifying Interaction

Interaction in the system can be quantified by the size of relative error matrix L_H. In this work a D-weighted induced Hölder l_∞ norm of L_H is used to quantify interaction. This norm is equal to the Perron root of the companion matrix which

is defined in the following.

Definition 3.3.1. *For an $n \times n$ transfer function matrix $G(s)$, $\langle G(j\omega)\rangle$ is the companion $n \times n$ positive matrix such that $\langle G(j\omega)\rangle_{kl}$ is the magnitude of $G(j\omega)_{kl}$ at the frequency ω.*

Definition 3.3.2. *The Perron root based interaction metric (PRIM) for the system G is defined as*

$$p_{L_H}(\omega) \triangleq \mathscr{P}(\langle L_H(j\omega)\rangle) \tag{3.1}$$

where $\mathscr{P}(\langle L_H(j\omega)\rangle)$ is the Perron root of the irreducible matrix $\langle L_H(j\omega)\rangle$ at frequency ω.

Since PRIM is a norm that quantifies the size of the relative error matrix L_H, a smaller value for it means less interaction. Note that PRIM does not provide information about interaction in each loop, but provides an overall picture of interaction in the multivariable system. And PRIM is bounded from below and above by the least and the worst possible interaction in individual loops as a consequence of Lemma 3.3.3 state below.

Lemma 3.3.3 (Lemma 3.1.1 in [38])**.** *Let $A \geq 0$ be an $n \times n$ matrix with row sums $r_1, \ldots, r_n$. If $\mathscr{P}(A)$ is the Perron root of A, then*

$$\min_{1\leq i\leq n} r_i \leq \mathscr{P}(A) \leq \max_{1\leq i\leq n} r_i.$$

And if A is primitive, then equality on either side implies equality throughout [39].

To study interaction, an interaction metric can also be defined based on the matrix $T \triangleq G\overline{G}^{-1}$ as

$$p_T(\omega) \triangleq \mathscr{P}(\langle T(j\omega)\rangle). \tag{3.2}$$

Note that the matrix $\langle T\rangle$ is the same as the matrix $g_{pq}(s_0)$ in [40] with $\langle T\rangle$ being a function of ω rather than a single frequency s_0. The matrix $\langle T\rangle$ possesses some

desirable characteristics, specifically $\langle T \rangle$ is primitive, that may be exploited to obtain stronger results when compared to $\langle L_H(j\omega) \rangle$. $\langle L_H(j\omega) \rangle$ is considered because it can be readily compared with the structured singular value interaction measure [35].

In the following, it is assumed that $\langle L_H \rangle$ is irreducible. For the sake of brevity, $\langle \cdot \rangle$ and ω will be dropped from the notation whenever there is no confusion between a rational transfer function matrix and a nonnegative matrix; when ω is dropped, it implies that the condition or statement is valid for all frequencies. The following lemma provides the relationship between p_{L_H} and p_T.

Lemma 3.3.4. $p_{L_H} = p_T - 1$.

Proof. The matrix T is related to L_H by

$$T = G\overline{G}^{-1} = \left(\overline{G} + \widetilde{G}\right)\overline{G}^{-1} = I + \widetilde{G}\overline{G}^{-1} = I + L_H$$

If v_i is an eigenvector of L_H corresponding to the eigenvalue $\lambda_{L_H i}$, then v_i is also an eigenvector of T and the corresponding eigenvalue is $\lambda_{T_i} = 1 + \lambda_{L_H i}$. It has to be shown that if $\lambda_{T_i} = p_T$, then the corresponding $\lambda_{L_H i}$ is p_{L_H}. Since L_H is irreducible, $T = I + L_H$ is irreducible (from Corollary 1.10.a of [41]). Also, since the trace of L_H is zero and the trace of $I = n > 0$, T is a primitive matrix (from Corollary 2.28 of [41]). Since T is primitive, p_T is the only eigenvalue of T that is on the spectral circle of T. Therefore, there exists a real $\lambda_p > 0$ such that $p_T = 1 + \lambda_p$ and λ_p is greater than or equal in magnitude to any eigenvalue of L_H, i.e., $\lambda_p \geq |\lambda_{L_H i}|$, $\forall i$. Since $\lambda_{Ti} = 1 + \lambda_{L_H i}$, and if $\lambda_{Ti} = p_T$, then it must be that $p_T = 1 + p_{LH}$. □

It is clear that the Perron eigenvectors are the same for both the matrices T and L_H. Additionally, T being primitive ensures that p_{L_H} is the only eigenvalue on the spectral circle of L_H, i.e., no other eigenvalue has magnitude greater than

or equal to the Perron root. This fact turns out to be important for the interaction minimization problem which is discussed in the following.

3.3.2 Minimizing Interaction

Lemma 3.3.5. *(Lemma 1.2 in [40]) Let T be a primitive square matrix with the Perron-Frobenius eigenvalue r. Then, for all $x > 0$,*

$$\min_i \frac{\sum_j T_{ij} x_j}{x_i} \leq r \leq \max_i \frac{\sum_j T_{ij} x_j}{x_i}.$$

Corollary 3.3.6. *(Corollary 1.3 in [40])*

$$\max_{x>0} \min_i \frac{\sum_j T_{ij} x_j}{x_i} = r = \min_{x>0} \max_i \frac{\sum_j T_{ij} x_j}{x_i},$$

and the optimal x is the Perron-Frobenius right eigenvector in both cases.

Remark 3.3.7. *If $\sup_\omega p_{L_H}(\omega) < 1$, then there exists a decentralized pre-filter that would ensure diagonal dominance (minimize interaction) at all frequencies. The pre-filter is obtained directly from the right Perron eigenvector of $L_H(\omega)$.*

From Lemma 3.3.5 and Corollary 3.3.6 it is evident that if an $n \times n$ primitive matrix T is pre-multiplied (scaled) by a diagonal matrix $D \triangleq \text{diag}\{x_1, \ldots, x_n\}$, where x_i are the elements of the Perron-Frobenius right eigenvector x, then the resulting primitive matrix has all the row sums equal to the Perron root of T; this is the optimal scaling matrix that minimizes the overall interaction in matrix T. Consequently, if $\sup_\omega p_T(\omega) < 2$ ($\sup_\omega p_{L_H}(\omega) < 1$) in the frequency range of interest, then diagonal dominance can be achieved by using an optimally scaled decentralized pre-filter whose magnitudes response is equal to the corresponding Perron vector in the frequency range of interest. The i^{th} decentralized pre-filter is this obtained by fitting a stable, non-minimum phase, rational transfer

function to the magnitude of the i^{th} element of the Perron eigenvector of $T(j\omega)$. Since the Perron eigenvector of $L_H(j\omega)$ is the same as that of $T(j\omega)$, the pre-filters obtained by using the right eigenvector of $L_H(j\omega)$ will minimize the interaction in the system.

Mees [40] introduced the concept of achieving diagonal dominance by using a static pre-compensator (post-compensator). He also showed that diagonal dominance can be achieved with a static pre-compensator over a range of frequencies. Since the static pre-compensator is conservative, results from that work are used and extended to obtain a dynamic pre-filter that reduces interaction and guarantees stability of the overall system for decentralized control applications.

Note that the Perron-Frobenius theory ensures that the Perron eigenvector is unique and none of the elements in the Perron eigenvector is non-positive. Moreover, the theory ensures that none of the elements of the Perron vector has magnitude greater than one; in fact the sum of the elements of the Perron vector is always equal to one. Hence, the pre-filter obtained from the Perron vector will always de-tune the system in order to minimize interaction. Interaction minimization does not guarantee performance of each individual section. In order to meet the performance requirements all the pre-filters can be scaled equally; the scaling does not change the underlying Perron eigenvector. One has to ensure that the stability is guaranteed with the scaled pre-filters. In the following the stability constraint based on PRIM is discussed.

Along with Lemma 3.3.5 and Corollary 3.3.6 another Lemma [40, Lemma 1.4] is used in [40] to design a static pre-filter that reduces interaction in the system. The static pre-filter is the right eigenvector of the nonnegative matrix Q which is obtained from $T(j\omega)$ as $Q_{kl} \triangleq \sup_\omega |T_{kl}(j\omega)|$.

3.3.3 Stability Constraints

Interaction metrics that quantify the destabilizing effect of interaction provide constraints on the size of relative error matrix based on diagonal closed-loop system [35, 36]. In a general framework, for the rational transfer function matrix $G(s)$ if K is a decentralized controller that stabilizes the diagonal plant $\overline{G}$, i.e., the diagonal closed-loop system $\overline{H}$ is stable where $\overline{H} = \overline{G}K(I + \overline{G}K)^{-1}$. From the multivariable Nyquist stability criteria we know that the closed-loop system with the diagonal controller K is stable if and only if

$$\det[I + G(s)K(s)] \neq 0, \forall s \in \mathscr{D}_{\mathscr{R}} \tag{3.3a}$$

$$\lim_{R\to\infty} N(0, \det[I + G(s)K(s)], \mathscr{D}_{\mathscr{R}}) = -q_0 \tag{3.3b}$$

where $N(0,(\cdot),\mathscr{D}_{\mathscr{R}})$ represents the number of clockwise encirclements of the origin by the image of the Nyquist contour $\mathscr{D}_{\mathscr{R}}$ (with appropriate indentations to avoid any open-loop poles on the imaginary axis) under $(\cdot)$ and q_0 is the number of open-loop unstable poles of GK. If G and $\bar{G}$ have the same number of unstable poles and if K stabilizes $\bar{G}$ then the stability condition reduces to

$$\det[I + G(s)K(s)] \neq 0, \forall s \in \mathscr{D}_{\mathscr{R}} \tag{3.4}$$

Then the condition for K to stabilize the overall plan G is given by the following theorem.

Theorem 3.3.8. *Assume G and $\overline{G}$ have the same number of unstable poles and $\overline{H}$ is stable. Then the closed-loop system $H = GK(I+GK)^{-1}$ is stable iff*

$$\det[I + L_H \overline{H}\,] \neq 0 \quad \forall s \in \mathscr{D}_{\mathscr{R}} \tag{3.5}$$

Proof.

$$\begin{aligned} I + GK &= I + \bar{G}K + \tilde{G}K \\ &= [I + \tilde{G}K(I+\bar{G}K)^{-1}][I+\bar{G}K] \\ &= [I + \tilde{G}\bar{G}^{-1}\bar{H}][I+\bar{G}K] \\ \implies \det[I+GK] &= \det[I+L_H\bar{H}]\det[I+\bar{G}K] \end{aligned}$$

Since $\det[I+\bar{G}K] \neq 0\ \forall s \in \mathscr{D}_{\mathscr{R}}$, H will be stable if and only if $\det[I+L_H\bar{H}] \neq 0\ \forall s \in \mathscr{D}_{\mathscr{R}}$ (from equation (3.4)). □

By using the small gain theorem, the sufficient condition for stability of the overall system based on the previous theorem is given by

$$||L_H(j\omega)\overline{H}(j\omega)|| < 1\ \forall \omega \tag{3.6}$$

where $||(\cdot)||$ is any compatible induced norm of $(\cdot)$. An interaction metric based on singular values would have the following constraint for stability given that the diagonal closed-loop system is stable:

$$||L_H(j\omega)\overline{H}(j\omega)||_2 \leq ||L_H(j\omega)||_2 ||\overline{H}(j\omega)||_2 < 1\ \forall \omega \tag{3.7a}$$

$$\overline{\sigma}(\overline{H}(j\omega)) < \frac{1}{\overline{\sigma}(L_H(j\omega))}\ \forall \omega \tag{3.7b}$$

where $\overline{\sigma}(\cdot)$ is the maximum singular value (MSV) of $(\cdot)$. The constraint indicates that the magnitude response of all the individual diagonal closed-loop systems

should be less than the MSV of the relative error matrix at all frequencies. The conservatism in equation (3.7a) arises due to the application of the multiplicative norm inequality.

By knowing that $\overline{H}$ is diagonal, it is possible to reduce the conservatism of the constraint. The matrix transformation theory provides useful relations between absolute norms and the Perron root of nonnegative matrices [42]. These transformations do not affect certain matrix structures such as diagonal matrices and hence are useful in obtaining bounds on transformed matrices.

Definition 3.3.9. *[43] Given a number $p \in [1,\infty]$ and a diagonal matrix $D \triangleq diag[d_1, d_2, \ldots, d_n] \in \mathscr{C}^{n\times n}$ with $d_i \neq 0$ for all $i = 1,\ldots,n$, the D-weighted Hölder l_p norm on $\mathscr{C}^n$ is*

$$||x||_{pD} \triangleq ||Dx||_p \triangleq \left(\sum_{i=1}^{n} |d_i x_i|^p\right)^{1/p} \quad \text{for all } x \in \mathscr{C}^n. \tag{3.8}$$

The subordinate bound norm induced in $\mathscr{C}^{n\times n}$ by the l_p-norm on $\mathscr{C}^n$ is

$$||A||_{pD} \triangleq \sup_{x\neq 0} \frac{||Ax||_{pD}}{||x||_{pD}} \quad \text{for all } A \in \mathscr{C}^{n\times n}. \tag{3.9}$$

Remark 3.3.10. *The diagonal pre-compensator (post-compensator) is optimal in minimizing the D-weighted induced Hölder l_p norm for $p = 1$ and ∞ and is sub-optimal for $1 < p < \infty$.*

Lemma 3.3.11. *[43, Lemma 2] The p-norm weighted D_p^* is optimal for $p = 1$ and $p = \infty$ in the sense that*

$$\|A(j\omega)\|_{pD_p^*} = \inf_D \|\langle A(j\omega)\rangle\|_{pD} = p_A(\omega) \tag{3.10}$$

For $1 < p < \infty$, the weight D_p^* is sub-optimal

$$\|A(j\omega)\|_{pD_p^*} \leq \inf_D \|\langle A(j\omega)\rangle\|_{pD} = p_A(\omega) \tag{3.11}$$

The optimal scaling D_p^* is obtained from the left and right Perron eigenvectors of $\langle A\rangle$.

The stability constraint based on the Perron root of L_H, that takes advantage of the fact that $\overline{H}$ is diagonal, may be obtained by using Lemma 3.3.11 and is given by

$$|\overline{h}_i(j\omega)| < \frac{1}{p_{L_H}(\omega)} \; \forall i, \omega. \tag{3.12}$$

Another stability constraint based on the structural information of $\overline{H}$ is obtained from the structured singular value interaction measure (SSVIM), or μ interaction measure, in [35]; the SSVIM is based on the structured singular value introduced in [44]. The stability constraint is given by

$$\overline{\sigma}(\overline{H}(j\omega)) < \frac{1}{\mu_{\overline{H}}(L_H(j\omega))} \; \forall \omega \tag{3.13}$$

where $\mu_{\overline{H}}$ is the structured singular value of $L_H(j\omega)$ with respect to the structure $\overline{H}$. In Section 3.5 further discussions comparing the PRIM and SSVIM are presented.

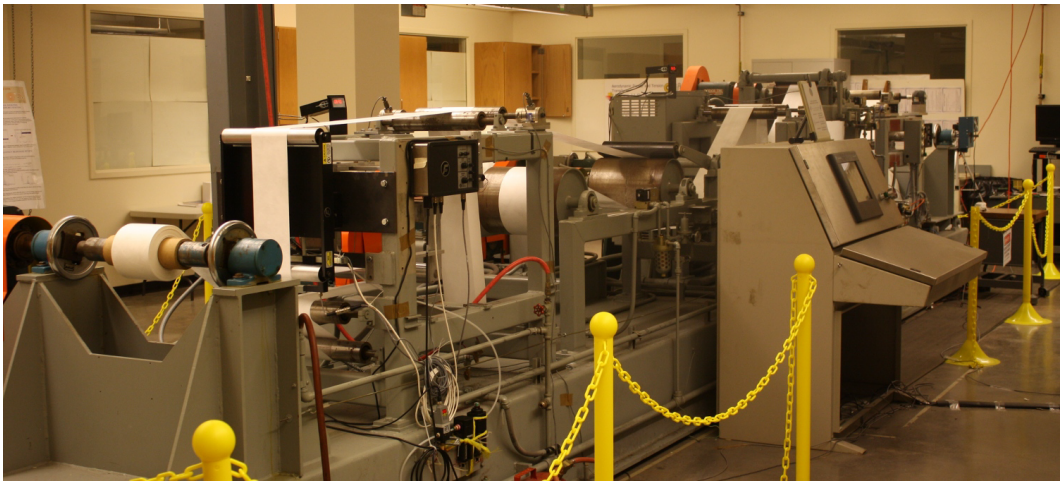

Figure 3.1: *Picture of the experimental web platform; a line schematic is shown in Figure 3.2.*

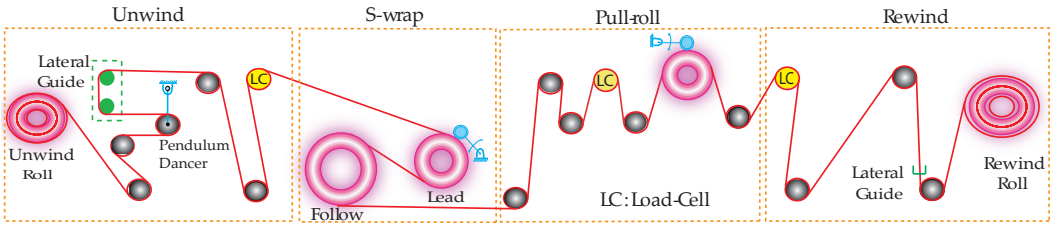

Figure 3.2: *Schematic of the experimental web platform*

3.4 Interaction Analysis and Minimization in Roll-to Roll Systems

The PRIM is used to analyze and minimize interaction in a large experimental R2R machine shown in Figure 3.1 (see Figure 3.2 for a schematic of the platform.). The R2R machine has three tension zones/sub systems namely, unwind section, pull roll section and rewind section, where web tension is regulated using driven rollers in these tension zones.

3.4.1 Governing Equations

The governing equations for each section of the R2R system is given in the following; a linearized variational longitudinal web dynamics for the experimental web platform is obtained using the procedure described in [26] with the same notations and subscript naming conventions (see Figure 3.3).

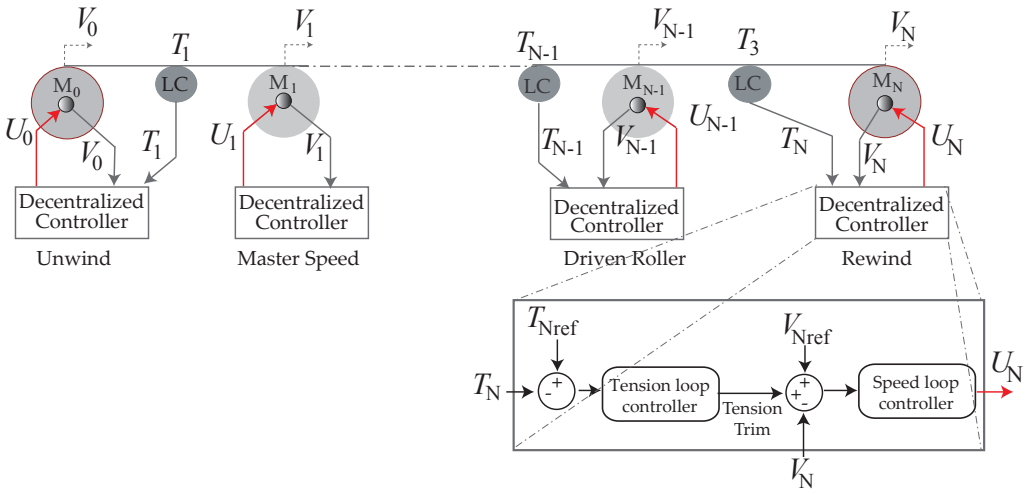

Figure 3.3: *Decentralized tension control structure for roll-to-roll systems with an inner velocity loop and an outer tension loop*

The following notations are used in the governing equations of the subsystems. J_i: driven roller moment of inertia, R_i: driven roller radius, V_i: web velocity at the driven roller, T_i: web span tensions, n_i: gear ratio, U_i: torque input, b_{f_i}: viscous friction coefficient, L_i: span length, t_0 wound on tension, v_{r_i}: velocity reference, t_{r_i}: tension reference, A the cross-sectional area of the web and E the Young's modulus of the web material.

Unwind Section:

$$\frac{J_0}{R_0}\dot{V}_0 = T_1 R_0 - n_0 U_0 - \frac{b_{f0}}{R_0} V_0 \tag{3.14a}$$

$$L_1 \dot{T}_1 = -T_1 v_{r_1} + \left[AE - t_{r_1}\right] V_1 + \left[t_0 - AE\right] V_0 \tag{3.14b}$$

Lead and Follower Section:

$$\frac{J_1}{R_1}\dot{V}_1 = (T_2 - T_1) R_1 + n_1 U_1 - \frac{b_{f1}}{R_1} V_1 \tag{3.15}$$

Pull Roll Section:

$$\frac{J_2}{R_2}\dot{V}_2 = (T_3 - T_2) R_2 + n_2 U_2 - \frac{b_{f2}}{R_2} V_2 \tag{3.16a}$$

$$L_2 \dot{T}_2 = -T_2 v_{r_2} + \left[AE - t_{r_2}\right] V_2 - \left[AE - t_{r_1}\right] V_1 + T_1 v_{r_1} \tag{3.16b}$$

Rewind Section:

$$\frac{J_3}{R_3}\dot{V}_3 = -T_3 R_3 + n_3 U_3 - \frac{b_{f3}}{R_3} V_3 \tag{3.17a}$$

$$L_3 \dot{T}_3 = -T_3 v_{r_3} + \left[AE - t_{r_3}\right] V_3 - \left[AE - t_{r_2}\right] V_2 + T_2 v_{r_2} \tag{3.17b}$$

Besides the interaction between the machine and web dynamics, coupling between tension zones is evident from Equations (3.14)–(3.17) which leads to interaction between tension zones (subsystems).

3.4.2 Interaction Analysis

Longitudinal control in roll-to-roll processing involves regulation of web tension by controlling the speed of the driven roller in that tension zone, based on web tension measurement; either a load cell or a dancer is used to measure web tension. The tension control strategy involves two loops: a well tuned inner velocity loop that is implemented within the motor drive for controlling the speed of

the driven roller motor; an outer tension loop implemented in a Programmable Logic Control (PLC) that provides the velocity correction to the inner loop to regulate tension (see Figure 3.3). Often in web processing machines, the inner loops are tuned and commissioned based on drive manufacturer specifications and are seldom re-tuned during the outer loop tuning process. The outer tension loops are tuned individually based on process and operating conditions until certain performance characteristics are met.

The goal is to analyze the overall interaction in this roll-to-roll system, i.e., the influence of the velocity correction provided by the outer tension loops on web tension in other sections. Figure 3.4 shows the PRIM with the three tension loop velocity corrections as the input and the web tensions in the three zones as the output; the web transport conditions and parameters values used in the linearized model is provided in Table 3.1. Since the Perron-root provides an indication of the size of L_H, a smaller value for the Perron-root indicates a smaller magnitude of interaction in the system; and if the Perron-root is zero, then no interaction exists. From the PRIM plot it is evident that interaction is dominant in a certain range of frequencies between 10^{-4} Hz to 1 Hz and is negligible above 1 Hz. The magnitude of interaction is close to 1 indicating that the velocity correction provided by a tension loop will have almost the same influence on one other tension zone. Note that the PRIM provides the worst case scenario for all the three tension zones and provides no information about the effect of any particular input-output pair.

Experiments were conducted on the experimental R2R system to characterize the interaction in the actual system and the results are compared with PRIM. Velocity disturbances at the S-wrap section were introduced to create tension

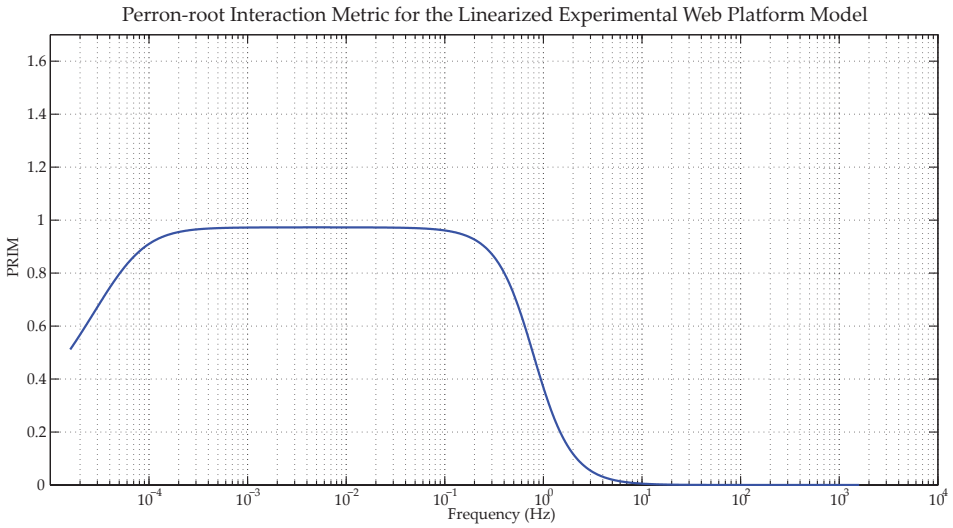

Figure 3.4: *Perron root interaction metric for the linearized model of the roll-to-roll system*

disturbances at the unwind and pull roll sections and the effect of these disturbances in the rewind section were observed to understand the interaction in the system. Experiments were conducted both in the forward direction (web travels from unwind to rewind) as well as in the reverse direction (web travels from the rewind to unwind) to see the effect of interaction both upstream and downstream of the disturbance section; for consistency the section names are the same irrespective of the direction of web transport. In the experiments a six inch polymer web (called Tyvek) was transported with a web speed of 150 feet-per-minute (fpm) and a web tension of 20 pounds (lbf). A sinusoidal speed disturbance of magnitude 5 fpm was introduced at the S-wrap driven rollers for a duration of one minute; six distinct frequencies were considered. Figures 3.5 and 3.6 show the tension signals in the three sections while the web is transported in the forward and reverse direction. Note that the tension disturbances observed in the unwind and the pull roll sections are due to the direct effect of the S-wrap velocity disturbance; the interaction is seen in the rewind section.

Symbol	Parameter	Value	Units
AE	Web Parameter	2200	lbf
t_{ri}	Nominal Tension	20	lbf
v_{ri}	Nominal Web Speed	150	fpm
n_i	Gear Ratio	1	
L_1	Span Length	22.15	ft
L_2	Span Length	18.175	ft
L_3	Span Length	17.1	ft
J_0	Moment of Inertia	2.93	lbf-ft-sec^2
J_1	Moment of Inertia	1.39	lbf-ft-sec^2
J_2	Moment of Inertia	1.47	lbf-ft-sec^2
J_3	Moment of Inertia	2.94	lbf-ft-sec^2
R_0	Radius of rewind	0.5	ft
R_1	Radius of S-wrap	0.5	ft
R_2	Radius of Pull-roll	0.25	ft
R_3	Radius of Unwind	0.5	ft
b_{fi}	Viscous Friction Coefficient	0.01	lbf-ft-sec

Table 3.1: *Parameter of the Euclid line and web transport conditions used in the linearized model.*

From the plots it is evident that the magnitude of interaction is small above 0.25 Hz and increases with decreasing frequency. At low frequencies the tension disturbance observed at the rewind section is as high as the tension disturbances observed in the unwind and the pull roll sections as predicted by the PRIM (see Figure 3.4). In many R2R manufacturing systems, webs with different physical and mechanical properties are transported through the same processing machines; seldom the control algorithm are changed based on the material used. Hence it would be beneficial to understand how the overall interaction changes when different web materials are transported within a same R2R system. Experiments were conducted to see the interaction in the experimental roll-to-roll system with different materials and the results are compared with the PRIM with different web materials. Figure 3.7 shows the PRIM with two different web materials transported in the same experimental roll-to-roll system. From the plot it is

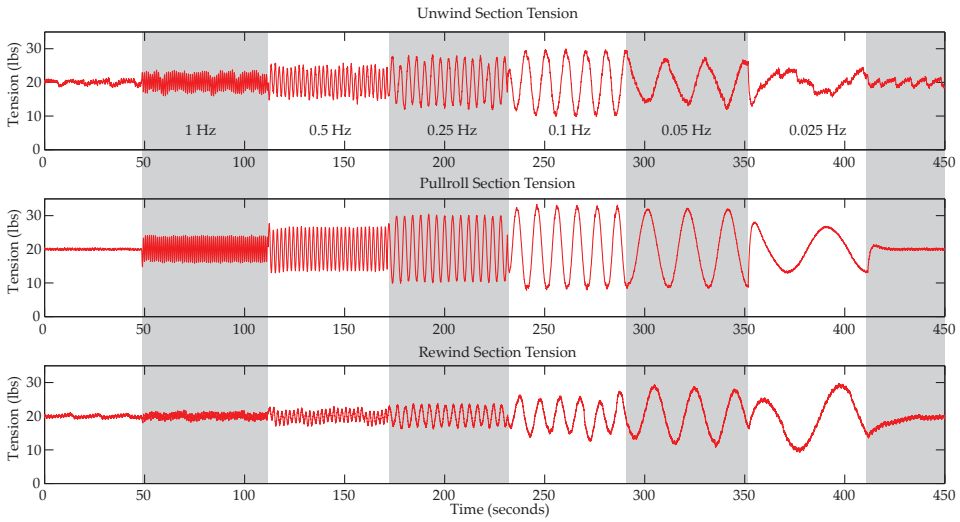

Figure 3.5: *Tension measurement at the unwind, pull roll and rewind section with sinusoidal velocity disturbances at the S-wrap section; web transport in the forward direction. The alternate shaded and light regions show the sinusoidal velocity disturbances with six distinct frequencies with a 5 ft/min magnitude; the annotation in the top plot indicates the frequencies.*

evident that the interaction is significantly higher for the polyethylene web in the frequency range of 0.1 Hz to 3 Hz when compared to the Tyvek web. Figures 3.8 and 3.9 show the tension signals at the three tension zones while the polyethylene web is transported in the forward and reverse direction within the experimental R2R system at a web speed of 150 fpm with the nominal tension of 20 lbs with the same set of sinusoidal velocity disturbances at the S-wrap driven rollers. From the data it is evident that the overall interaction is higher for polyethylene web when compared to the Tyvek web in the frequency range of 0.1 Hz to 1 Hz as predicted by PRIM. To clearly see the effect the FFT of the time domain signals with Tyvek and polyethylene web for forward and reverse is shown in Figures 3.10 and 3.11. From the experiments it is evident that PRIM is valuable in providing insights into overall interaction in the system and in fact PRIM can be used to make mechanical design and process design changes in order to minimize inter-

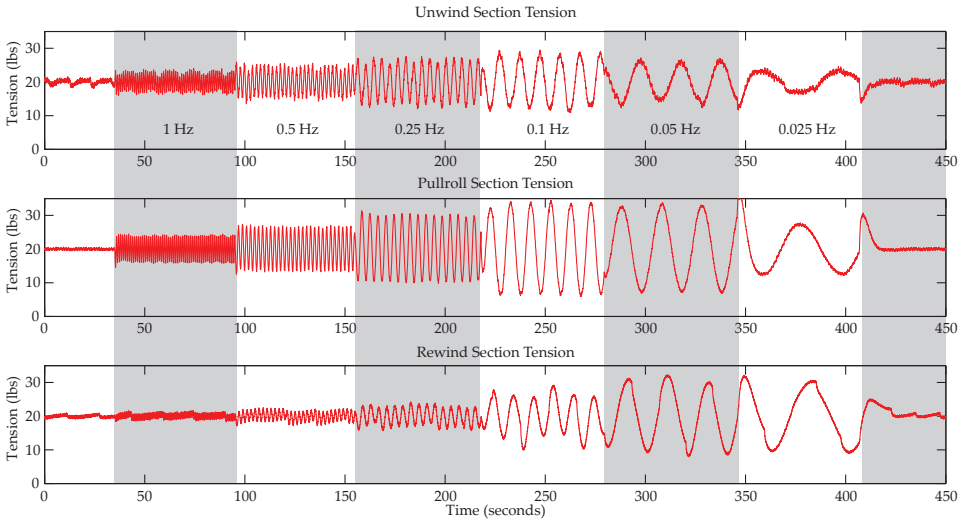

Figure 3.6: *Tension measurement at the unwind, pull roll and rewind section with sinusoidal velocity disturbances at the S-wrap section; web transport in the reverse direction. The alternate shaded and light regions show the sinusoidal velocity disturbances with six distinct frequencies with a 5 ft/min magnitude.*

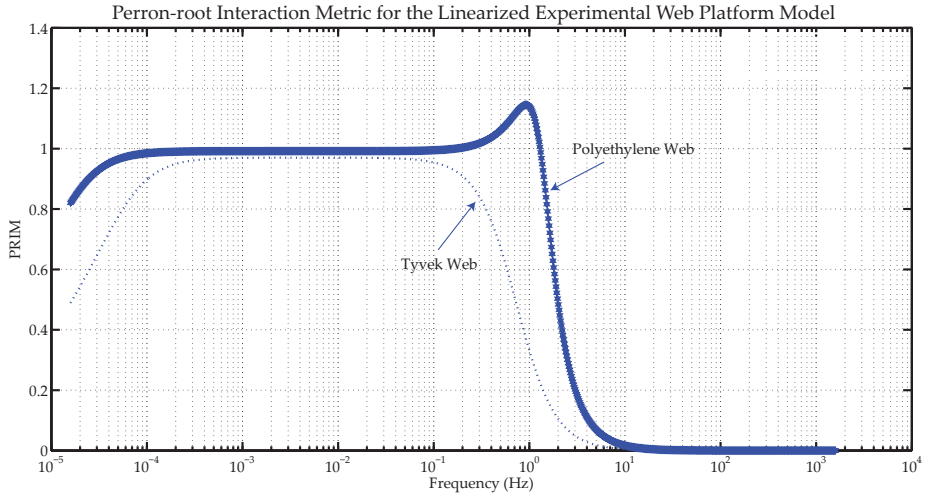

Figure 3.7: *Comparison of PRIM for two different web materials. Tyvek web: EA=2200 lbf; Polyethylene web: EA=7000 lbf.*

action in the system. Such a design based on interaction analysis is not currently available in literature and may be a valuable tool for industrial practitioners. Note that the governing equations (3.14) through (3.17) used in computing the PRIM are linearized equations and derived under several simplifying assump-

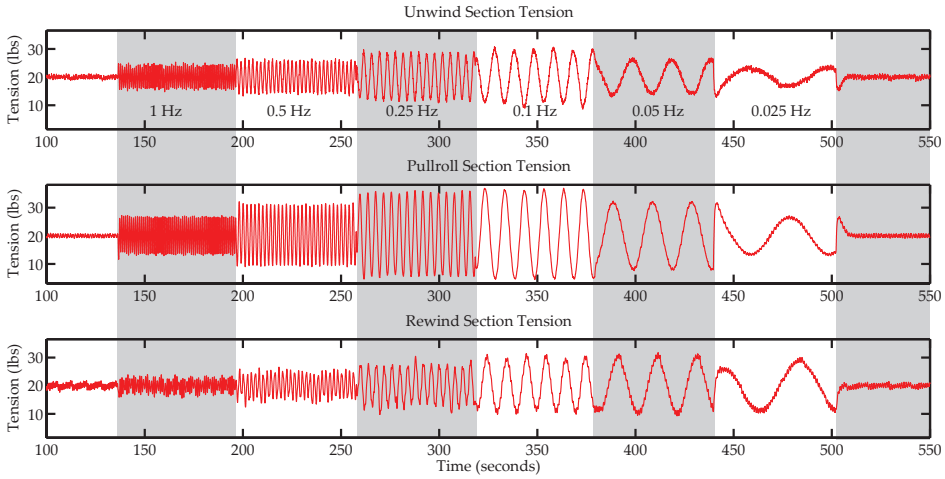

Figure 3.8: *Tension measurement at the unwind, pull roll and rewind section with sinusoidal velocity disturbances at the S-wrap section; web transport in the forward direction.*

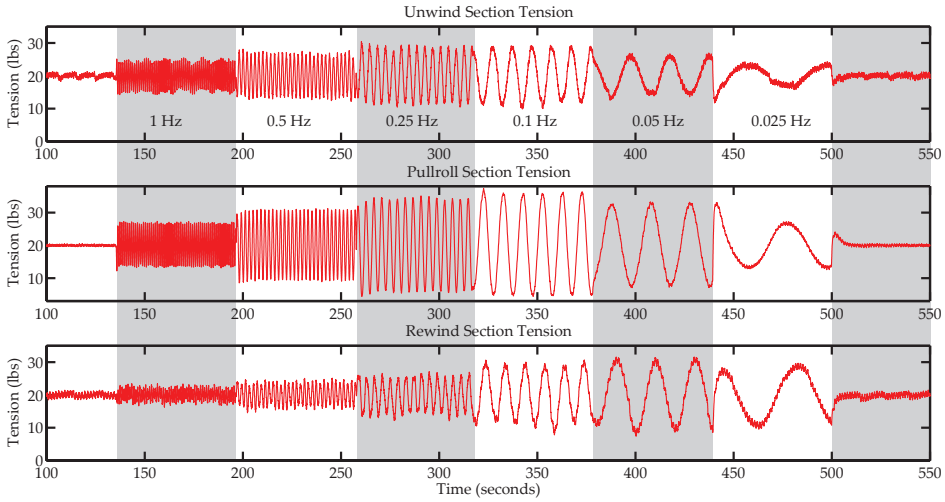

Figure 3.9: *Tension measurement at the unwind, pull roll and rewind section with sinusoidal velocity disturbances at the S-wrap section; web transport in the reverse direction.*

tions: web does not slip on the rollers, the effect of backlash and compliance in transmissions are neglected, the effect of idle rollers are neglected, etc. Additionally, the nonlinear web tension dynamics is linearized around a nominal operating condition to obtain the linearized model. In spite of these assump-

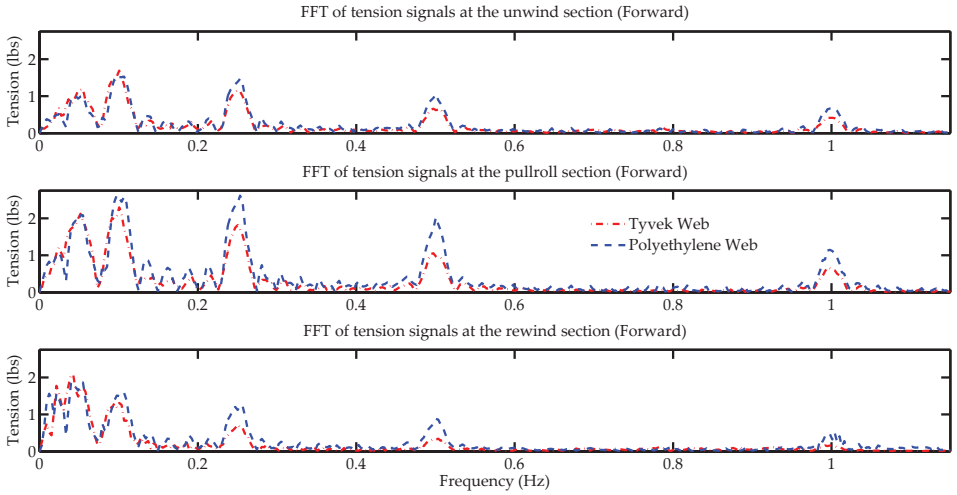

Figure 3.10: *FFT of tension measurement in the three tension zones with Tyvek and polyethylene webs; web is transported in the forward direction.*

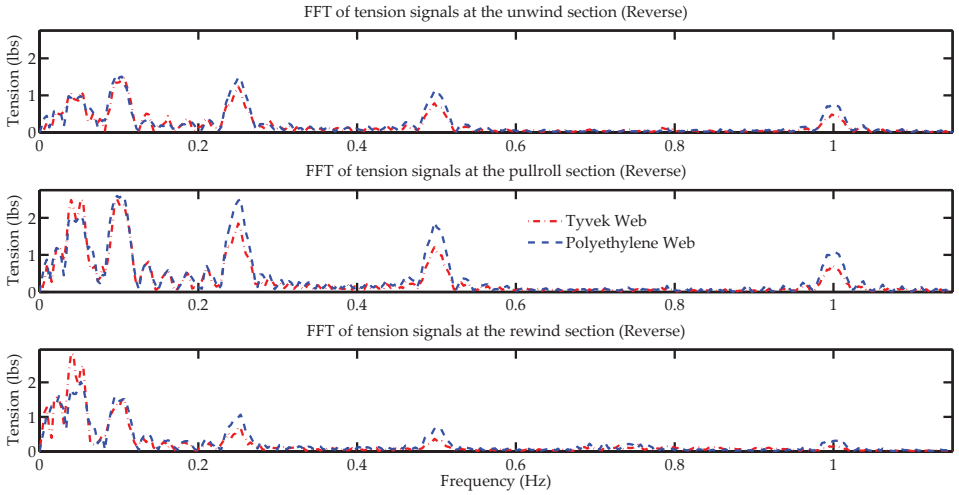

Figure 3.11: *FFT of tension measurement in the three tension zones with Tyvek and polyethylene webs; web is transported in the reverse direction.*

tions and constraints, the interaction in the actual system is predicted to a good degree by the PRIM.

3.4.3 Interaction Minimization

The optimal scaling vector that minimizes the interaction is given by the Perron right eigenvector; Figure 3.12 shows the magnitude of the Perron vector elements corresponding to each tension zone for a range of frequencies. A pre-filter for each tension zone is obtained by fitting a stable, minimum phase rational transfer function whose magnitude response is equal to the magnitude of the corresponding Perron vector element at that frequency. Figure 3.13 shows

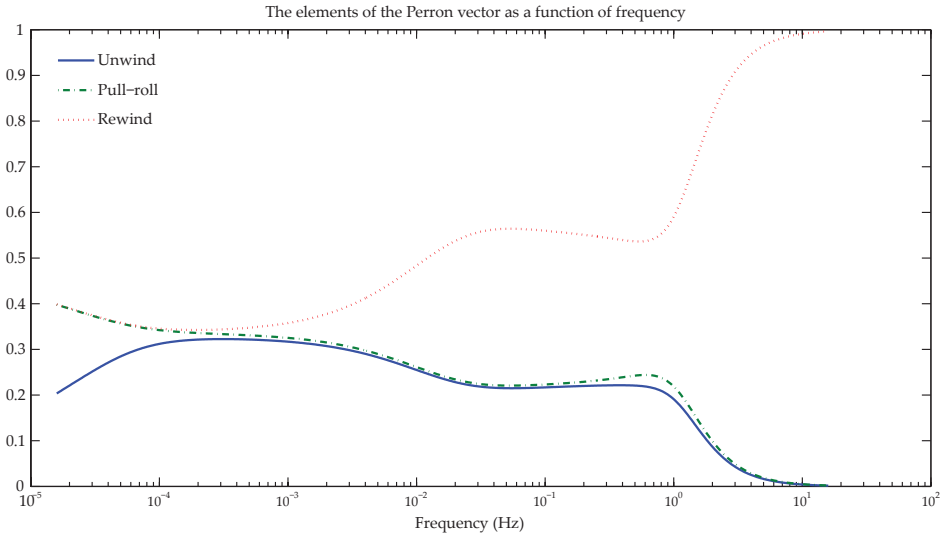

Figure 3.12: *Perron vector elements in the frequency range of interest*

the Bode magnitude response of the stable, minimum phase pre-filters fitted to match the magnitude of the Perron vector elements for the frequency range of interest. These fifth order lead-lag filters were used to filter the output of the existing outer tension loops in the experimental web platform.

Experiments were conducted with Tyvek web to observe the effect of the pre-filters in minimizing the interaction in the system; similar to the previous

Note that the Perron-Frobenius theorem ensures that the Perron vector is unique and its elements are positive, non-zero and their one norm is unity.

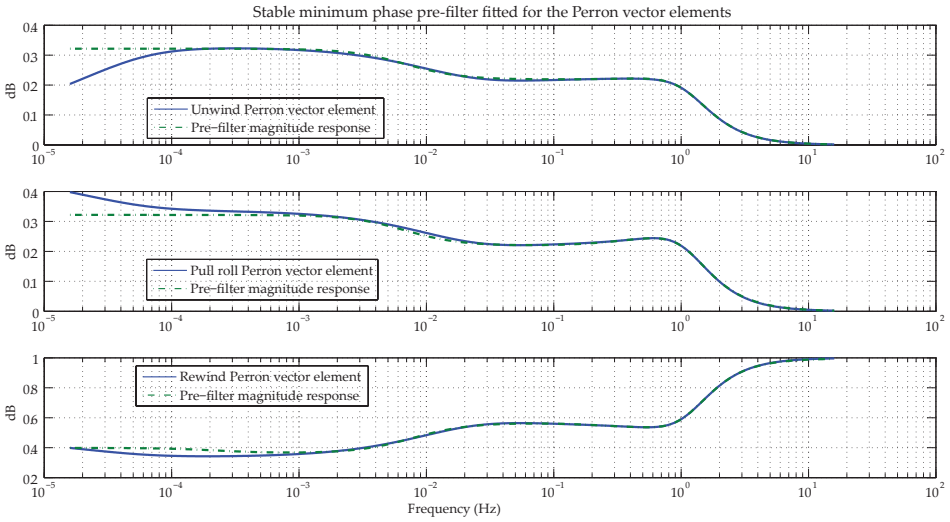

Figure 3.13: *Pre-filters for the three tension loops designed by fitting stable, minimum phase ration transfers for the elements of the Perron right eigenvector*

experiments, a sinusoidal velocity disturbance at the S-wrap is injected and the propagation of interaction in the system is evaluated by observing the tension measurement at the rewind section. Figures 3.14 and 3.15 show the experimental results with pre-filters. When compared to the experimental results shown in Figures 3.5 and 3.6, the results with the pre-filter show significant interaction reduction at the rewind section. Figure 3.16 shows the Fast Fourier Transform (FFT) of the tension signals in the three tension zones for the data shown in Figures 3.5 and 3.14. Figure 3.17 shows the FFT of tension signals for data shown in Figures 3.6 and 3.15. From the plots it is evident that the pre-filter minimizes the interaction at the rewind section. The experimental results shown in Figures 3.14 and 3.15 use the pre-filters shown in Figure 3.13 with a scaling factor of 4. Figure 3.18 shows the stability constraint with and without the scaled pre-

Note that a sinusoidal velocity disturbance at the S-wrap section acts as a sinusoidal input disturbance to the tension dynamics in both the unwind section and the pull roll section; this results in a sinusoidal tension disturbance in both these sections that contribute to the interaction in the rewind section.

filter, which shows the constraint is met for both cases.

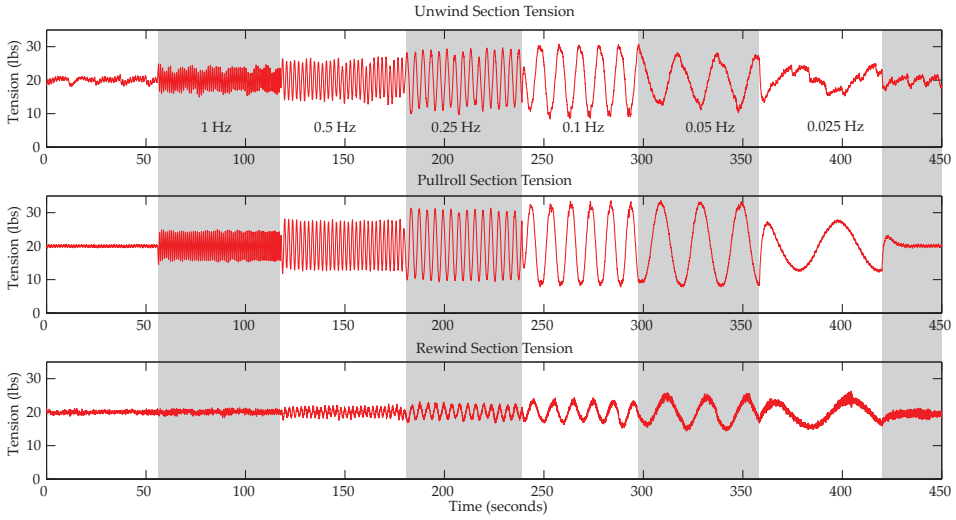

Figure 3.14: *Interaction in the experimental platform with pre-filter; tension measurement at the unwind, pull roll and rewind section with sinusoidal velocity disturbances at the S-wrap section; web transport in the forward direction.*

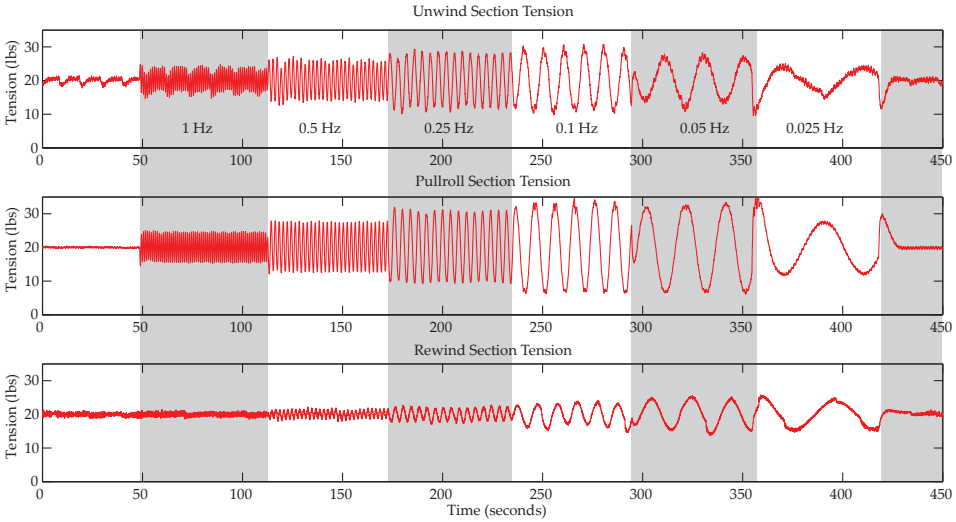

Figure 3.15: *Interaction in the experimental platform with pre-filter; tension measurement at the unwind, pull roll and rewind section with sinusoidal velocity disturbances at the S-wrap section; web transport in the reverse direction.*

The Perron vector of $\langle L_H \rangle$ also provides useful information regarding the interaction in the system. The relative magnitude of the elements of the Perron

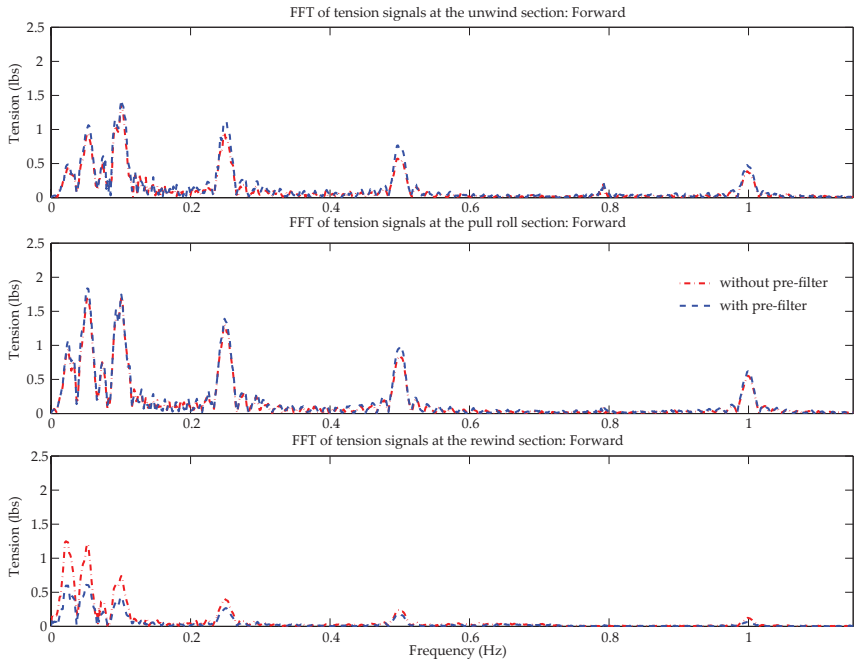

Figure 3.16: *FFT of tension measurement in the three tension zones with and without pre-filter; web is transported in the forward direction.*

vector indicate the effect of each input on the overall interaction in the system. From Figure 3.12 it can be observed that the magnitudes of all the Perron vector elements are equal between 10^{-4} Hz to 10^{-3} Hz indicating that all three sections have equal influence on the overall interaction in the system. As the frequency increases, the magnitude of the Perron vector element corresponding to the rewind tension loop is larger than the other two elements indicating that the rewind section has less influence on the interaction at those frequencies when compared to the unwind and the pull roll tension loops.

3.5 Discussion of PRIM and Other Interaction Metrics

In order to apply the Perron-Frobenius theory the non-negative matrix $\langle L_H \rangle$ needs to be irreducible for all frequencies. For the R2R processing applications, inter-

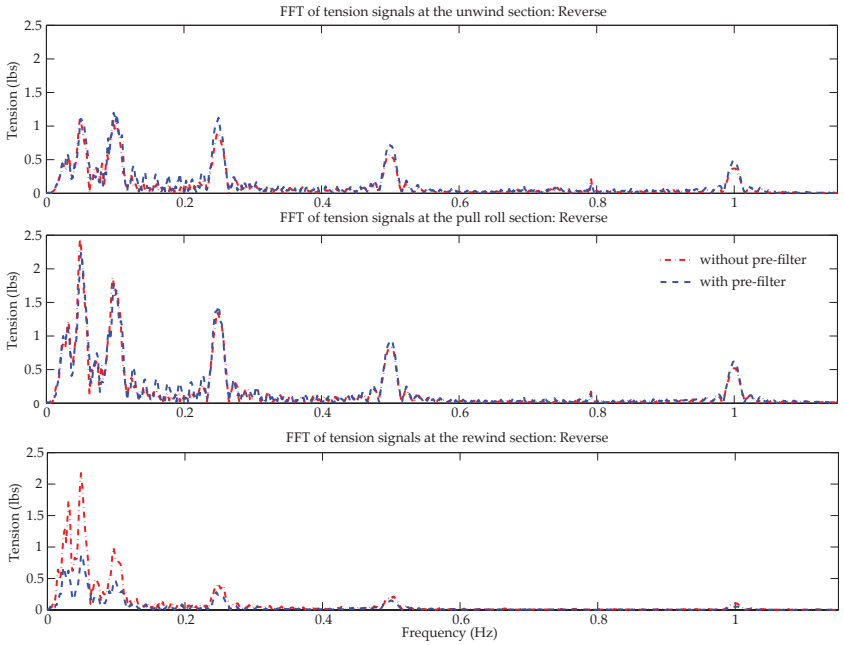

Figure 3.17: *FFT of tension measurement in the three tension zones with and without pre-filter; web is transported in the reverse direction.*

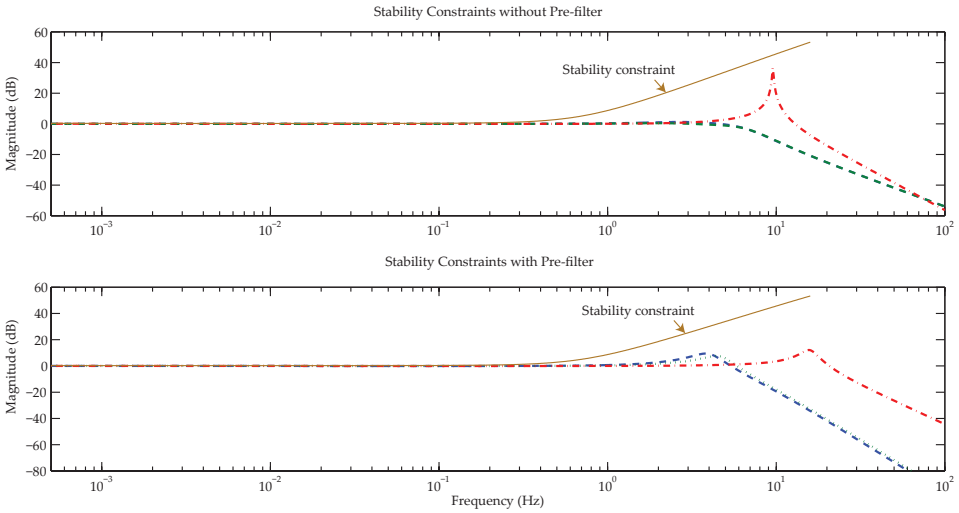

Figure 3.18: *Top and bottom plots show the closed-loop magnitude response ($|\overline{h}_i(s)|$) for the three tension loops (dashed and dotted lines) without and with pre-filter for the diagonal system $\overline{G(s)}$. The solid line is the stability constraint ($\frac{1}{p_{L_H}}$) for the overall system G.*

action between neighboring sections is unavoidable due to the physical connection of the web between sections. This results in a matrix $\langle L_H \rangle$ that is at least tridiagonal, and hence $\langle L_H \rangle$ is guaranteed to be irreducible. And for most large-scale interconnected systems such a connection between neighboring subsystems can be expected and hence PRIM would provide a valuable tool for interaction analysis.

It has to be noted that even though the Perron root can be computed only for square, irreducible, nonnegative matrices, the application of PRIM is not just limited to systems with equal number of inputs and outputs. In fact the practical example considered in the chapter is a R2R system with four inputs (motor torques) and seven outputs (web velocity at each driven roller and web tension in the three tension zones). By closing the inner velocity loops in the drive, the large-scale system was reduced to three SISO subsystems with the inputs being the tension trim to the tension loop and the outputs the web tension in the tension zones (subsystems). Since a large class of large-scale systems have, or can be reduced to SISO subsystems with decentralized controllers, the PRIM will serve as a valuable tool in those applications.

Both the PRIM and the SSVIM utilize the structural information of $\overline{H}$ to reduce the conservatism in the MSV based constraint. It is not always possible to compute the SSV exactly, rather an upper bound and lower bound for the SSV is computed using matrix transformation. It has been shown that for some special cases the upper bound is equal to the SSV and the lower bound is always equal to the SSV [45]. But for the decentralized control problem considered in this chapter (complex uncertainty structure with repeated scalar blocks), the exact computation of SSV is hard, especially when $n \geq 4$ [46, 47] and hence the

upper bound is typically used. The upper bound is computed using convex optimization techniques based on transformed matrices. For complex uncertainty structure the upper bound can be obtained from the following matrix transformation as

$$\mu_{\overline{H}}(L_H) \leq \inf_{D\in\mathscr{D}} \overline{\sigma}(DL_HD^{-1}) \tag{3.18}$$

where $\mathscr{D} \in \mathscr{R}^{n\times n}$ is the family of diagonal matrices with the diagonal entries $d_i > 0,\ \forall i \in [0,n]$. Hence the relationship between SSVIM and PRIM can be obtained from Lemma 3.3.11 as

$$\mu_{\overline{H}}(L_H) \leq \inf_{D\in\mathscr{D}} \overline{\sigma}(DL_HD^{-1}) \leq p_{L_H}. \tag{3.19}$$

Additionally, for the decentralized problem considered here the upper bound for SSV is bounded by the Perron root from above and below by [48]

$$\frac{1}{\sqrt{n}} p_{L_H} \leq \inf_{D\in\mathscr{D}} \overline{\sigma}(DL_HD^{-1}) \leq p_{L_H}. \tag{3.20}$$

Even though the PRIM is more conservative than the SSVIM, there are several reasons to choose PRIM for the decentralized control problem considered in this chapter. First, the Perron root can be computed accurately using simple iterative algorithms that are very fast [40, 49]. The numerical results shown in this chapter uses the algorithm presented in [49] that neither use diagonal transformations nor use Perron complement idea and attains a convergence rate of at least quadratic. The SSV computation on the other had is computationally complex involving many steps depending on the complexity of the uncertainty structure [50, 51]. For the problem considered in this chapter the SSV upper bound computation involves purely complex uncertainty structure with repeated scalar blocks that can be solved using a fast algorithm presented in [52, 51]. The first step of the multi-step algorithm involves balancing the complex matrix L_H with

diagonal transformation D^* so that the optimization problem is numerically stable and efficient. A modified Osborne's algorithm [53] that minimizes the Frobenius norm of

$$\inf_{D^* \in \mathscr{D}} ||(D^* L_H D^{*-1})||_F$$

is used to obtain the diagonal transformation for balancing. Alternatively, the Perron eigenvector of $\langle L_H \rangle$ which is the suboptimal scaling for the transformation in Equation (3.18) is used for balancing the complex matrix L_H; the Osborne's scaling and the Perron vector scaling have similar computational speeds [52]. Hence the use of PRIM is computationally inexpensive when compared to SSVIM that requires the computation of Perron vector just to complete the initial step.

Second, the Perron root is equal to the SSV upper bound if a pair of unitary diagonal matrices exist such that [43]

$$\langle L_H(j\omega) \rangle = \Theta(j\omega) L_H(j\omega) \Psi^{-1}(j\omega). \tag{3.21}$$

For the problem considered in this work PRIM is a good approximation of the upper bound for SSVIM and in fact for R2R system in this paper the PRIM and SSVIM are identical as evident from Figure 3.19.

Finally, the algorithm for the computation of the Perron root also readily provides the optimal pre-filter magnitudes that minimize interaction in the system. Note that the frequency shaping effect of the pre-filter from PRIM is similar to the filter in multiloop internal model control (IMC) design [36] and a similar interpretation related to the constraints of the filter in multiloop IMC control is closely related to the magnitude of Perron eigenvector elements. Moreover, the stability constraint provided using IMC control is very similar to the stability constraint provided in equation (3.6). The distinction is that PRIM provides an

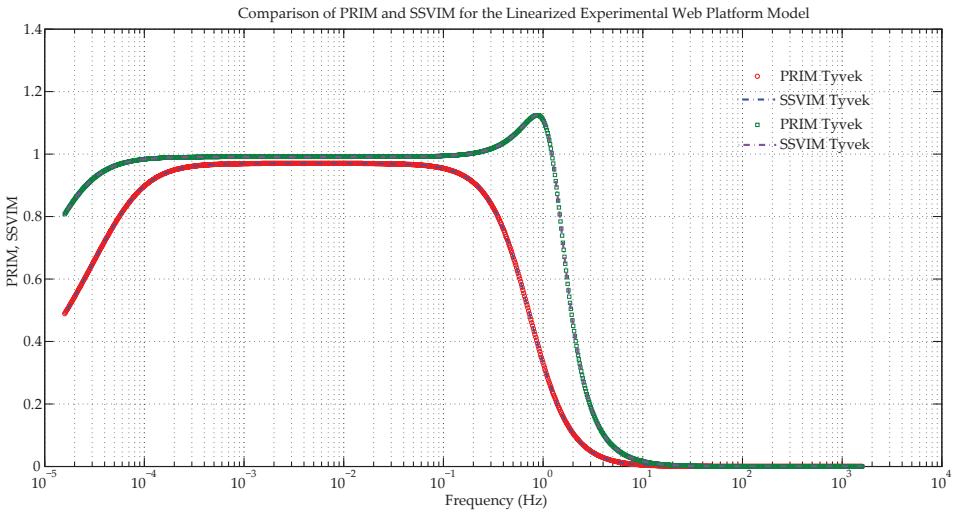

Figure 3.19: *PRIM and SSVIM for the linearized R2R platform model with Tyvek and Polyethylene webs.*

overall level of interaction while IMC interaction measure provides both interaction in terms of row sum and column sum of $\langle L_H \rangle$ that is primarily used for loop-paring. Neither SSVIM nor IMC interaction measure provide a systematic procedure to minimize the overall interaction in the system.

In the decentralized design example illustrated in this chapter the diagonal pre-filter that was obtained from the Perron right eigenvector minimized interaction without degrading individual subsystem performance. It may not be possible to guarantee that the pre-filter maintains the individual subsystem performance. Hence it is necessary to look at possible ways to design the controller and the pre-filter simultaneously so that interaction is minimized and some nominal performance is guaranteed. This problem is similar to the μ-synthesis problem (D-K iteration) in robust control applications [54]. Some of the results in non-negative matrix theory [55, 56, 57] may be used as a possible starting point for solving the simultaneous controller and pre-filter design problem.

CHAPTER 4

Analysis and Control of Print Registration

The primary objective of this work is to control registration error in order to improve print output and productivity. It is possibel to minimized registration error passively by appropriate machine design that reduces machine induced disturbances (based on the model analysis similar to those presented in Chapter 2), or actively by controlling the propagation of machine induced disturbances (by using a pre-filter such as the one described in Chapter 3), or a combination of both. Apart from minimizing the effect of machine induced disturbances, registration error may be controlled actively by using either: (1) a compensator that changes the web path length in the print unit or (2) a print cylinder where the angular position is controlled to correct for registration error. Current industrial trend is to directly control the angular position of the print cylinder to control registration error. The analysis presented in Chapter 2 indicate that a compensator provides an additional degree of freedom to control both registration error

and web strain. A systematic comparison of these control strategies will enable the R2R printing community to choose a control strategy based on their requirements and capabilities. In this chapter the two registration controls strategies, Compensator based Registration Control (CRC) and Print cylinder Angular position based Registration Control (PARC), are analyzed based on the model developed in Chapter 2 and the analysis tool developed in Chapter 3; open loop analysis in terms of disturbance propagation with the two control strategies is presented in Section 4.1 and closed loop analysis in terms of control design and stability characteristic is presented in Section 4.2. In both CRC and PARC the angular velocities of the print cylinders are regulated using independent motors, which is referred to as electronic line shafting.

Existing registration control algorithms in the literature are developed predominantly for PARC with one or two print units [20, 58, 22, 59]. These control algorithms involve communication of measurements such as web speed and tension between print units and also require past values of these measurements to stabilize the system. Moreover, propagation of disturbances due to registration error correction in one print unit with PARC affects other print units and this disturbance propagation is often minimized using a cooperative control strategy where the control input from one print unit is fed forward to the subsequent print unit [22, 59]. Even the existing CRC algorithms in literature require a centralized control structure with exchange of information between print units and storage of past measurements [60, 21].

Typical industrial controllers for web tension and velocity regulation are simple, decentralized controllers based on measurements from the respective tension zones. A centralized or a cooperative controller is seldom used because of

the complexity involved in data communication between different sections in a R2R machine, and more importantly, because of erroneously providing control corrections in those sections of the web line where compensation is not required. From a practical implementation stand point simple, decentralized controllers for R2R printing applications will have a high likelihood of adoption in industrial controllers when compared to complex cooperative control algorithms currently available in the literature.

4.1 Analysis of Interaction in R2R Printing

Like any other R2R process, printing involves more than one print unit and hence R2R printing machines can be considered as a large scale interconnected system with several subsystems, the subsystems being the print units or the tension zones between the driven print cylinders. Because of the interconnections due to web transport, tension disturbances propagate between different tension zones. Since the registration error is affected primarily by tension disturbances, it is important to understand and control propagation of tension disturbances within the R2R system in order to achieve the stringent registration requirements for flexible printed electronics. Moreover, control of registration error using either CRC or PARC will affect web strain and registration error in adjacent print units. The analysis of interaction using PRIM will provide insights on both machine design and control design for better print registration control.

The model developed in Chapter 2 is considered for analysis in this chapter. For a single print unit with two print cylinders and the web span between the two

cylinders (see Figure 4.1) the registration error governing equation is given by

$$e_1(t) = l - \int_{t-\tau_1}^{t} \frac{r_1\omega_1(\tau)}{1+\bar{\epsilon}_2(\tau)}d\tau - \left[r_2\theta_2(t) - \frac{r_1\theta_1(t-\tau_1)}{1+\bar{\epsilon}_2(t)}\right] + \int_{t-\tau_1}^{t-\tau_2} \dot{\tilde{l}}(\tau)d\tau$$

and the governing equation for strain is given by

$$\dot{\epsilon}_2(t) = \frac{1+\epsilon_2(t)}{l+\tilde{l}(t)}\left[r_2\omega_2(t) + \dot{\tilde{l}}(t) - r_1\omega_1(t)\frac{1+\epsilon_2(t)}{1+\epsilon_1(t)}\right]. \tag{4.1}$$

These governing equations are linearized around nominal operating conditions,

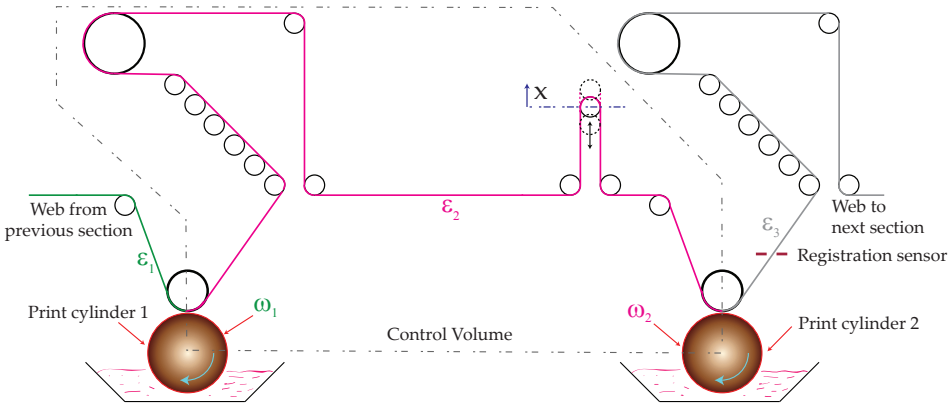

Figure 4.1: *A schematic showing the web between two successive print cylinders; some of the idle rollers are ignored.*

such as, nominal web speed and nominal web tension to obtain a linear model that can be analyzed using PRIM. It is assumed that all the print cylinders have the same radius r, nominal angular velocity ω^* and the angular velocity variation above the nominal speed $\Delta\omega_i$. It is also assumed that the impression roller dynamics can be neglected and that the web dynamics directly affect the print cylinder dynamics. The web is assumed to be elastic and the tensile force experienced by the web is related to web strain through the constitutive relationship $\epsilon_i = T_i/EA$ where ϵ is the web strain and T_i is the tension in the i^{th} web span, E is the modulus of elasticity of the web material and A is the cross sectional area

of the web. Moreover, the modulus of web material used in most R2R printing systems is sufficiently large and hence the strain experienced by the web is typically small. By assuming web strain (or relative strain) is small, the following approximation is introduced

$$\frac{1}{1+\epsilon_i} \approx (1-\epsilon_i). \tag{4.2}$$

The subscript convention for various parameters in print unit i is as follows. The angular velocities of the print cylinders in print unit i are ω_i (upstream print cylinder) and ω_{i+1} (downstream print cylinder). The web strain within the i^{th} print unit span is ϵ_{i+1}, the change in span length due to compensator roller in that span is $\tilde{l}_i$ and the registration error is e_i. With this convention, the linearized registration error for each print unit i (using the small strain assumption) is

$$\dot{e}_i = r\omega^*[\overline{\epsilon}_{i+1}(t)-\overline{\epsilon}_{i+1}(t-\tau_1)]+r[\Delta\omega_i(t-\tau_1)-\Delta\omega_{i+1}(t)]+\dot{\tilde{l}}_i(t-\tau_2)-\dot{\tilde{l}}_i(t-\tau_1), \tag{4.3}$$

the linearized strain equation is

$$l\dot{\epsilon}_{i+1} = -r\omega^*[\epsilon_{i+1}(t)-\epsilon_i(t)]+\dot{\tilde{l}}_i(t)+r[\Delta\omega_{i+1}(t)-\Delta\omega_i(t)] \tag{4.4}$$

and the variational print cylinder velocity dynamics is

$$J_{i+1}\Delta\dot{\omega}_{i+1} = -b_{f_{i+1}}\Delta\omega_{i+1}+\overline{\tau}_{i+1}+rEA[\epsilon_{i+1}-\epsilon_i] \tag{4.5}$$

where $\overline{\epsilon}_i = \epsilon_i - \epsilon_{i-1}$ is the relative web strain, J_i is the rotational inertia, b_{f_i} is the viscous friction coefficient and $\overline{\tau}_i$ is the torque above the nominal torque for the i^{th} print cylinder. Equations (4.3)–(4.5) clearly show the interconnection between the print units which contribute to the interaction within printing presses.

The interaction analysis is carried out on a print section with eight print cylinders and seven print units as shown which is Figure 4.2. The control inputs in each print unit are the torque supplied to the print cylinder and the rate

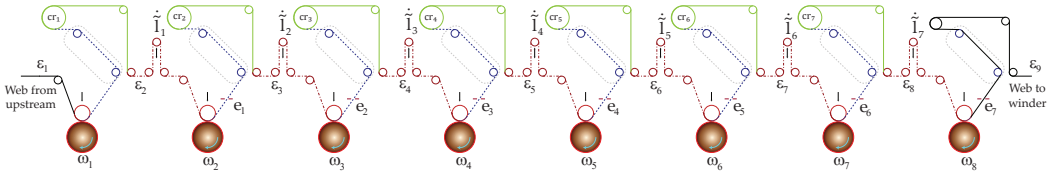

Figure 4.2: *Schematic of a print section with seven print units and eight print cylinders.*

of change of span length due to the compensator motion. The outputs in each print unit are the three state variables, the downstream print cylinder velocity, the web strain within the print unit span and the registration error in the print unit. The overall linearized dynamics, including machine, web and registration error dynamics, for the print section with seven print units is represented in the state space form as

$$\dot{x}(t) = A_0 x(t) + A_1 x(t-\tau_1) + B_{0c} u_1(t) + B_{0t} u_2(t) + B_{1c} u_1(t-\tau_1) + B_{2c} u_1(t-\tau_2) \quad (4.6)$$

where $x \in \mathscr{R}^{22\times 1}, u_1 \in \mathscr{R}^{7\times 1}, u_2 \in \mathscr{R}^{8\times 1}$ are given by

$$x(t) = [\Delta\omega_1, \epsilon_2, e_1, \Delta\omega_2, \epsilon_3, e_2, \Delta\omega_3, \ldots, \epsilon_8, e_7, \Delta\omega_8]^\top,$$
$$u_1(t) = \left[\dot{\bar{l}}_1, \dot{\bar{l}}_2, \ldots, \dot{\bar{l}}_7\right]^\top, \; u_2(t) = [\overline{\tau}_1, \overline{\tau}_2, \ldots, \overline{\tau}_8]^\top,$$

A_0 is the state matrix corresponding to the states without delays, A_1 is the state matrix corresponding to the states with delay τ_1, B_{0c} and B_{0t} are the input matrices corresponding to inputs u_1 and u_2 without delays, and B_{1c}, B_{2c} are input matrices corresponding to input u_1 with delays τ_1 and τ_2, respectively.

The PRIM is used to analyze the level of interaction in the print section with seven print units with CRC and PARC. It quantifies the overall effect of each control input on all other outputs, i.e., the effect of compensator motion in one print unit on registration error in all other print units for a compensator based registration control, and the effect of print cylinder angular position correction in one

print unit on registration error in all other print units for PARC. A linear fractional transform based modeling of linear time invariant systems with delay is used to compute the frequency response of the system described in Equation(4.6) using MATLAB [61]. For CRC the frequency response is computed with rate of change of span length at each print unit ($\dot{\tilde{l}}_i, i = 1,\ldots,7$) as input and registration error ($e_i, i = 1,\ldots,7$) at the respective print units as the output. And for PARC the frequency response is computed with the torque to print cylinder ($\overline{\tau}_i, i = 2,\ldots,8$) at each print unit as input and registration error ($e_i, i = 1,\ldots,7$) at the respective print units as the output.

For the sake of comparison, parameters from the Armstrong print line is used to compute PRIM and the values of the parameters are given in Table 4.1. Figure 4.3 shows the PRIM for the two control strategies where the top plot shows the interaction in registration error due to CRC and the bottom plot shows the interaction due PARC. From these plots it is evident that the magnitude of interaction in print units with PARC is much larger than for print units CRC at low frequencies. And as the frequency increases beyond 10 Hz the interaction is about the same with both control strategies.

The magnitude of interaction is lower in CRC when compared to PARC because of the manner in which strain is transported. As the compensator is positioned to reduce the registration error in one print unit, the motion of the compensator directly affects web strain within that span. This strain variation affects the velocity dynamics of the print cylinders within that span and thereby affects web strain in adjacent spans. Therefore the motion of the compensator has an

The high frequency interaction behavior is consistent with analysis presented in the previous chapter where the interaction in the experimental platform is zero beyond 10 Hz. This is because the strain dynamics acts as a low pass filter that filters the high frequency disturbance propagation.

Symbol	Parameter	Value	Units
EA	Web Parameter	28080	lbf
$r\omega^*$	Nominal Web Speed	36	in/sec
b_f	Friction Coefficient	0.1	lb-in-sec
J	Print Cylinder Moment of Inertia	192	lb-in-sec^2
l	Span Length	650	inch
r	Print Cylinder Radius	8.6	inch
τ_1	Time Constant	18	second
τ_2	Time Constant	6.3	second

Table 4.1: *Web transport parameters used in interaction analysis.*

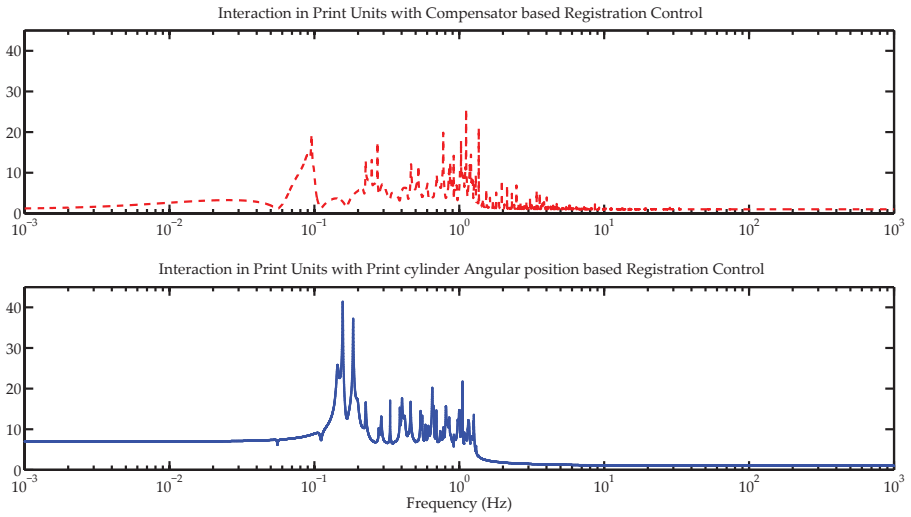

Figure 4.3: *Perron root interaction metric for print units with CRC and PARC.*

indirect effect on web strain in adjacent spans. But for print units with PARC, the control of the angular position or the angular velocity of a print cylinder directly affects web strain in the spans immediately upstream and downstream of that print cylinder. Therefore, the control of registration error with PARC has a direct effect on web strain in adjacent spans, contributing to a larger magnitude of interaction.

Interaction in print units employing CRC and PARC is further studied based on open loop time domain simulations and a representative sample of results

is shown in Figures 4.8–4.21. In all the simulations the initial conditions for the states are set to zero and an input is provided to correct registration error in print unit 1; for CRC the input is the rate of change of span length to print unit 1 and for PARC the input is the torque input to print cylinder 2. The magnitudes of the inputs are appropriately scaled so that the registration error correction provided by the control input for the two strategies are almost the same; the magnitude of rate of change of span length due to compensator motion is taken as 0.0401 in/sec and the magnitude of torque input to the print cylinders is taken as 0.5643 lb-in for all the simulations. The top plot in all the figures shows the registration error correction in print unit 1 and the second plot shows the registration error in all other print units, i.e., the interaction in the system. The bottom two plots in all the figures show web strain ($\epsilon_i, i = 2,3,4,5,6,7,8$) in all print units and web speed ($r\Delta\omega_i, i = 1,2,3,4,5,6,7,8$) above the nominal web speed ($r\omega^*$) at all print cylinders. Inputs in the form of pulse and sinusoidal disturbances are used to analyze interaction in the system with CRC and PARC.

Figures 4.8–4.11 show the open loop response with CRC and PARC for a pulse input in print unit 1. These simulations indicate that interaction in CRC is an order of magnitude less than the magnitude of registration error correction seen in print unit 1. While with PARC the magnitude of correction provided in print unit 1 is propagated to subsequent print units. This observation is consistent with the PRIM analysis.

To further see the interaction as a function of frequency, sinusoidal inputs were introduced to simulate the open loop system response for CRC and PARC. Figures 4.12–4.21 show the time domain response with sinusoidal inputs with CRC and PARC for frequencies $0.05, 0.1, 0.5, 1$ and 1.5 Hz. From these plots it is

This is a typical magnitude for registration correction rate in Armstrong print line.

evident that at low frequencies (0.05 and 0.1 Hz) the magnitude of interaction with PARC is greater than or equal to the magnitude of the correction provided in print unit 1; while CRC exhibits a smaller magnitude of interaction at those frequencies. Consistent with the PRIM analysis, interaction with CRC increases when the input frequencies are 0.5 and 1 Hz and decreases significantly as the input frequency increases beyond 1.5 Hz.

Even though the interaction is lower with CRC, the compensator motion introduces additional delay in control input while adding an additional degree of freedom to control the state variables. For PARC the dynamics of the print section given in Equation 4.6 reduces to

$$\dot{x}(t) = A_0 x(t) + A_1 x(t-\tau_1) + B_{0c} u_1(t) \tag{4.7}$$

which is simpler when compared to CRC. In the following section the two control strategies are compared based on control design and stability characteristic.

4.2 Comparison of Registration Control Strategies

In this section a closed loop analysis of registration control in print units with CRC are PARC strategies is presented. The comparison of the two control strategies is based on the stability analysis of the two types of delayed systems. The system with the CRC strategy involves both internal delays (delay in state variables) and control delays (delay in control input) while the system with the PARC strategy involves only an internal delay.

Stability of time delay systems may be analyzed using either time or frequency domain techniques; a frequency domain based analysis is considered in this work. Some preliminaries related to the stability of time delay systems are presented in Section 4.2.1 and control design based on these stability conditions

is discussed in Sections 4.2.2 and 4.2.3 for CRC and PARC, respectively. Readers unfamiliar with analysis and control of time delay systems are referred to the book [62] and overview articles on recent advances, open problems and opportunities [63, 64]. Most of the results available in the control literature are based on results from functional differential equations theory provided in [65].

4.2.1 Stability of Time Delay Systems

Consider the following LTI system described by the state-space equations

$$\dot{x}(t) = \tilde{A}_0 x(t) + \sum_{k=1}^{m} \tilde{A}_k x(t - r_k), \quad r_k \geq 0, k = 1, \ldots, m, \tag{4.8}$$

$x(t) \in \mathscr{R}^{n\times 1}, \tilde{A}_k \in \mathscr{R}^{n\times n}$ and r_k are independent incommensurate delays; the LTI system is a special case of a retarded functional differential equation with a linear operator having time-invariant coefficients. The stability of the system is ascertained from the characteristic quasipolynomial (or characteristic function)

$$p(s; e^{-r_1 s}, \ldots, e^{-r_m s}) = \det\left(sI - \tilde{A}_0 - \sum_{k=1}^{m} \tilde{A}_k e^{-r_k s} \right) \tag{4.9}$$

and is defined below.

Definition 4.2.1 (Definition 2.1 [62]). *The characteristic function (4.9) is said to be stable if*

$$p(s; e^{-r_1 s}, \ldots, e^{-r_m s}) \neq 0, \quad \forall s \in \overline{\mathscr{C}}_+.$$

It is said to be stable independent of delay if (4.9) holds for all $r_k \geq 0, k = 1, \ldots, m$. The system (4.8) is said to be stable if its characteristic function (4.9) is stable, and is stable independent of delay if its characteristic function is stable independent of delay.

Stability analysis for systems with commensurate delays where $r_k = k\tau$, $k = 1, \ldots, m$ are relatively easier than for systems with incommensurate delays where r_k are assumed to be independent of each other.

Definition 4.2.2 (Delay-Independent Stability)**.** *The time delay system* (4.8) *is said to be stable independent of delay if the stability condition is satisfied for all possible nonnegative delay values.*

Definition 4.2.3 (Delay-Dependent Stability)**.** *If the time delay system* (4.8) *is stable only for a subset of nonnegative delay values then the stability is dependent on delay.*

From the above definitions it is clear that delay-independent stability is a stronger condition than a delay-dependent stability condition.

The necessary condition for the system to be stable independent of delay is that $\tilde{A}_0$ be stable since the characteristic polynomial should have no right half plane roots when the delay is infinite. The system (4.8) is stable independent of delay if and only if

$$\det\left(I-(sI-\tilde{A}_0)^{-1}\sum_{k=1}^{m}\tilde{A}_k e^{-r_k s}\right)\neq 0,\quad \forall s\in\overline{\mathscr{C}}_+,\ \forall r_k\geq 0. \tag{4.10}$$

A small gain type approach may be followed to provide sufficient conditions for stability. The system in (4.8) can be represented in the M-Δ loop structure using a lower linear fractional transformation with $\dot{x}(t)=\mathscr{F}_l(M,\Delta)x(t)$ as shown in Figure 4.4 with M given by

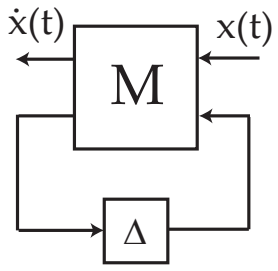

Figure 4.4: *$M-\Delta$ loop representation of the system in* (4.8)

$$M = \begin{bmatrix} M_{11} & M_{12} \\ M_{21} & M_{22} \end{bmatrix} = \begin{bmatrix} \tilde{A}_0 & [\tilde{A}_1 \dots \tilde{A}_m] \\ \begin{bmatrix} I \\ \vdots \\ I \end{bmatrix} & \mathbf{0} \end{bmatrix}$$

and Δ is the delay operator represented as the block diagonal uncertainities as

$$\Delta = \begin{pmatrix} \Delta_1 & & \\ & \ddots & \\ & & \Delta_m \end{pmatrix}$$

with $\Delta_k x(t) = x(t - r_k)$. From the small gain theorem the sufficient condition for delay-independent stability, provided $\tilde{A}_0$ is stable, is that

$$\sup_{s \in \overline{\mathscr{C}}_+} ||M(s)|| < 1 \quad \text{or} \quad \sup_{\omega > 0, \omega \in \mathscr{R}} ||M(j\omega)|| < 1 \tag{4.11}$$

where $||\cdot||$ is any induced matrix norm. The second condition is valid since $M(s)$ and $\Delta(s)$ are analytic in the closed right half plane and hence any induced matrix norm will reach its maximum on the boundary $\partial \mathscr{C}_+$ [66]. The conservativeness in the small gain condition is overcome by using the structured singular value based stability conditions that provide both necessary and sufficient conditions. The following theorem provides the stability conditions using the structured singular value.

Theorem 4.2.4 (Theorem 3.5 [62]). *Let $r_k \geq 0, k = 1,\ldots,m$ be independent, incommensurate delays. Then the system (4.8) is stable independent of delay if and only if*

1. *$\tilde{A}_0$ is stable,*
2. *$\sum_{k=0}^{m} \tilde{A}_k$ is stable,*
3. *$\mu_{\mathscr{X}_m}(M(j\omega)) < 1, \quad \forall \omega > 0,$*

where

$$M(s) \triangleq \begin{pmatrix} I \\ \vdots \\ I \end{pmatrix} \left(sI - \tilde{A}_0\right)^{-1} \left(\tilde{A}_1 \ldots \tilde{A}_m\right),$$

$\mathscr{X}_m$ is a block diagonal uncertainty of the form

$$\mathscr{X}_m \triangleq \{diag(\delta_1 I_{k_1}, \ldots, \delta_m I_{k_m}) | \delta_k \in \mathscr{C}\}$$

and $\mu_{\mathscr{X}_m(.)}$ is the structured singular value of $(.)$ with respect to the uncertain diagonal structure $\mathscr{X}_m$.

Apart from the well known computational complexity involved in the accurate computation of the structured singular value, especially for uncertainty structures with repeated scalar blocks [46], it has been shown that the delay independent stability problem for systems with incommensurate delays is a NP-hard problem [62] with respect to the number of incommensurate independent delays. Hence, less demanding sufficient conditions are used to show stability in systems with incommensurate delays and often is the only available tool for systems with incommensurate delays.

Theorem 4.2.5 (Theorem 3.15 [62]). *Let $r_k \geq 0, k = 1,\ldots,m$ be independent, incommensurate delays. Suppose that $\tilde{A}_0$ is stable. Then the system (4.8) is stable independent of delay if one of the following conditions hold.*

1. $\mu_{\mathscr{X}_m}(M(j\omega)) < 1,\ \forall \omega \geq 0.$
2. *For any absolute or unitary invariant induced matrix norm $||.||$,*
$$||M(j\omega)|| < 1,\ \forall \omega \geq 0.$$
3. $||(sI - \tilde{A}_0)^{-1}(\tilde{A}_1,\ldots,\tilde{A}_m)||_\infty < 1/\sqrt{m}.$

Hence a sufficient condition based on a D-weighted l_p Holder norm given by the Perron root of a nonnegative matrix can be obtained as

Corollary 4.2.6. *Let $r_k \geq 0, k = 1,\ldots,m$ be independent, incommensurate delays. Suppose that $\tilde{A}_0$ is stable. Then the system (4.8) is stable independent of delay if*

$$\sup_{\omega \geq 0} \mathscr{P}(\langle M(j\omega)\rangle) < 1$$

where $\mathscr{P}(.)$ is the Perron root of the nonnegative matrix $\langle M(j\omega)\rangle$ and $\langle M(j\omega)\rangle$ is a nonnegative matrix such that $\langle M(j\omega)\rangle_{kl}$ is the magnitude of $M(j\omega)_{kl}$ at the frequency ω.

Proof. Since Δ is diagonal, $\mathscr{P}(\langle M(j\omega)\rangle)$ is a D-weighted induced Hölder l_p norm in $\mathscr{C}^n$ for $||M(j\omega)||$. Hence from Theorem 4.2.5 the sufficient condition for delay-independent stability is satisfied if $\sup_{\omega\geq 0} \mathscr{P}(\langle M(j\omega)\rangle) < 1$. □

It is noted that the Perron root based sufficient condition is more conservative than the SSV based condition because of the structure of the uncertainty or the delays. The conservativeness reduces with the order of the system. Hence for large systems, the Perron root based stability condition will result in an overly

conservative constraint which might serve to be impractical. A SSV based analysis will be used in the rest of our analysis.

In many situations the sufficient conditions for delay-independent stability criteria may not be satisfied since the stability is checked for all possible delay values. For many practical problems, such as, registration in roll-to-roll printing, an upper bound for the delay can be found and this information can be used to obtain a delay dependent stability condition. A model transformation is typically used to convert the retarded delayed differential equation with discrete incommensurate delays into a retarded delayed differential equation with distributed delay [62]. For the system in Equation 4.8, the model transformation can be obtained from the fact that

$$x(t-r_i) = x(t) - \int_{t-r_i}^{t} \dot{x}(u)\,du \tag{4.12a}$$

$$= x(t) - \int_{t-r_i}^{t} \left[\sum_{k=0}^{m} \tilde{A}_k x(u-r_k)\right] du. \tag{4.12b}$$

Hence the original system in Equation 4.8 can be rewritten with the additional dynamics as

$$\dot{x}(t) = \left(\sum_{i=0}^{m} \tilde{A}_i\right) x(t) - \sum_{i=1}^{m} \tilde{A}_i \int_{t-r_i}^{t} \left[\sum_{k=0}^{m} \tilde{A}_k x(u-r_k)\right] du. \tag{4.13}$$

The stability of the transformed system (4.13) implies stability of the original system (4.8) but the reverse is not true because of the additional dynamics [62]. The characteristic quasipolynomial of the transformed system (4.13) can be obtained as [62, pg. 85]

$$\det\left[sI - \left(\sum_{i=0}^{m} \tilde{A}_i\right) - \sum_{i=1}^{m} \tilde{A}_i \frac{e^{-r_i s}-1}{s} \left(\sum_{k=0}^{m} \tilde{A}_k e^{-r_k s}\right)\right] \neq 0, \quad \forall s \in \overline{\mathscr{C}}_+ \tag{4.14}$$

and hence stability can be derived from an equivalent condition, provided $\tilde{A} = \sum_{i=0}^{m} \tilde{A}_i$ is stable,

$$\det\left[I-(sI-\tilde{A})^{-1}\sum_{i=1}^{m}\tilde{A}_i\frac{e^{-r_i s}-1}{s}\left(\sum_{k=0}^{m}\tilde{A}_k e^{-r_k s}\right)\right]\neq 0, \quad \forall s \in \overline{\mathscr{C}}_+. \tag{4.15}$$

With the knowledge of the maximum allowable delay for the system (4.8), the delay-dependent stability condition is obtained using the following theorem.

Theorem 4.2.7 (Theorem 3.9 [62]). *Let $r_k \geq 0, k = 1,\ldots,m$ be independent, incommensurate delays. Then the system (4.8) is stable for all $r_k \in [0,\overline{r}_k)$, $k = 1,\ldots,m$, if*

1. $\sum_{k=0}^{m}\tilde{A}_k$ *is stable*
2. $\mu_\Delta(M(j\omega;\overline{r}))<1, \ \forall\omega>0$

where $\Delta = \mathscr{X}_{m^2+m}$,

$$M(s;\overline{r}) \triangleq \begin{pmatrix} I \\ \vdots \\ I \end{pmatrix}\left(sI-\left(\sum_{i=0}^{m}\tilde{A}_i\right)\right)^{-1}\left(\overline{r}_1\tilde{A}_1C \ \ \overline{r}_2\tilde{A}_2C \ \ldots \overline{r}_m\tilde{A}_mC\right),$$

$$C \triangleq \left(\tilde{A}_0 \ \ \tilde{A}_1 \ \ldots \ \tilde{A}_m\right)$$

It is noted that, because of the additional dynamics from the model transformation, the delay-dependent stability condition may or may not be conservative than the delay-independent stability condition.

4.2.2 Control Design for Print Units with CRC

Recall the system dynamics for a print section with compensator based registration control.

$$\dot{x}(t) = A_0x(t)+A_1x(t-\tau_1)+B_{0c}u_1(t)+B_{0t}u_2(t)+B_{1c}u_1(t-\tau_1)+B_{2c}u_1(t-\tau_2) \tag{4.16}$$

The presence of delays in both states and inputs in the system dynamics complicates the control design and stability analysis. For the sake of generality, the delays τ_1 and τ_2 are considered to be incommensurate even though the location of the compensator within the print unit span can be changed so that the delays are commensurate.

Systems with delayed control are typically transformed into a delay-free system and the transformed system is then controlled using state feedback either with or without past state measurements (see [67, 68, 69] and references therein). Whereas for systems with both internal delays and delayed control the system is first transformed into a system with delay free control and then a stabilizing state feedback control, with or without past state measurements, is obtained for the transformed system with internal delays (see [70, 71] and references therein). The control law from these techniques are complicated from a practical stand point and typically require memory to store past state measurements.

The objective in this section is to design a decentralized control laws for the system in Equation (4.6) which results in a stable, autonomous, retarded functional differential equation. The system is first transformed into an equivalent system without control delays (motivated by the idea presented in [72, 70]) by using integral action. A memorlyless state feedback control law is then designed for the transformed system so that the resulting system is stable. The stability of the closed loop system with state feedback is analyzed based on the frequency domain based stability conditions provided in Theorems 4.2.5 and 4.2.7.

The system (4.6) can be rewritten by combining all inputs into a single vector as

$$\dot{x}(t) = A_0 x(t) + A_1 x(t-\tau_1) + B_0 u(t) + B_1 u(t-\tau_1) + B_2 u(t-\tau_2) \tag{4.17}$$

where $x \in \mathscr{R}^{n\times 1}, u \in \mathscr{R}^{m\times 1}, u(t) = \left[\overline{\tau}_1, \dot{\overline{l}}_1, \overline{\tau}_2, \dot{\overline{l}}_2 \ldots, \dot{\overline{l}}_7, \overline{\tau}_8\right]^\top$ with $n = 22$ state variables and $m = 15$ control inputs. The system in (4.17) can be transformed into a system with internal delay by using dynamic feedback with m integrators. The augmented system can be represented as

$$\dot{z}_1(t) = A_0 z_1(t) + A_1 z_1(t-\tau_1) + B_0 z_2(t) + B_1 z_2(t-\tau_1) + B_2 z_2(t-\tau_2) \tag{4.18a}$$

$$\dot{z}_2(t) = \omega(t) \tag{4.18b}$$

where $z_1 \in \mathscr{R}^{n\times 1}$ and $z_2, \omega \in \mathscr{R}^{m\times 1}$. Alternatively, the transformed system is represented as

$$\dot{z}(t) = \underbrace{\begin{bmatrix} A_0 & B_0 \\ \mathbf{0} & \mathbf{0} \end{bmatrix}}_{\overline{A}_0} z(t) + \underbrace{\begin{bmatrix} A_1 & B_1 \\ \mathbf{0} & \mathbf{0} \end{bmatrix}}_{\overline{A}_1} z(t-\tau_1) + \underbrace{\begin{bmatrix} \mathbf{0} & B_2 \\ \mathbf{0} & \mathbf{0} \end{bmatrix}}_{\overline{A}_2} z(t-\tau_2) + \underbrace{\begin{bmatrix} \mathbf{0} \\ I \end{bmatrix}}_{\overline{B}_0} \omega(t)$$

$$\dot{z}(t) = \overline{A}_0 z(t) + \overline{A}_1 z(t-\tau_1) + \overline{A}_2 z(t-\tau_2) + \overline{B}_0 \omega(t) \tag{4.19a}$$

where $\overline{A}_0, \overline{A}_1, \overline{A}_2 \in \mathscr{R}^{n+m\times n+m}$ and $\overline{B}_0 \in \mathscr{R}^{n+m\times m}$. Consider a state feedback control law with $w(t) = -Kz(t) = -K_1 z_1(t) - K_2 z_2(t)$ where $K_1 \in \mathscr{R}^{m\times n}, K_2 \in \mathscr{R}^{m\times m}$ so that the closed loop system is reduced to

$$\dot{z}(t) = \begin{bmatrix} A_0 & B_0 \\ -K_1 & -K_2 \end{bmatrix} z(t) + \begin{bmatrix} A_1 & B_1 \\ \mathbf{0} & \mathbf{0} \end{bmatrix} z(t-\tau_1) + \begin{bmatrix} \mathbf{0} & B_2 \\ \mathbf{0} & \mathbf{0} \end{bmatrix} z(t-\tau_2). \tag{4.20}$$

If there exist K_1 and K_2 such that the closed loop system (4.20) is stable using either Theorem 4.2.5 or Theorem 4.2.7, then the dynamic feedback control law given by

$$\dot{u}(t) = -K_1 x(t) - K_2 u(t) \tag{4.21}$$

will stabilize the system in Equation 4.17.

For a decentralized control structure for CRC K_1 should be block diagonal with $K_1 = \text{diag}[k_0, k_{11}, k_{22}, \ldots, k_{77}]$ with $k_0 \in \mathscr{R}$ and $k_{ii} \in \mathscr{R}^{2\times 3}$ for $i = 1, \ldots, 7$ and

K_2 should be diagonal. The state feedback gain k_0 corresponds to the torque input for the first print cylinder which acts as the master speed for the print section. The first row in k_{ii} corresponds to the rate of change of span length correction provided by the compensator in print unit i and the second row corresponds to the torque input to the print cylinder in print unit i. In this analysis strain and registration error measurements are used to compute the control input for the compensator roller and speed feedback is used to compute the print cylinder torque input. For the sake of simplicity the feedback gains in all the print units are chosen to be equal, i.e., $k_{ii} = k_{jj}$ for $i, j = 1, \ldots, 7$.

For the transformed system (4.19) with parameter values defined in Table 4.1 the following state feedback gains are chosen:

$$k_0 = 1000, \qquad k_{ii} = \begin{bmatrix} 36 & 0.1 & 0 \\ 0 & 0 & 1000 \end{bmatrix} \text{ for } i = 1, \ldots, 7 \qquad K_2 = 10I \tag{4.22}$$

where I is a 15×15 identity matrix.

The stability of the closed loop system in (4.20) with these gains is checked using the stability constraints in Theorems 4.2.5 and Theorem 4.2.7 which are shown in Figure 4.5. From the figure it is evident that the delay-dependent stability constraint is not satisfied while the delay-independent condition is. The stability of the system is guaranteed as long as the maximum delay value for τ_1 and τ_2 are $r_1 = 19$ seconds and $r_2 = 7$ seconds since $\mu_\Delta(M(j\omega; \overline{r})) < 1, \ \forall \omega > 0$ for the closed loop system (4.20).

It is noted that the seven open loop poles of $\overline{A}_0$, corresponding to the registration error states in A_0, are shifted away from the origin to the left half plane whenever the control gain corresponding to the registration error in the compensator input is nonnegative. The magnitude of this gain plays an important role in

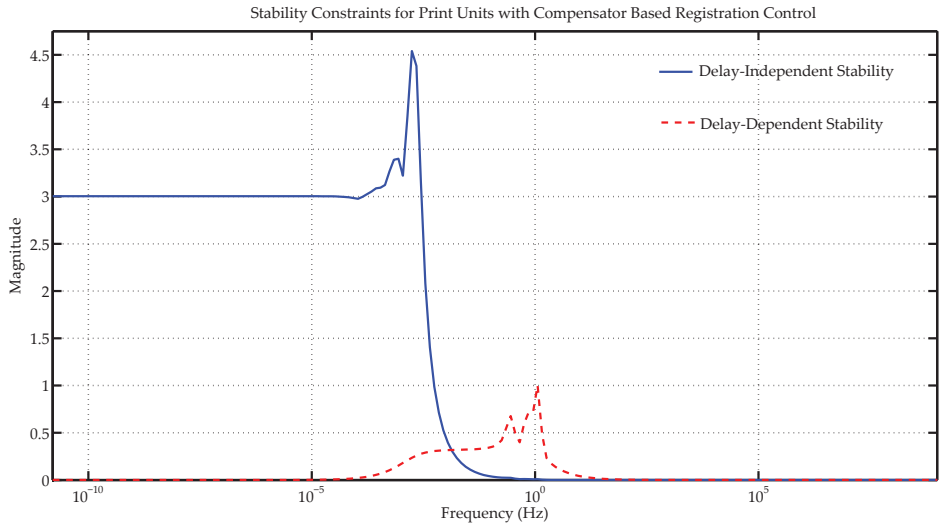

Figure 4.5: *Stability constraints for print units with compensator based control for print registration. For the stability condition dependent on delay the maximum delay for τ_1 was chosen as $r_1 = 19$ seconds and $r_2 = 7$ seconds for τ_2.*

stability. A gain value of 0.1 corresponds to 10% correction in registration error every second or a 15% correction of registration error per revolution of the print cylinder. Any span length change correction provided with a compensator has a delay of at least 6 seconds before its effect is seen at the registration sensor but the effect of span length change on web strain is experienced instantaneously. A large correction in span length based on registration error feedback will instantaneously affect the registration error, through the web strain dynamics, before the effect of the web path length change due to the compensator is observed after a delay of 6 seconds. This effect may destabilize the system when large span length correction rate is provided by the compensator. The destabilizing effect of the magnitude of correction provided by the feedback gain corresponding to the registration error is shown in Figure 4.6. The magnitude of span length correction is varied from 10% correction to 100% of registration error correction per second. From the plot it is evident that as the correction increases beyond 10%

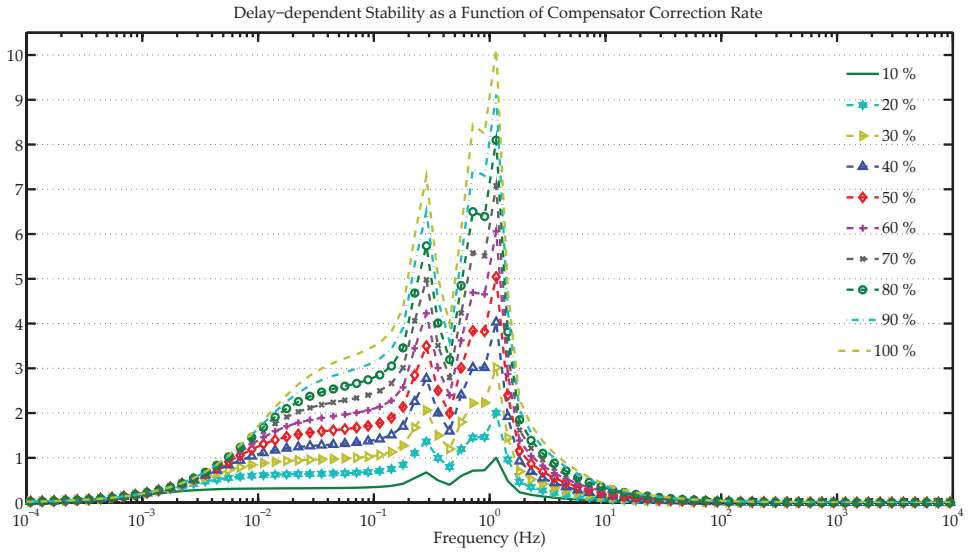

Figure 4.6: *Delay-dependent stability condition as a function of magnitude of span length correction. The plots show 10 to 100 % of the registration error correction per second.*

the stability condition is not satisfied.

A similar destabilizing effect is observed with PARC during practical implementation when registration error correction to the angular position is provided based on the developed algorithms [20, 58, 59]; to overcome this instability the time period for correction per revolution of the print cylinder is restricted to 4 ms in an adhoc manner in these studies. The time domain analysis does not provide a visual tuning process to scale the magnitude of correction. With the graphical stability conditions, the frequency domain analysis provides a more intuitive understanding on the effect of magnitude of correction provided by each inputs and hence will serve as a valuable tool for industrial practitioners.

The feedback gain corresponding to web strain in the compensator input does not move the open loop system poles significantly and can even be zero for a closed loop system that is stable. It is noted that the control gains are not synthesized but are found by tuning the controller parameters so that the stability

constraint is satisfied and not based on performance. One set of controller gains that satisfy the stability condition is presented. The delay-independent stability condition with proposed control structure was not satisfied for any set of gains that were analyzed because of the size of the A_1 matrix which has a destabilizing effect on the retarded differential equation.

Time domain simulations were carried out to observe the performance characteristics of the closed loop system with the control gains and a representative sample of the simulation results is shown in Figures 4.22–4.31. For simulation purposes the variational strain dynamics is used in the model and it is assumed that the nominal web strain is known and equal to the nominal web strain in the span upstream of the print unit; the variational strain dynamics can be obtained from the following relation $\epsilon_i = \tilde{\epsilon} + \Delta\epsilon_i$ where $\tilde{\epsilon}$ is the nominal strain and $\Delta\epsilon_i$ is the variational strain. Note that the dynamics of the overall system is identical with either the strain dynamics or the variational strain dynamics. Moreover, even with the variational strain dynamics, the registration error is based on the relative variational strain since $\overline{\epsilon}_2 = \epsilon_2 - \epsilon_1 = \Delta\, epsilon_2 - \Delta\epsilon_1$.

Figures 4.22–4.27 show the initial condition response, with and without the correction provided by the compensator, for three sets of initial conditions involving web strain, registration error and variational web speed. For all the simulations the print cylinder velocity loop is closed based on the velocity feedback with the gains corresponding to the second row of k_{ii} in (4.22). For the simulations without the compensator correction, the first row of k_{ii} is set to zero and for the simulations with compensator correction the first row of k_{ii} from (4.22) are used. From these simulations it is evident that CRC actively controls the registration error.

The disturbance rejection performance of CRC is also evaluated from simulations. Disturbances in the form of incoming variational web strain $\Delta\epsilon_1$ to the print unit section were introduced and the performance of the closed loop system is evaluated. Figures 4.28–4.31 show the response of the system with and without the compensator correction provided by CRC for pulse and sinusoidal disturbances. Simulation results indicate the effectiveness of CRC to reject disturbances. Note that with the sinusoidal disturbances, even with active control the registration error is not minimized in the first print unit. This is because $\Delta\epsilon_1$ acts as an input disturbance which cannot be controlled without actively controlling the strain in the incoming web span. But the registration error in all other print units are minimized when the compensator is used.

4.2.3 Control Design for Print Units with PARC

Recall from Equation (4.7) the system dynamics for print units employing the PARC strategy is

$$\dot{x}(t) = A_0 x(t) + A_1 x(t-\tau_1) + B_{0c} u_1(t) \tag{4.23}$$

where $u_1(t) = [\overline{\tau}_1, \ldots, \overline{\tau}_8]$. The system dynamics is simple when compared to that using the CRC strategy with just a single delay in the state. The objective is to design a decentralized, state feedback control law with current state measurement ($u_1(t) = -Kx(t)$) so that the closed loop system

$$\dot{x}(t) = [A_0 - B_{0c}K]\, x(t) + A_1 x(t-\tau_1) \tag{4.24}$$

is stable by using either Theorem 4.2.5 or Theorem 4.2.7. For decentralized control the gain matrix K should have the following structure $K = \text{diag}\,[k_0, k_{11}, k_{22}, \ldots, k_{77}]$ with $k_0 \in \mathscr{R}$ and $k_{ii} \in \mathscr{R}^{1\times 3}$ for $i = 1, \ldots, 7$. The gain k_0 corresponds to the torque

to print cylinder 1 based on its velocity measurement and the gains k_{ii} correspond to torque to the print cylinder in i^{th} print unit used for registration error correction based on web strain, registration error, and print cylinder velocity measurements.

With the decentralized state feedback control structure, the necessary condition for stability using either Theorem 4.2.5 or Theorem 4.2.7 is not satisfied for any set of gains. This is because of the fact that the seven open loop poles of A_0 corresponding to registration error state cannot be moved from the origin to the left-half plane unless large values for gains corresponding to the registration error state are used; this may be attributed to the fact that the control input has an indirect effect on the registration error dynamics. Even with large gains it is not possible to move one of the eigenvalues of the matrix $A_0 - B_{0c}K$ which violates the necessary condition for delay-independent stability, i.e., the matrix $A_0 - B_{0c}K$ be Hurtwitz. The necessary condition for stability dependent on delay, i.e., the matrix $A_0 - B_{0c}K + A_1$ be Hurwitz is satisfied for a set of gains K but the stability constraint $\mu_\Delta(M(j\omega;\overline{r})) < 1,\ \forall\ \omega > 0$ in Theorem 4.2.7 is not satisfied unless the delay $\tau_1 < 0.27$ seconds (see Figure 4.7).

Instead of regulating the print cylinder velocity variations to zero, a servo type control can be used to regulate the velocities to a non-zero value in order to correct for registration error. This type of control is similar to existing PARC based control strategies where the angular position of the print cylinders are varied based on registration error feedback. The control law is given by $u_1(t) = -K_1x(t) + G_g r(t)$ where $G_g \in \mathscr{R}^{7\times 7}$ is the input gain matrix and $r(t) \in \mathscr{R}^{7\times 1}$ is the reference for the print cylinder velocity variation; G_g is diagonal for decentralized control. The reference $r(t)$ is computed based on the registration error and

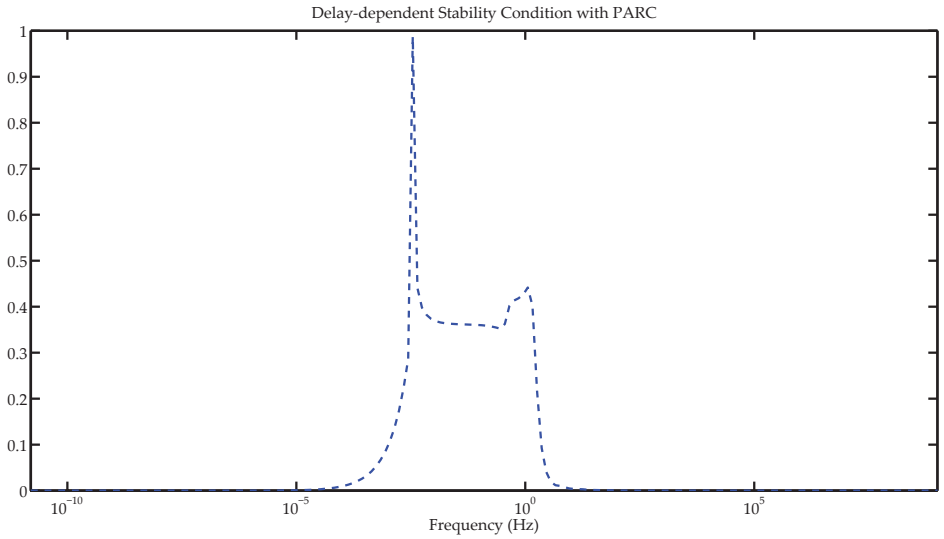

Figure 4.7: *Stability condition dependent on delay for the print section with the dynamics in Equation 4.7 controlled using a electronic line shaft based registration control with gain* $k_0 = 1000$ *and* $k_{ii} = [0 \quad -275 \quad 1000]$ *for a maximum delay value for* τ_1 *to be* $\overline{r}_1 = 0.27$ *seconds.*

is given by $r(t) = \alpha_g C_e x(t)$ where α_g is the registration error correction scaling factor, and C_e is the output matrix of the system corresponding to the registration error states. Depending on the amount of correction needed, the angular velocity reference is scaled using the term α_g footnoteIf $\alpha_g = 1/r$ where r is the radius of the print cylinder then 100% of registration error is corrected in a second. and the input gain matrix is chosen such that the steady-state tracking error is zero. The servo type control for PARC can then be represented as

$$\dot{x}(t) = \left[A_0 - B_{0c}K + \alpha_g G_g C_e\right] x(t) + A_1 x(t-\tau_1). \tag{4.25}$$

Even with this control strategy the matrix $\left[A_0 - B_{0c}K + \alpha_g G_g C_e\right]$ is not Hurtwitz for any value of α_g. For values of $\alpha_g > 0.3103$ the matrix $\left[A_0 - B_{0c}K + \alpha_g G_g C_e + A_1\right]$ has all eigenvalues with negative real part but the delay-dependent stability condition based on the structured singular value is also not satisfied. It is noted that $\alpha_g > 0.3103$ implies that at least 2.6 times the registration error is corrected every

second, which is basically a large magnitude of correction that can indeed lead to instability as discussed in the previous section.

4.3 Remarks

Based on the analysis presented in this chapter it can be concluded that CRC has a number of advantages over PARC. First, the propagation of tension disturbances due to registration control is smaller with CRC than with PARC. This is attributed to the fact that the control of registration error with PARC has a direct effect on web strain in adjacent print units which results in more interaction. While the direct effect of compensator motion on web strain in one print unit is propagated to the adjacent span through the print cylinder dynamics, which reduces the magnitude of disturbance propagation. In order to avoid the propagation of disturbances due to PARC, a cooperative control strategy is employed in [59, 22] where a disturbance attenuation based on angular correction provided in adjacent print units is employed. Therefore, when multiple print units are employed, the complexity of the cooperative control strategy will increase significantly.

The CRC strategy can stabilize the print section dynamics with a decentralized state feedback control law based on current state measurements. A decentralized state feedback law is simple to implement and hence would be an ideal choice for commercial registration controllers. Without the need to store past measurements, the memory requirement of the controller during practical implementation is reduced significantly; for example, with a 10 millisecond sampling time at least 1800 measurements are needed to be stored for each state for the Armstrong print unit, which is a significant memory requirement even for

modern advanced signal process based industrial controllers.

It is possible to stabilize the system with PARC by using methods such as those presented in [20, 58, 22, 59]. But the advantages of using the CRC presented in this chapter over the exiting PARC are that (1) past measurements are not necessary, (2) control law computation is not complex and hence can be implemented in commercial registration controllers, and (3) state measurements from adjacent print units is not necessary hence a decentralized control can be implemented.

In [20, 58, 22, 59] past measurements of states as well as the communication of state measurements between registration controllers in adjacent print units are necessary for the PARC algorithms. The complex control algorithm for PARC presented in [20, 58, 59] had to be implemented on a dedicated DSP since commercial registration controllers were unable to handle the computation complexity of the nonlinear control laws. And even though the control law was shown to be stable with the PARC algorithms presented in [20, 58, 59], during practical implementation instability in the system was observed because of the rapid change in angular velocity that resulted in slippage or web breakage. This instability was avoided in experimentation by limiting the angular velocity correction based on registration error to be 4 millisecond per revolution of the print cylinder in an adhoc manner.

The stability analysis presented in this chapter is preliminary in the sense that it is applicable for a restricted set of control structures and controller complexity. It is anticipated that improvements to the registration control performance may be made by using advanced decentralized control strategies with both CRC and PARC. Moreover, the comparison presented in this chapter did

not consider the achievable performance with either control strategies. Future work should consider control design based on desired performance.

It is noted that the stability of the print section with CRC was achieved with a simple control structure. This may be attributed to the structure of the plant and the additional degree of freedom available with the compensator. For example, the delay τ_1 corresponding to the state delay matched with one of the input delays and also the two input matrices with delays are equal in magnitude. Further, the complexity of the stability analysis for CRC may be reduced if the delays are commensurate. Note that the delays can be made commensurate by positioning the compensator in the web path so that the transport delay τ_1 for the web to travel from one print cylinder to the other is an integer multiple of the transport delay τ_2 for the web to travel from the compensator to the downstream print cylinder. Future work should further investigate this aspect based on the structure of the print section dynamics.

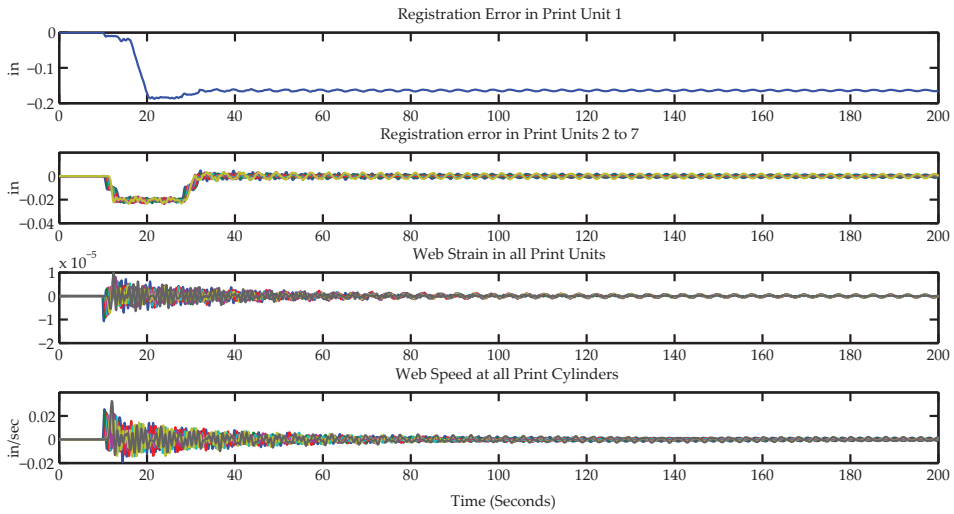

Figure 4.8: *Interaction in CRC with a pulse width of 14 seconds and magnitude of* 0.0401 *in/sec.*

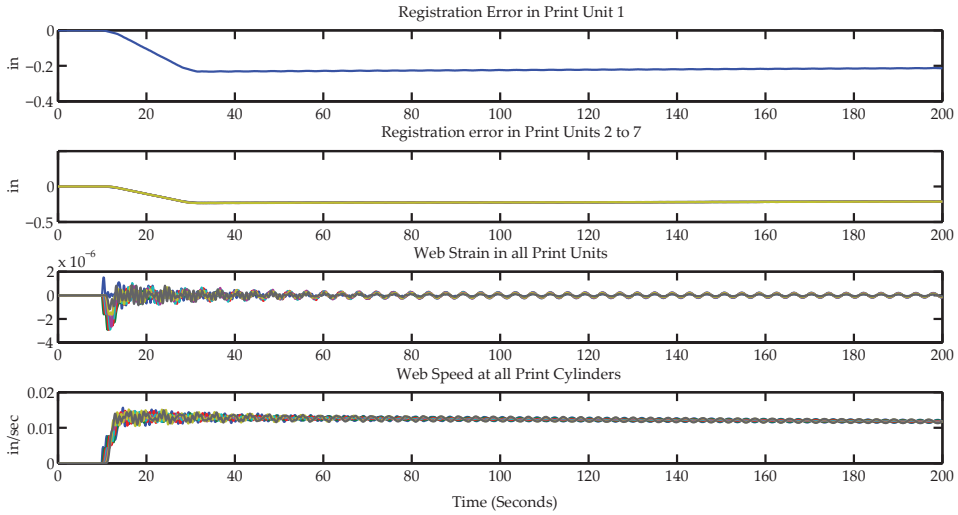

Figure 4.9: *Interaction in PARC with a pulse width of 14 seconds and input torque magnitude of* 0.5643 *lb-in.*

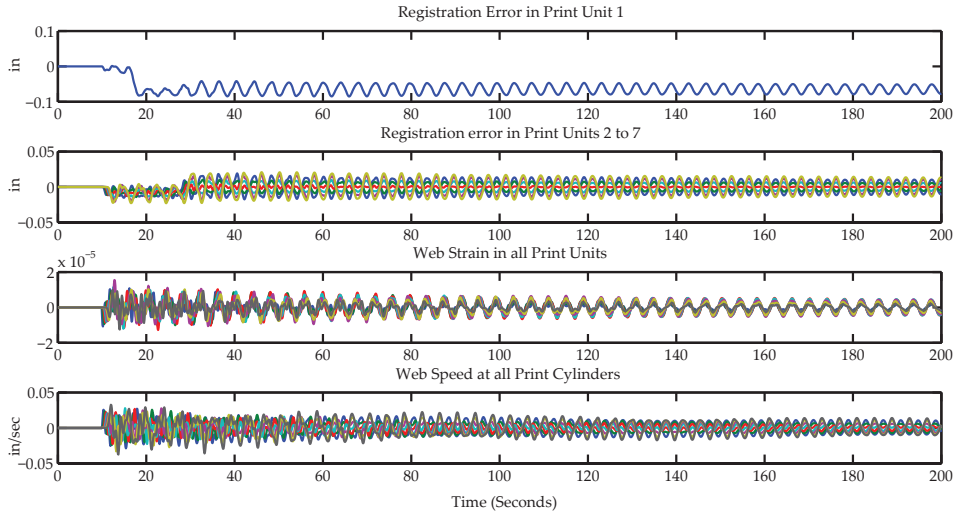

Figure 4.10: *Interaction in CRC with a pulse width of 1.5 seconds and magnitude of* 0.0401 *in/sec.*

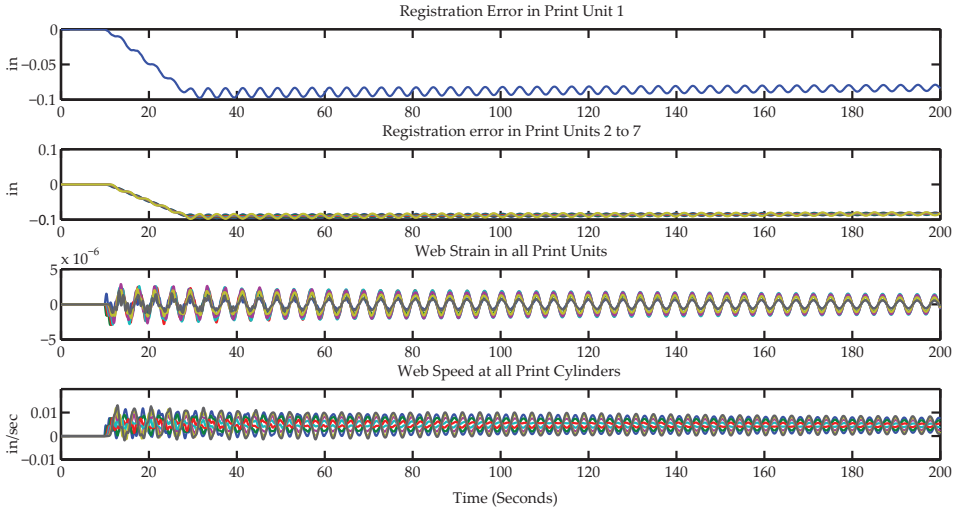

Figure 4.11: *Interaction in PARC with a pulse width of 1.5 seconds and input torque magnitude of* 0.5643 *lb-in.*

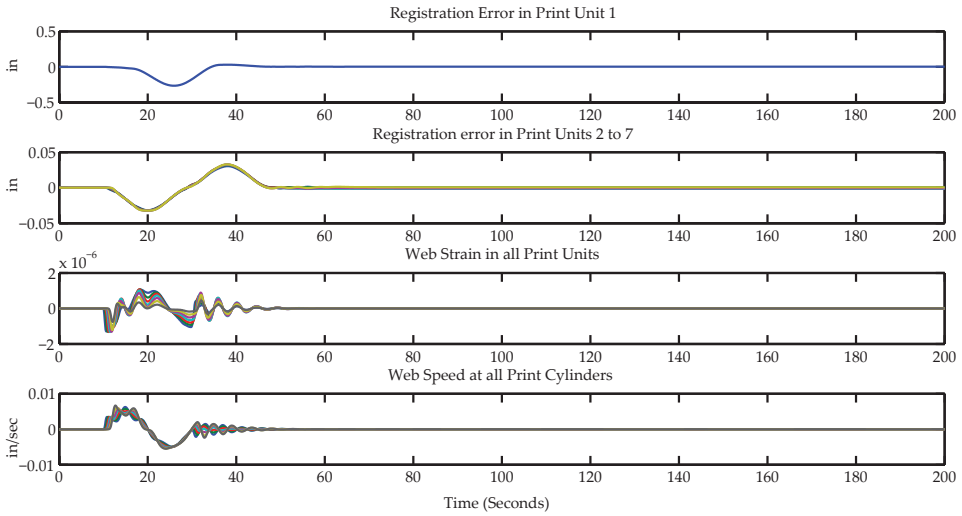

Figure 4.12: *Interaction in CRC with a sinusoidal input magnitude of* 0.0401 *in/sec and frequency of* 0.05 *Hz.*

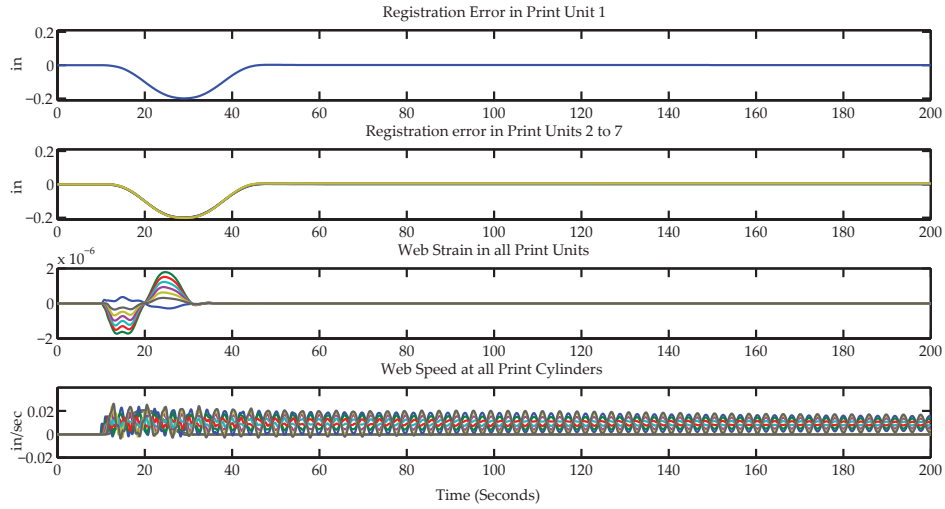

Figure 4.13: *Interaction in PARC with a sinusoidal torque input magnitude of* 0.5643 *lb-in and frequency of* 0.05 *Hz.*

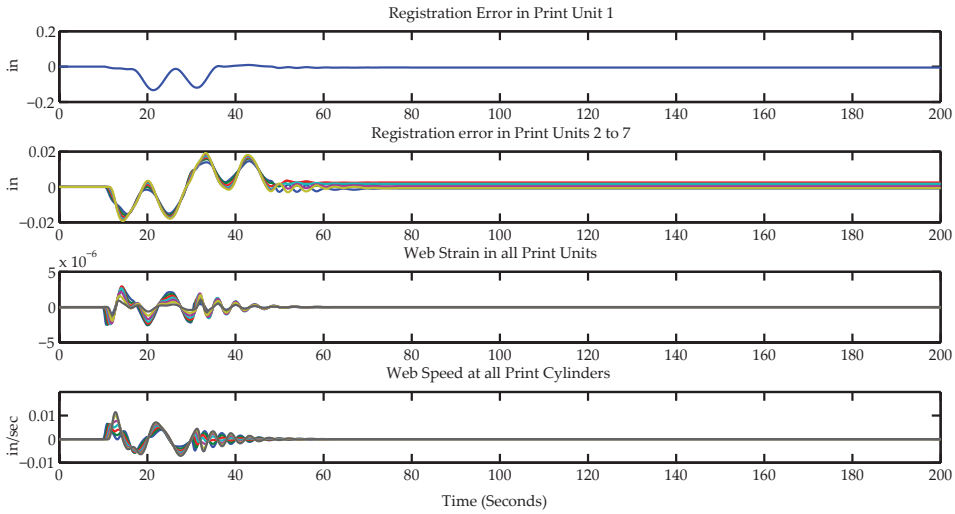

Figure 4.14: *Interaction in CRC with a sinusoidal input magnitude of* 0.0401 *in/sec and frequency of* 0.1 *Hz.*

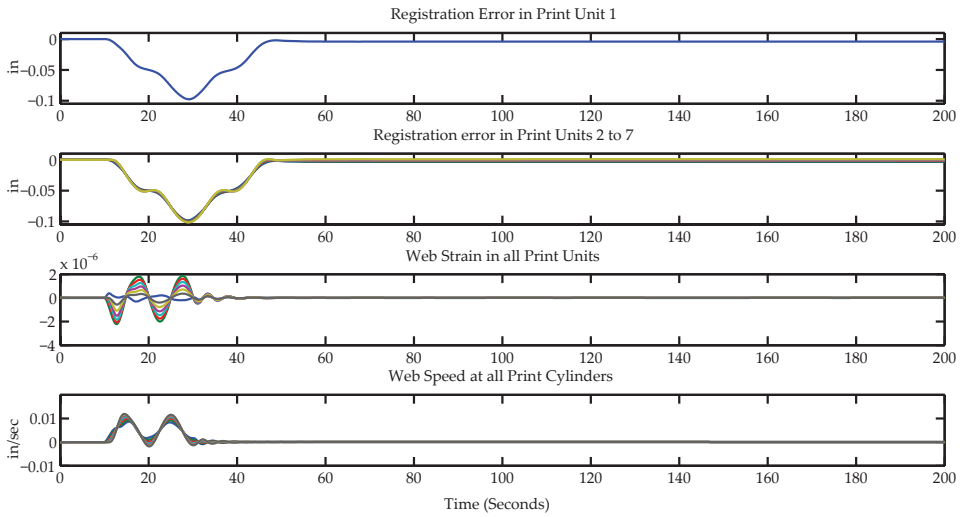

Figure 4.15: *Interaction in PARC with a sinusoidal torque input magnitude of* 0.5643 *lb-in and frequency of* 0.1 *Hz.*

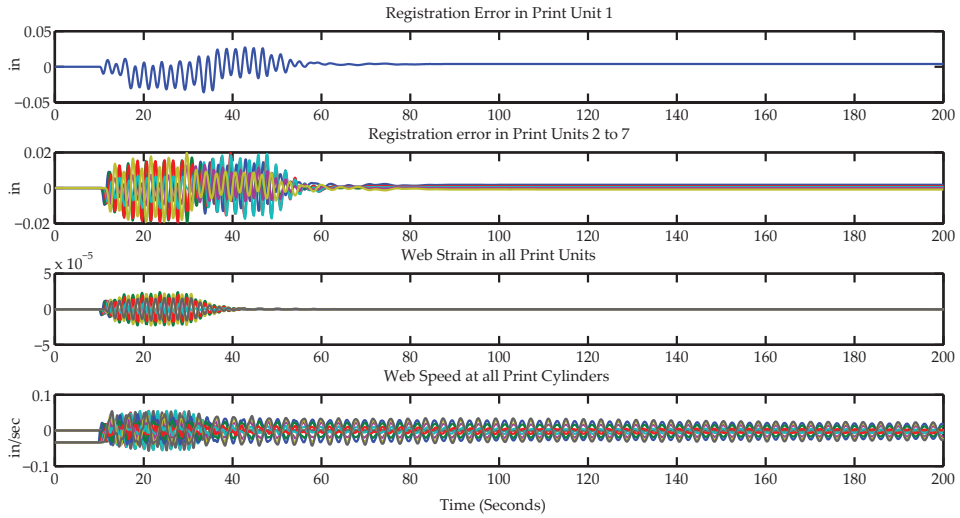

Figure 4.16: *Interaction in CRC with a sinusoidal input magnitude of* 0.0401 *in/sec and frequency of* 0.5 *Hz.*

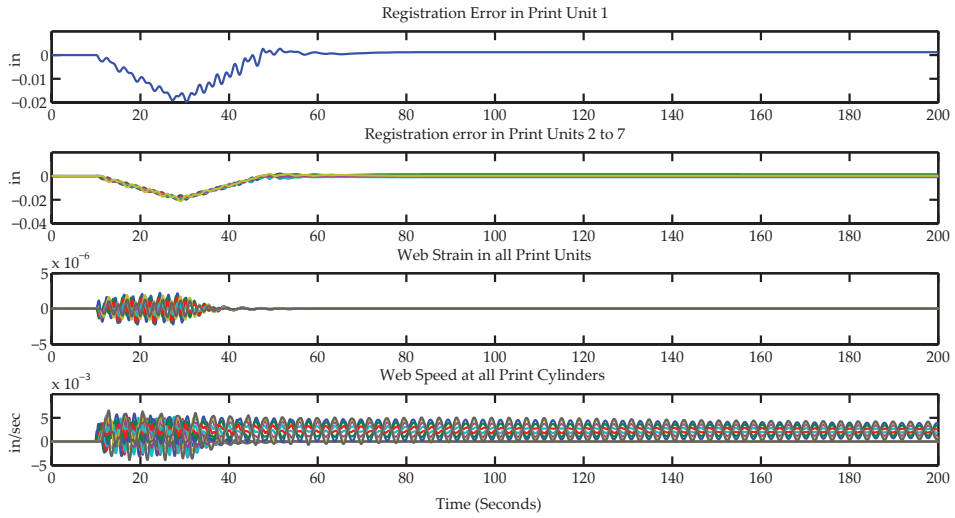

Figure 4.17: *Interaction in PARC with a sinusoidal torque input magnitude of* 0.5643 *lb-in and frequency of* 0.5 *Hz.*

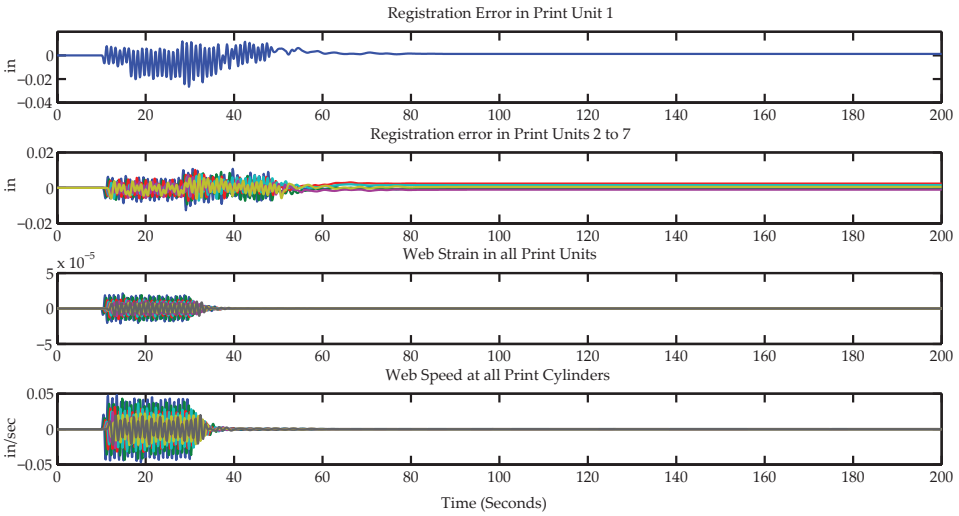

Figure 4.18: *Interaction in CRC with a sinusoidal input magnitude of* 0.0401 *in/sec and frequency of* 1 *Hz.*

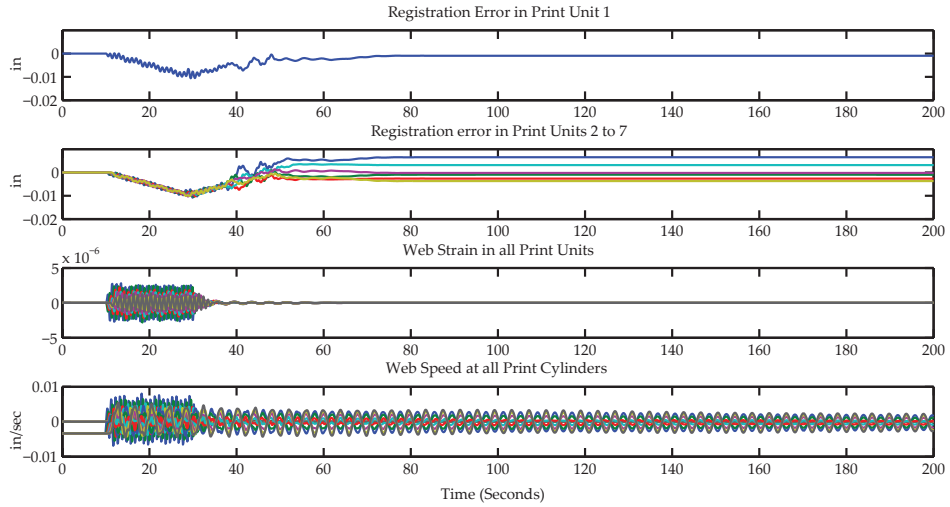

Figure 4.19: *Interaction in PARC with a sinusoidal torque input magnitude of* 0.5643 *lb-in and frequency of* 1 *Hz.*

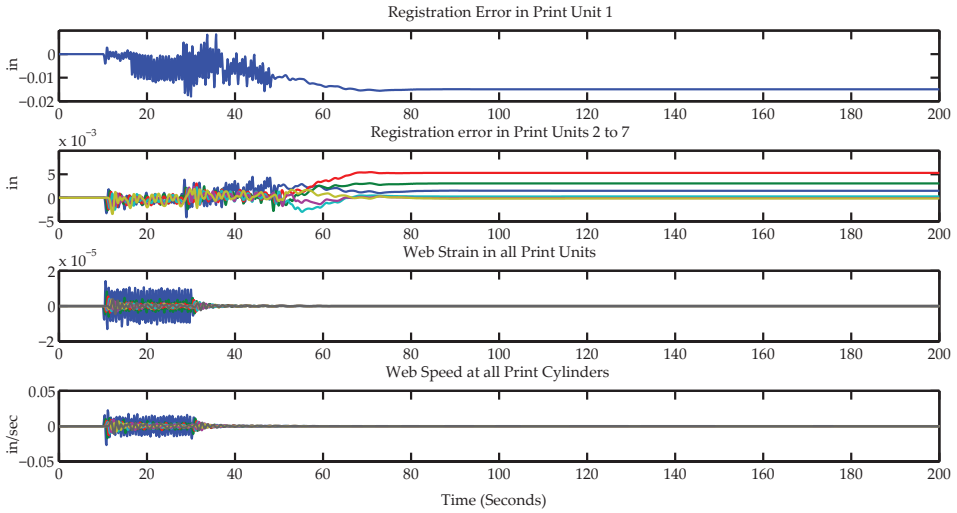

Figure 4.20: *Interaction in CRC with a sinusoidal input magnitude of* 0.0401 *in/sec and frequency of* 1.5 *Hz.*

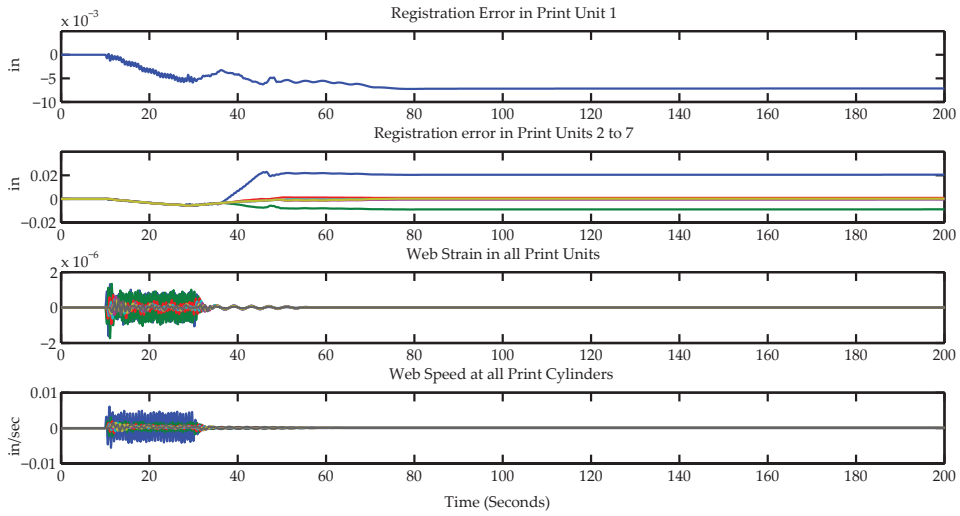

Figure 4.21: *Interaction in PARC with a sinusoidal torque input magnitude of* 0.5643 *lb-in and frequency of* 1.5 *Hz.*

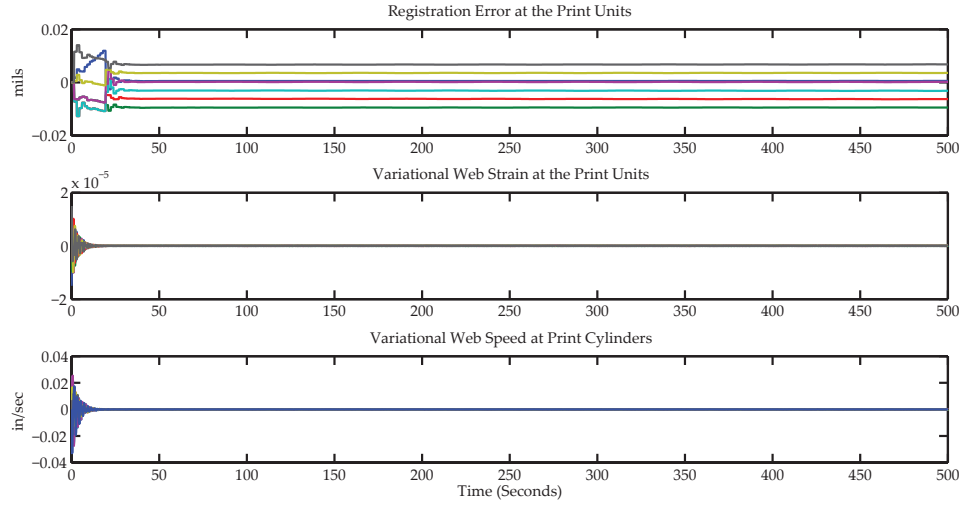

Figure 4.22: *Initial condition response of the print section dynamics without compensator correction. The initial conditions for the variational web strain in the seven print units were taken as* $[-1.5,\ -1,\ -0.5,\ 0,\ 0.5,\ 1,\ 1.5] \times 10^{-5}$.

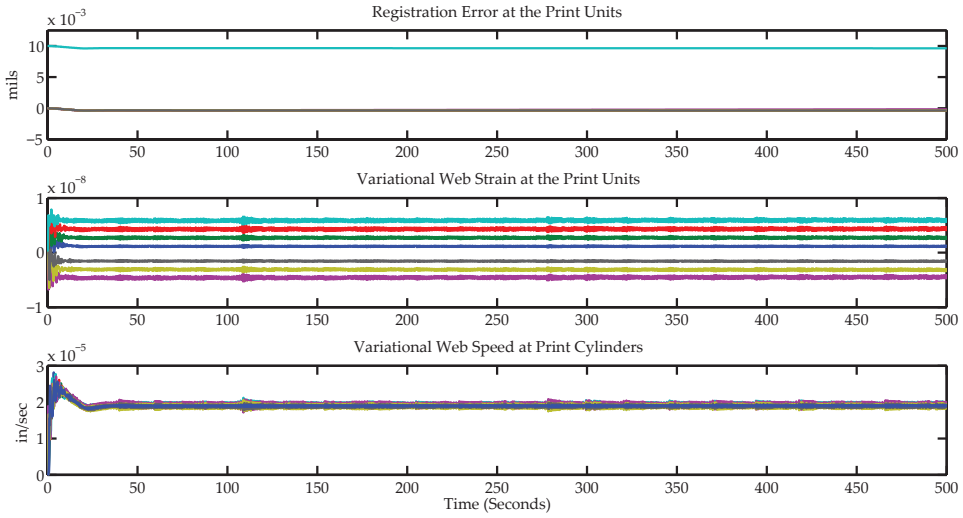

Figure 4.23: *Initial condition response of the print section dynamics without compensator correction. The initial conditions for registration error in print unit 4 was taken as* 0.01 *mils.*

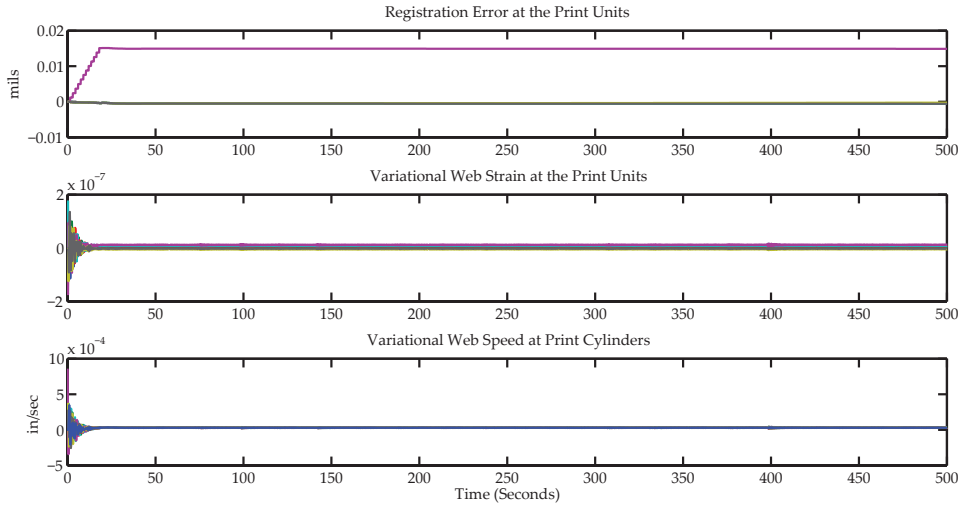

Figure 4.24: *Initial condition response of the print section dynamics without compensator correction. The initial conditions for variational web velocity in print cylinder 4 was taken as* 10^{-4} *rad/sec or* 8.5944×10^{-4} *in/sec.*

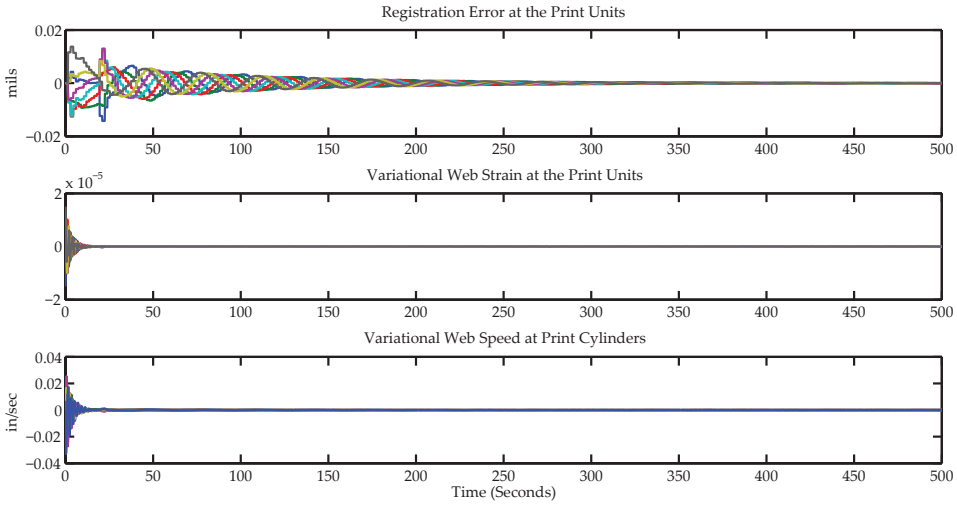

Figure 4.25: *Initial condition response of the print section dynamics with state feedback CRC. The initial conditions for the variational web strain in the seven print units were taken as* $[-1.5,\ -1,\ -0.5,\ 0,\ 0.5,\ 1,\ 1.5] \times 10^{-5}$.

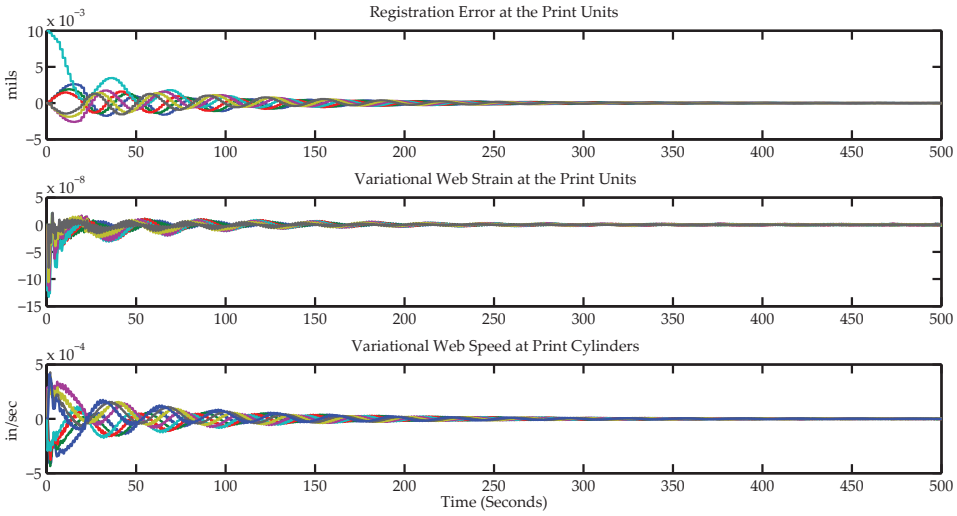

Figure 4.26: *Initial condition response of the print section dynamics with state feedback CRC. The initial conditions for registration error in print unit 4 was taken as* 0.01 *mils.*

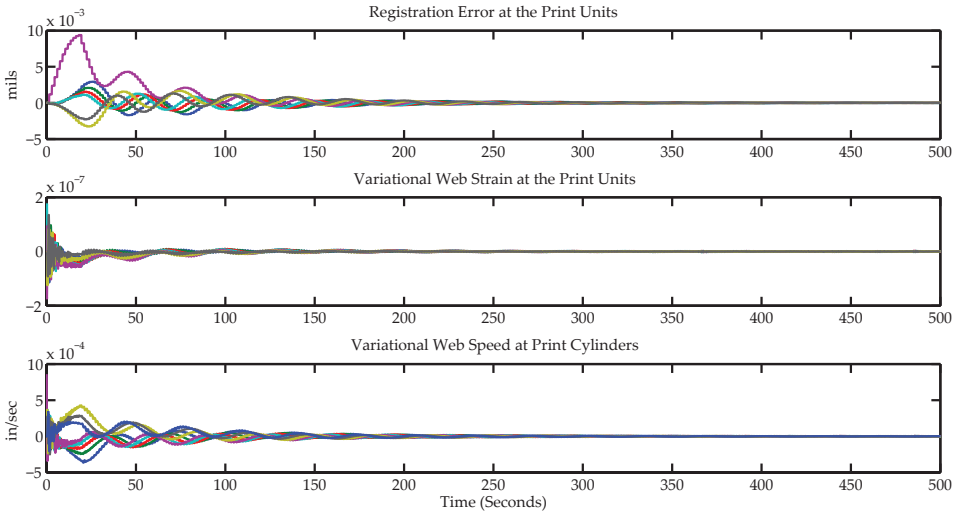

Figure 4.27: *Initial condition response of the print section dynamics with state feedback CRC. The initial conditions for variational web velocity in print cylinder 4 was taken as* 10^{-4} *rad/sec or* 8.5944×10^{-4} *in/sec.*

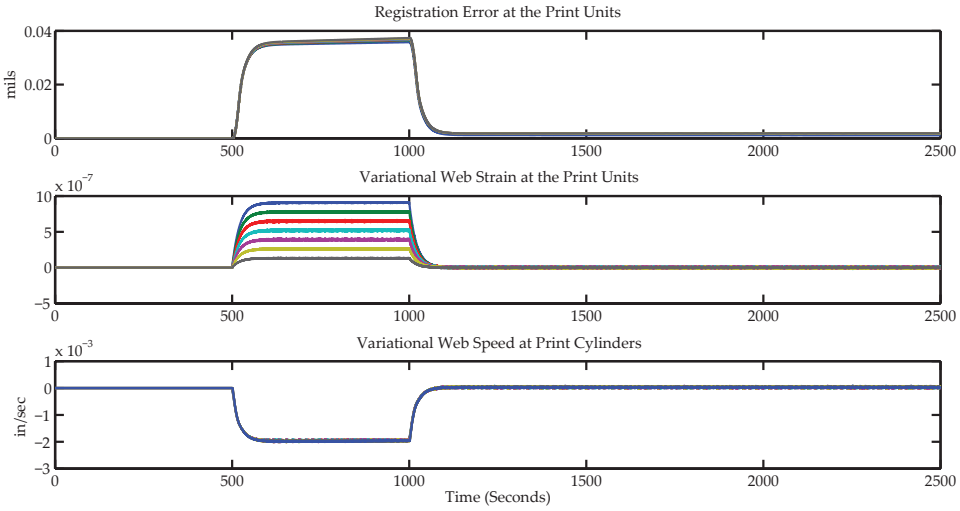

Figure 4.28: *Propagation of disturbance in the print section without compensator correction. A pulse disturbance magnitude of* 1×10^{-6} *in variational web strain was introduced in the span upstream of the print section.*

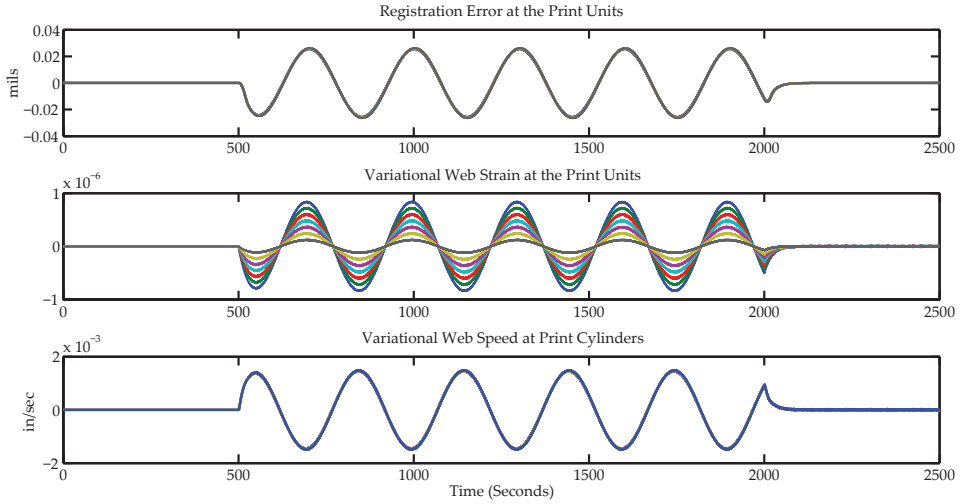

Figure 4.29: *Propagation of disturbance in the print section without compensator correction. A sinusoidal disturbance with magnitude of* 1×10^{-6} *and frequency of (1/300) Hz in variational web strain was introduced in the span upstream of the print section.*

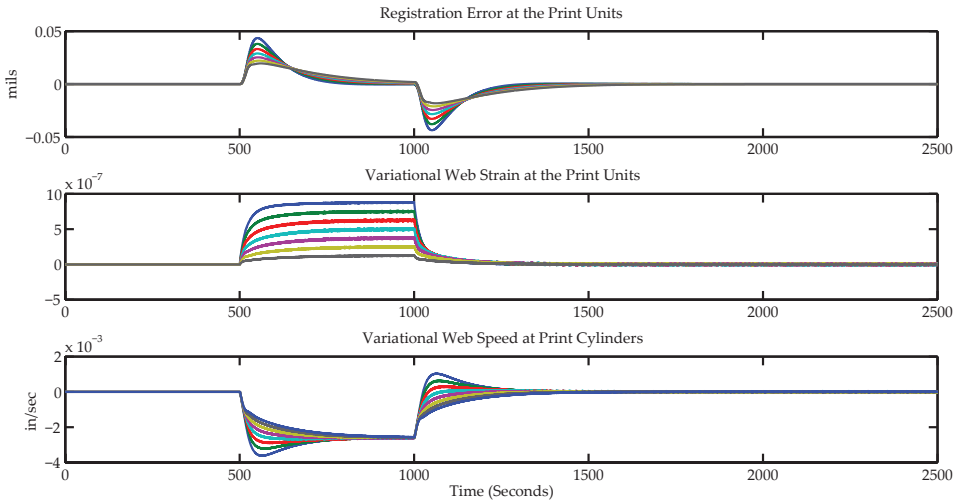

Figure 4.30: *Propagation of disturbance in the print section with CRC. A pulse disturbance magnitude of* 1×10^{-6} *in variational web strain was introduced in the span upstream of the print section.*

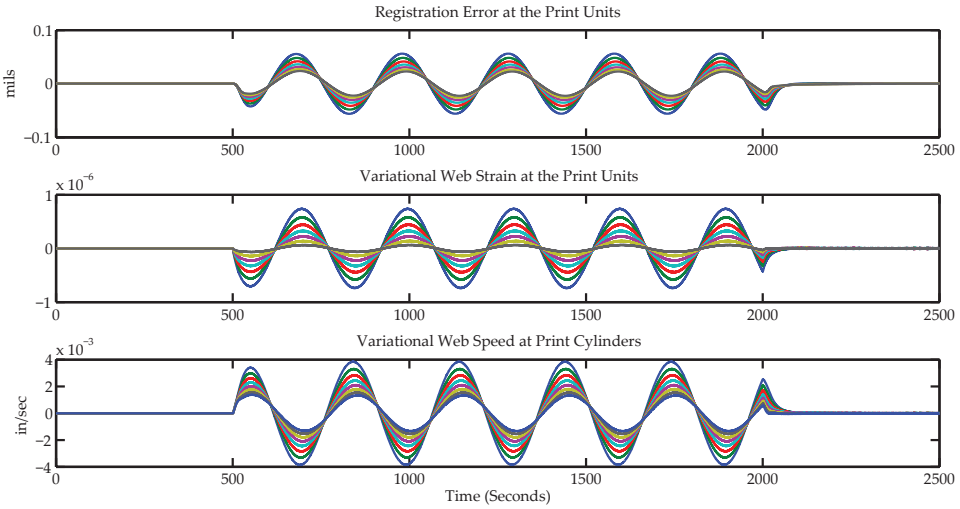

Figure 4.31: *Propagation of disturbance in the print section with CRC. A sinusoidal disturbance with magnitude of* 1×10^{-6} *and frequency of (1/300) Hz in variational web strain was introduced in the span upstream of the print section.*

CHAPTER 5

Summary and Conclusions

Roll-to-roll printing of electronics on a flexible substrate has a significant potential to become the primary manufacturing method for the semiconductor industry, especially for the manufacture of flexible solar cells, displays and lighting. But in order to realize that potential it is important to minimize registration error in the print process. In this dissertation a systematic study to minimize registration error in roll-to-roll printing presses is presented. A summary of the contributions are listed in the following.

5.1 Summary

A new mathematical model for print registration that considers the effect of machine introduced disturbances due to non-ideal elements as well as the effect of various web handling parameters on print registration are presented. The mathematical model differs from existing models available in the literature based on the way in which the effect of web strain is accounted for in the registration error dynamics. Unlike the existing models, the new mathematical model is based on

the relative strain between print units and is neither a function of absolute strain in a print unit nor a function of the difference between the absolute strain and its nominal value. Data from actual productions runs from an industrial printing press are used to show that the relative strain registration model captures the dynamic behavior of print registration process better than the existing models in the literature. Additionally, the analysis of registration error model and the production data indicate the importance of tension regulation within print units in order to minimize registration error. Web tension is seldom regulated in commercial printing presses and active tension regulation is expected to significantly improve print registration.

Machine and web dynamics for a rotogravure print section driven by a mechanical line shaft are modeled based on first principles. Based on the analysis of the model, it is concluded that primary sources of machine induced disturbances in print units are compliant transmission elements. Transmission compliance affects print cylinder velocities and thereby the registration error. If doctor blades are used to wipe excess ink of the rotogravure print cylinders, their motion must be appropriately designed and actuated in order to reduce the effect of machine induced disturbances. For instance, print cylinder velocity variations can be minimized if the stroke length of the doctor blade motion is small and if the doctor blade is independently actuated using a separate actuator. Excessive contact force between the doctor blade and print cylinder should also be reduced in order to reduce print cylinder velocity variations due to doctor blade contact. Depending on the choice of the material for the doctor blade it may be possible to reduce doctor blade loading force.

In roll-to-roll printing with multiple print units, control of registration er-

ror in one print unit will affect registration error in adjacent print units because of strain transport. This propagation of tension disturbances in roll-to-roll processing machinery is studied using a new interaction metric which is based on the Perron root of a nonnegative matrix associated with the system dynamics. The Perron root based interaction metric (PRIM) provides a systematic way to quantify interaction in decentralized large-scale interconnected systems, such as roll-to-roll processing machines. The PRIM also provides a procedure to minimize the interaction via the design of decentralized pre-filters. Stability constraints for decentralized controllers are also derived based on the PRIM analysis. Experimental results from a roll-to-roll platform show the effectiveness of the PRIM in analyzing the tension disturbance propagation behavior within the R2R platform. The experimental results also indicate the effectiveness of PRIM based decentralized pre-filters to minimize tension propagation within the R2R platform.

Two types of control strategies are typically used to control print registration: compensator based registration control (CRC) strategy where the web path length between the print cylinders in a print unit is changed to compensate for registration error and a print cylinder angular position based registration control (PARC) strategy where the angular position of the print cylinder is controlled to compensate for registration error. A systematic analysis of the two control strategies based on their disturbance propagation behavior is performed using the PRIM. From the PRIM analysis it is found that CRC results in a smaller magnitude of disturbance propagation when compared to PARC. This is because of the manner in which strain is transported with these control strategies. The control of registration error with PARC has a direct effect on web strain in adjacent

print units, therefore, it results in more interaction. The direct effect of compensator motion on web strain in one print unit is propagated to the adjacent span through the print cylinder dynamics, which reduces the magnitude of disturbance propagation.

Control of registration error with either CRC or PARC is complicated due to the presence of internal delays associated with the transport of web from one print cylinder to the other. Moreover, additional delay in control input is introduced when CRC is used. But a compensator based control strategy provides an additional degree of freedom to control registration error. Control design and stability characteristics of the two control strategies are compared based on a simple control structure that involves decentralized, memoryless, state feedback controllers. Stability of the delayed system is ascertained based on frequency domain delay-dependent conditions.

A memoryless state feedback decentralized controller is designed for the CRC strategy where the print cylinder velocity is regulated based on the angular velocity feedback and the compensator motion is controlled based on web strain and registration error feedback. The original system with state and input delays is transformed into a system without input delays using dynamic feedback. The control design and stability analysis is carried out on a transformed system since the stability of the transformed system imply the stability of the original system. Delay-dependent stability conditions are satisfied for the CRC strategy for a set of controller gains and the effect of various controller gains on stability is discussed. It is found that the compensator rate plays an important role in the stability of the system and large correction rates will destabilize the system.

A controller for PARC with a decentralized, memoryless, state feedback con-

trol structure was not found, possibly due to the fact that a single control input needs to regulate three state variables in each print unit. Existing controllers in literature that employ a PARC strategy involve computation of a control law based on past measurements and communication of information between different print units. From a practical implementation perspective CRC strategies are attractive because of their decentralized structure and computational simplicity.

5.2 Conclusions

The print quality using R2R printing can be improved by using print cylinders driven by tightly controlled electronic line shafts that regulate the web velocity, and a compensator based control strategy for registration control. With electronic line shafts, the machine induced disturbances due to compliant transmission can be avoided and with a CRC the propagation of registration error between print units can be minimized. The registration performance can be further improved by using an independent actuator for doctor blade motion, actively regulating the web tension within the print units, choosing process conditions such as, transport velocity, web tension, web span length, web material properties, etc., based on PRIM analysis of the model in order to minimize the tension propagation behavior within print units. Moreover, pre-filters designed to minimize propagation of tension disturbances will possibly improve registration performance.

5.3 Future Work

The PRIM was used to compare the two control strategies in terms of disturbance propagation behavior. Minimization of interaction based on the decentralized pre-filter design from PRIM should be considered as part of the future work. Interaction can also be minimized by appropriate machine design and process design. The use of Perron root interaction metric to make machine and process design modifications that would reduce interaction in the print section may be considered as future work.

The decentralized pre-filter design based on PRIM acts more like a detuning gain that ensures stability of the closed-loop system. The addition of the pre-filter does not guarantee closed-loop performance. It is necessary to look at possible ways to design the controller and the pre-filter simultaneously so that interaction is minimized and nominal performance is guaranteed.

It is expected that improvements to the registration control performance may be made by using advanced decentralized control strategies with both CRC and PARC. Moreover, the comparison presented in this work did not consider the achievable performance with either control strategies. Future work should consider control design based on performance.

It is noted that the stability of the print section with CRC was achieved with a simple control structure. This may be attributed to the structure of the plant and the additional degree of freedom available with the compensator. Further, the complexity of the stability analysis for CRC can be reduced if the delays are commensurate. Future work should investigate stabilizability and achievable performance based on the structure of the print section dynamics.

Bibliography

[1] J. J. Shelton, "Dynamics of web tension control with velocity or torque control," in *American Control Conference*, 1986. 3, 57

[2] R. V. Dwivedula, Y. Zhu, and P. R. Pagilla, "Characteristics of active and passive dancers: A comparative study," *Control Engineering Practice, A Journal of the International Federation of Automatic Control*, vol. 14, no. 4, pp. 409 – 423, 2006. 3

[3] J. J. Shelton, "Lateral dynamics of a moving web," Ph.D. dissertation, Oklahoma State University, Stillwater, 1968. 3

[4] J. J. Shelton and K. N. Reid, "Lateral Dynamics of an Idealized Web," *ASME Journal of Dynamic Systems, Measurment, and Control*, vol. 93, no. 3, pp. 187 – 192, 1971. 3

[5] ——, "Lateral Dynamics of Real Moving Web," *ASME Journal of Dynamic Systems, Measurment, and Control*, vol. 93, no. 3, pp. 180 – 186, 1971. 3

[6] A. Seshadri and P. R. Pagilla, "Optimal web guiding," *ASME Journal of Dynamic Systems, Measurement, and Control*, vol. 132, no. 1, pp. 011 006–1–10, 2010. 3

[7] ——, "Adaptive control of web guides," *Control Engineering Practice*, vol. 20, no. 12, pp. 1353 – 1365, 2012. 3

[8] C. F. Puckhaber, "Print-registration control in a rotogravure printing press combined with extrusion-coating or lamination processes," *TAPPI Journal*, vol. 78, no. 3, pp. 144 – 154, 1995. 5

[9] P. R. Pagilla, I. Singh, and R. V. Dwivedula, "A study on control of accumulators in web processing lines," *ASME Journal of Dynamic Systems, Measurement, and Control*, 2004. 8

[10] S. E. Molesa, "Ultra-low-cost printed electronics," Ph.D. dissertation, EECS Department, University of California, Berkeley, May 2006. 10

[11] V. Subramanian and D. Sung, "Gravure as an industrially viable process for printed electronics," Master's thesis, EECS Department, University of California, Berkeley, May 2008. 10

[12] S. H. Ahn and L. J. Guo, "High-speed roll-to-roll nanoimprint lithography on flexible plastic substrates," *Advanced Materials*, vol. 20, no. 11, pp. 2044–2049, 2008. 10

[13] A. D. la Fuente Vornbrock, "Roll printed electronics: Development and scaling of gravure printing techniques," Ph.D. dissertation, EECS Department, University of California, Berkeley, December 2009. 10

[14] F. C. Krebs, S. A. Gevorgyan, and J. Alstrup, "A roll-to-roll process to flexible polymer solar cells: model studies, manufacture and operational stability studies," *J. Mater. Chem.*, vol. 19, pp. 5442–5451, 2009. 10

[15] J. Noh, D. Yeom, C. Lim, H. Cha, J. Han, J. Kim, Y. Park, V. Subramanian, and G. Cho, "Scalability of roll-to-roll gravure-printed electrodes on plastic foils," *Electronics Packaging Manufacturing, IEEE Transactions on*, 2010. 10

[16] M. Jung, J. Kim, J. Noh, N. Lim, C. Lim, G. Lee, J. Kim, H. Kang, K. Jung, A. Leonard, J. Tour, and G. Cho, "All-printed and roll-to-roll-printable 13.56-mhz-operated 1-bit rf tag on plastic foils," *Electron Devices, IEEE Transactions on*, 2010. 10

[17] M. Ponjanda-Madappa, "Roll to roll manufacturing of flexible electronic devices," Master's thesis, School of Mechanical and Aerospace Engineering, Oklahoma State University, December 2011. 10

[18] R. Søndergaard, M. HÖsel, D. Angmo, T. T. Larsen-Olsen, and F. C. Krebs, "Roll-to-roll fabrication of polymer solar cells," *Materials Today*, vol. 15, no. 1–2, pp. 36 – 49, 2012. 10

[19] G. Brandenburg, "New mathematical models for web tension and register error," in *Proceedings of the Third International IFAC Conference on Instrumentation and Automation in the Paper, Rubber and Plastics Industries*, Brussels, 1976, pp. 411 – 438. 15, 18, 24, 25

[20] T. Yoshida, S. Takagi, Y. Muto, and T. Shen, "Register control of sectional drive rotogravure printing press," in *Manufacturing Systems and Technologies for the New Frontier*, M. Mitsuishi, K. Ueda, and F. Kimura, Eds. Springer London, 2008, pp. 417 – 420. 15, 18, 24, 25, 27, 90, 110, 116

[21] K. Choi, T. Tran, P. Ganeshthangaraj, K. Lee, M. Nguyen, J. Jo, and D. Kim, "Web register control algorithm for roll-to-roll system based printed elec-

tronics," in *Automation Science and Engineering (CASE), 2010 IEEE Conference on*, 2010. 15, 90

[22] H.-K. Kang, C.-W. Lee, and K.-H. Shin, "Compensation of machine directional register in a multi-layer roll-to-roll printed electronics," in *Control Automation and Systems (ICCAS), 2010 International Conference on*, 2010. 15, 90, 115, 116

[23] G. Brandenburg, "Advanced process models and control strategies for rotary printing presses," in *Proceedings of the Eleventh International Conference on Web Handling*, Stillwater, Oklahoma, 2011. 18, 24, 25, 27

[24] C. Branca, P. R. Pagilla, and K. N. Reid, "Modeling and identification of the source of oscillations in web tension," in *Proceedings of the Tenth International Conference on Web Handling*, Stillwater, Oklahoma, 2009. 31

[25] G. Brandenburg, S. Geissenberger, C. Kink, N.-H. Schall, and M. Schramm, "Multimotor electronic line shafts for rotary offset printing presses: a revolution in printing machine techniques," *IEEE/ASME Transactions on Mechatronics*, vol. 4, no. 1, pp. 25 – 31, 1999. 46, 55

[26] P. R. Pagilla, N. B. Siraskar, and R. V. Dwivedula, "Decentralized control of web processing lines," *IEEE Transactions on Control Systems Technology*, vol. 15, no. 1, pp. 106 – 117. 57, 71

[27] A. Benlatreche, D. Knittel, and E. Ostertag, "Robust decentralised control strategies for large-scale web handling systems," *Control Engineering Practice*, vol. 16, no. 6, pp. 736 – 750, 2008. 57

[28] D. Knittel, A. Arbogast, M. Vedrines, and P. R. Pagilla, "Decentralized robust control strategies with model based feedforward for elastic web winding systems," in *American Control Conference*, 2006. 57

[29] R. V. Dwivedula, "Modeling the effects of belt compliance, backlash, and slip on web tension and new methods for decentralized control of web processing lines," Ph.D. dissertation, Oklahoma State University, 2005. 57

[30] P. R. Pagilla and Y. Diao, "Resonant frequencies in web process lines due to idle rollers and spans," *Journal of Dynamic Systems, Measurement, and Control*, vol. 133, no. 6, p. 061018, 2011. 57

[31] E. Bristol, "On a new measure of interaction for multivariable process control," *Automatic Control, IEEE Transactions on*, 1966. 58

[32] A. Niederlinski, "A heuristic approach to the design of linear multivariable interacting control systems," *Automatica*, vol. 7, no. 6, pp. 691 – 701, 1971. 58

[33] P. Campo and M. Morari, "Achievable closed-loop properties of systems under decentralized control: conditions involving the steady-state gain," *Automatic Control, IEEE Transactions on*, 1994. 58

[34] A. Conley and M. Salgado, "Gramian based interaction measure," in *Decision and Control, 2000. Proceedings of the 39th IEEE Conference on*, vol. 5, 2000, pp. 5020 –5022 vol.5. 58

[35] P. Grosdidier and M. Morari, "Interaction measures for systems under decentralized control," *Automatica*, vol. 22, no. 3, pp. 309–320, 1986. 58, 63, 66, 69

[36] C. G. Economou and M. Morari, "Internal model control: multiloop design," *Industrial & Engineering Chemistry Process Design and Development*, vol. 25, no. 2, pp. 411–419, 1986. 58, 66, 87

[37] C. D. Meyer, *Matrix Analysis and Applied Linear Algebra*. Society of Industrial and Applied Mathematics, 2000. 59, 60

[38] R. B. Bapat and T. E. S. Raghavan, *Nonnegative Matrices and Applications*. Cambridge University Press, 1997. 62

[39] E. Seneta, *Non-negative Matrices and Markov Chains*. Springer–Verlag, 1981. 62

[40] A. I. Mees, "Achieving diagonal dominance," *Systems & Control Letters*, vol. 1, no. 3, pp. 155 – 158, 1981. 62, 64, 65, 86

[41] A. Berman and R. J. Plemmons, *Nonnegative Matrices in the Mathematical Sciences*. Academic Press, 1979. 63

[42] J. Stoer and C. Witzgall, "Transformations by diagonal matrices in a normed space," *Numerische Mathematik*, vol. 4, no. 1, pp. 158 – 171, 1962. 68

[43] M. Safonov, "Stability margins of diagonally perturbed multivariable feedback systems," *Control Theory and Applications, IEE Proceedings D*, 1982. 68, 69, 87

[44] J. C. Doyle, "Analysis of feedback systems with structured uncertainties," *Control Theory and Applications, IEE Proceedings D*, 1982. 69

[45] A. K. Packard, "What's new with mu: Structured uncertainty in multivariable control," Ph.D. dissertation, University of California, Berkeley, 1988. 85

[46] A. Packard and J. Doyle, "Structured singular value with repeated scalar blocks," in *American Control Conference*, 1988. 85, 102

[47] ——, "The complex structured singular value," *Automatica*, vol. 29, no. 1, pp. 71 – 109, 1993. 85

[48] J. Chen and C. N. Nett, "Bounds on generalized structured singular values via the perron root of matrix majorants," *Syst. Control Lett.*, vol. 19, no. 6, pp. 439–449, 1992. 86

[49] P. Chanchana, "An algorithm for computing the perron root of a nonnegative irreducible matrix," Ph.D. dissertation, North Carolina State University, 2007. 86

[50] P. Young and J. Doyle, "Computation of μ; with real and complex uncertainties," in *Decision and Control, 1990., Proceedings of the 29th IEEE Conference on*, 1990. 86

[51] P. M. Young, M. P. Newlin, and J. C. Doyle, "Practical computation of the mixed μ problem," in *American Control Conference*, 1992. 86

[52] M. Fan, A. Tits, and J. Doyle, "Robustness in the presence of mixed parametric uncertainty and unmodeled dynamics," *Automatic Control, IEEE Transactions on*, 1991. 86, 87

[53] E. E. Osborne, "On pre-conditioning of matrices," *J. ACM*, vol. 7, no. 4. 87

[54] J. C. Doyle, "Synthesis of robust controllers and filters," in *Proc. CDC*, San Antonio, 1983, pp. 109 – 114. 88

[55] S. J. Kirkland, M. Neumann, N. Ormes, and J. Xu, "On the elasticity of the perron root of a nonnegative matrix," *SIAM Journal on Matrix Analysis and Applications*, vol. 24, no. 2, pp. 454–464, 2002. 88

[56] S. J. Kirkland, M. Neumann, and J. Xu, "Convexity and elasticity of the growth rate in size-classified population models," *SIAM Journal on Matrix Analysis and Applications*, vol. 26, no. 1, pp. 170–185, 2004. 88

[57] E. Deutsch and M. Neumann, "First and second order derivatives of the perron vector," *Linear algebra and its applications*, vol. 71, pp. 57 – 76, 1985. 88

[58] T. Yoshida, S. Takagi, T. Shen, and Y. Muto, "Register control method for sectional-drive-type rotogravure printing press – application of nonlinear control law and tension observer," in *Asia International Symposium on Mechatronics 2008*, 2008. 90, 110, 116

[59] T. Yoshida, S. Takagi, Y. Muto, and T. Shen, "Register control of rotogravure printing press. application of nonlinear control theory to sectional drive printing press," *Electronics and Communications in Japan*, vol. 94, no. 1, pp. 17–24, 2011. 90, 110, 115, 116

[60] H. Komatsu, T. Yoshida, S. Takagi, T. Shen, and Y. Muto, "Improvement of printing accuracy via web handling control in multi-colors printing machines," in *Control, Automation and Systems, 2007. ICCAS '07. International Conference on*, 2007. 90

[61] P. Gahinet and L. Shampine, "Software for modeling and analysis of linear systems with delays," in *American Control Conference*, 2004. 95

[62] K. Gun, V. L. Kharitonov, and J. Chen, *Stability of Time-Delay Systems*, ser. Control Engineering. BirkhÃd'user Boston, 2003. 99, 102, 103, 104, 105

[63] J.-P. Richard, "Time-delay systems: an overview of some recent advances and open problems," *Automatica*, vol. 39, no. 10, pp. 1667 – 1694, 2003. 99

[64] R. Sipahi, S. Niculescu, C. Abdallah, W. Michiels, and K. Gu, "Stability and stabilization of systems with time delay," *Control Systems, IEEE*, 2011. 99

[65] J. K. Hale and S. M. Verduyn Lunel, *Introduction to functional-differential equations*, ser. Applied Mathematical Sciences. New York: Springer-Verlag, 1993, vol. 99. 99

[66] S. Boyd and C. Desoer, "Subharmonic functions and performance bounds on linear time-invariant feedback systems," *IMA Journal of Mathematical control and Information*, vol. 2, no. 2, pp. 153–170, 1985. 101

[67] W. Kwon and A. Pearson, "Feedback stabilization of linear systems with delayed control," *Automatic Control, IEEE Transactions on*, 1980. 106

[68] Z. Artstein, "Linear systems with delayed controls: A reduction," *Automatic Control, IEEE Transactions on*, 1982. 106

[69] K. Watanabe and M. Ito, "A process-model control for linear systems with delay," *Automatic Control, IEEE Transactions on*, 1981. 106

[70] A. Manitius and A. Olbrot, "Finite spectrum assignment problem for systems with delays," *Automatic Control, IEEE Transactions on*, 1979. 106

[71] Y. Fiagbedzi and A. Pearson, "Feedback stabilization of linear autonomous time lag systems," *Automatic Control, IEEE Transactions on*, 1986. 106

[72] A. Olbrot, “Stabilizability, detectability, and spectrum assignment for linear autonomous systems with general time delays,” *Automatic Control, IEEE Transactions on*, 1978. 106

VITA

Aravind Seshadri

Candidate for the Degree of

Doctor of Philosophy

Dissertation: Modeling, Analysis And Control of Print Registration in Roll-to-Roll Printing Presses

Major Field: Mechanical and Aerospace Engineering

Biographical:

Education:

Received Bachelor of Engineering in Mechanical Engineering from University of Madras, Chennai, India, in 2003;
Received the Master of Science in Mechanical Engineering from Oklahoma State University in May, 2007.
Completed the requirements for the Doctor of Philosophy in Mechanical and Aerospace Engineering at Oklahoma State University, Stillwater, Oklahoma in May 2013.

Experience:

Research Assistant/Associate at Oklahoma State University from June 2004 - May 2013;
Visiting Researcher at Louis Pasteur University, Strasbourg, France from May 2007 - July 2007;
Teaching Assistant at Oklahoma State University from August 2004 - December 2005.

Professional Memberships:

American Society of Mechanical Engineers (ASME)